# *Numerical modelling of slab breakoff and its magmatic effects*

REBECCA JANE FREEBURN

# Numerical modelling of slab breakoff and its magmatic effects


**Rebecca Jane Freeburn**

**Department of Earth Sciences**

**Durham University**

A thesis submitted for the degree of

Master of Philosophy (MPhil)

2016

# Numerical modelling of slab breakoff and its magmatic effects

**Rebecca Jane Freeburn**

## Abstract

The process of slab breakoff following the collision of continental plates has been invoked to account for many magmatic observations in post-collisional areas. These interpretations are often based upon the results of kinematic modelling of slab breakoff, which find this process can induce a thermal perturbation in the overriding plate, possibly generating lithospheric melting. Such a process requires that breakoff occurs at depths shallower than the base of the overriding lithosphere. This thesis aims to investigate more thoroughly the magmatic effects that breakoff may have. 2D numerical experiments are conducted, which make use of a thermodynamic database to determine the generation of melts and (de)hydration processes that occur within a collisional environment. A systematic parametric study is designed, which investigates those factors which may have a significant control on the breakoff depth. The breakoff timing and resulting mantle flow patterns are also investigated, as these may affect the magmatic processes. The strength of the subducting continental lithosphere is found to have a key control on the breakoff depth, whilst the timing and flow are significantly dependent upon the mantle rheology. By investigating further those conditions which promote shallow breakoff, it is found that breakoff appears unable to induce any significant melting of the overriding mantle lithosphere. In most cases, breakoff localises deeper than the overriding plate, preventing melting. Even following very shallow breakoff, the rapid descent of the detached slab gives way to a subsequent cooling of the overriding plate. A more commonly observed feature is the melting of continental crust upon breakoff, which may be a more reliable indicator of the occurrence of breakoff than lithospheric melting. Despite this, post-collisional magmatic observations show a wide range of compositions, timings, and localities. It is unlikely that melting across a post-collisional area can be attributed to any one geodynamic process.

# Contents

# List of Tables

# List of Figures

# Declaration

I, Rebecca Jane Freeburn, declare that this thesis, presented for the degree of Master of Philosophy at Durham University, is a result of my own original research and has not been previously submitted to Durham University or any other institution. I have clearly indicated, when appropriate, the contributions of colleagues and have made every effort to acknowledge all collaborative work.

Rebecca Jane Freeburn

Durham University

September 2016

# Acknowledgements

My thanks firstly goes to Jeroen van Hunen for all his support and guidance with the project over the last two years. He has always been willing to listen, to discuss, and to provide endless help with all aspects of the project, and to give up much of his very busy time. Ben Maunder has also been a huge help with this project, helping me to understand the way the numerical code works and to implement new features. He has shown great patience with my regular lack of understanding and constant questions. He also has provided much amusement at many conferences, providing he manages to board his flights. I am also grateful for the help of Valentina Magni and Pierre Bouilhol throughout this project. Like Ben, Valentina has often been a source of advice and help when working with the models. Her implementations have been crucial to the development of this work. Pierre has helped greatly with the petrological aspects, without whom I would have made many incorrect assumptions and conclusions about magmatism, and this thesis would still be entirely written 'like a geodynamicist' would. This work has been made possible through grant funding from the Topomod and the use of the Durham University High Performance Computing service. Thanks should also be given to Henk Slim, who has made Hamilton work again many, many times and shows great patience with HPC novices. This study was also supported by the European Research Council (ERC StG 279828).

My thanks also goes to Jordan, who has been my best desk buddy for the past two years, despite being seemingly boring for the first few months of knowing him. He has livened up my days many times, listened to me chattering away to him about my work (even when he doesn't have a clue what I'm talking about), cheered me up when I'm glum, and provided me with lots of food and hot chocolate when I'm hungry. Thanks also has to go to him for introducing me to afternoon tea breaks, which I have found make for a much more productive days work. I am grateful for friendship and laughter with many other colleagues in the department: Jack, Helena, Sarah, Eleanor, Kate, Miles, Anna, Vili, Julien, Fienke, Li, Hongliang, Andrew and many others. Thanks also goes to my family, for their support and provision since moving away from their home, despite them still being unable to describe what my project has involved other than 'plate tectonics'. I am also very grateful for my husband, who has been so caring and loving over the past year and a half. He has flown over to San Francisco with me, pretended to be a nameless professor in the department so that he

could listen to the presentation I gave at AGU, and now knows it so well he could present it better than I could. Thanks also goes to him for his patience with my absence over the past month whilst I finished writing this thesis, despite him moving house and starting a new job.

Finally, my greatest thanks goes to my heavenly Father, who has sustained me and provided everything I have needed over the past two years. The work in this thesis provides only a glimpse of his glory in creating everything that is around us:

> ‘The heavens declare the glory of God,
> and the sky above proclaims his handiwork.
> Day to day pours out speech,
> and night to night reveals knowledge.’
>
> Psalm 19:1-2

I look forward to the day when he will remake a new world, where we will see Jesus in glory:

> ‘Then I saw a new heaven and a new earth, for the first heaven and the first earth had passed away, and the sea was no more. And I saw the holy city, new Jerusalem, coming down out of heaven from God, prepared as a bride adorned for her husband. And I heard a loud voice from the throne saying, “Behold, the dwelling place of God is with man. He will dwell with them, and they will be his people, and God himself will be with them as their God. He will wipe away every tear from their eyes, and death shall be no more, neither shall there be mourning, nor crying, nor pain anymore, for the former things have passed away.”’
>
> Revelation 21:1-4

Chapter 1

# Introduction

## 1.1 Convergent margin magmatism

### 1.1.1 Arc magmatism

Globally, magmatic activity is observed within boundary zones where tectonic plates meet (Fig. 1.1). Arc volcanism occurs at sites of oceanic subduction, both beneath oceanic and continental overriding plates. Characteristically, lines of volcanism are formed parallel to the subduction trench, which range in width from between 50 and 200 km and often appear to have a constant depth of around 110 km to the subducting slab (Schmidt and Poli, 1998; Tatsumi, 1986). The magmas have a comparatively higher $H_2O$ content than mid-ocean ridge basalts (MORBs), varying between 1.0 - 2.9 wt%, and are also more enriched in incompatible elements, which is suggested to be a result of a transfer of elements by the fluid phase from the downgoing slab (Sobolev and Chaussidon, 1996; Tatsumi et al., 1986). These observations suggest that melting is not solely formed through simple decompression melting, as at oceanic spreading centres.

Water is known to considerably lower the melting temperature of rock (Ernst, 1999; Thompson, 1992). Multiple sources of fluid are present within the subduction zone: the oceanic crust can become hydrated initially through alteration at the mid-oceanic ridge (Rüpke et al., 2004); further hydration of the crust and of the lithospheric mantle can occur through bend faults, as the plate starts to be subducted (Faccenda et al., 2008; Ranero et al., 2005); and sediments deposited upon the oceanic plate can also contain both pore and chemically bound water (Rüpke et al., 2004). Experiments at high pressures and temperature show that fluids can be released from the subducting oceanic crust and lithospheric mantle at the conditions reached in typical subduction zones, due to the breakdown of hydrous minerals during progressive metamorphism within the downgoing slab (Peacock, 1990;

Schmidt and Poli, 1998). The volcanic front therefore forms above the location where the melt reaches a sufficient volume to be extracted. It is possible that the slab chemical signature observed in arc magmas could originate from melting of the subducted lithospheric mantle, but experiments suggest that this would only occur in relatively hot subduction zones (Peacock, 1996, 1990). Instead, it is more feasible that fluids transfer this signature to material flowing into the mantle wedge area, which subsequently melts.

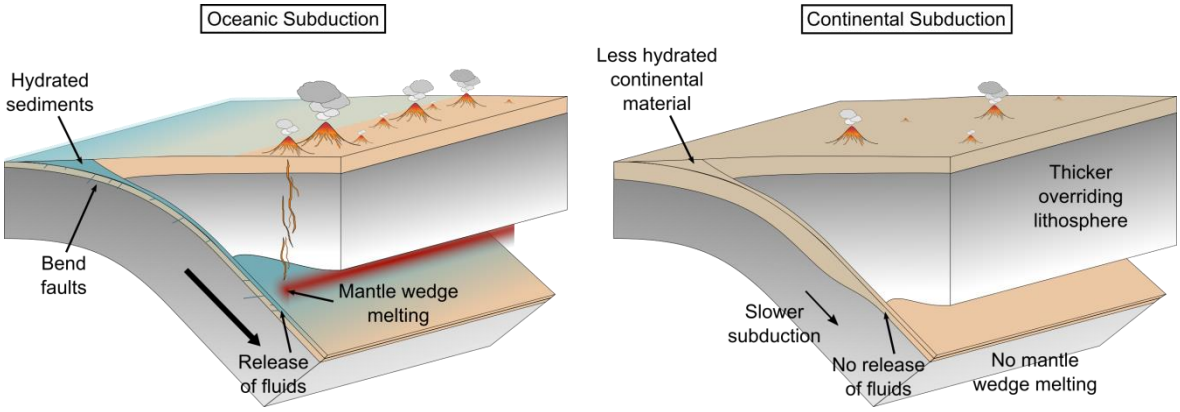


**Figure 1.1: The differences in dynamics, hydration and melting processes between the subduction of the oceanic and continental lithosphere.** The subduction of buoyant continental crust may act to alter the thermal structure of the mantle wedge, but the absence of arc volcanism in continent-continent collision zones is most likely the result of a lack of available fluids to generate partial melting in the mantle wedge.

## 1.1.2 Post-collisional magmatism

### 1.1.2.1 Differences between oceanic and continental subduction

Magmatism is also observed across post-collisional areas, but is very different in nature to the continuous calc-alkaline arc volcanism observed at subduction zones (Ernst, 1999; Zhao et al., 2013; Zheng, 2009; Zheng and Hermann, 2014). Hence, post-collisional magmatism may not solely be generated by the dehydration of the subducting lithosphere. Before analysing the mechanisms that have been suggested to account for magmatic observations in these areas, it is useful to consider why melting may not occur in the same way and what the differences are between sites of oceanic and continental subduction (Fig. 1.1).

The structure of a continental plate is significantly different to an oceanic plate, and hence differences in the dynamics of subduction are to be expected. The continental lithosphere consists of thicker, more buoyant crust, which provides a resistive force to subduction.

Although in many areas the introduction of continental material slows the rate of subduction, it does not fully terminate subduction, and the continent is subducted beneath the overriding plate. This decrease in velocity may alter the thermal structure of the mantle wedge. Corner flow during oceanic subduction, induced by the continual downgoing of the slab, brings hot undepleted mantle towards the subduction zone. This flow may be hindered in the case of continental subduction by a slower rate of subduction, which could prevent melt generation.

The presence of fluid is also crucial for the generation of arc volcanism during oceanic subduction. For the same dehydration and melting processes during continental subduction, the continental plate would both need to be sufficiently hydrated before subduction, and then be capable of dehydrating at depth when subducted. Based upon the lack of ocean water to infiltrate into the continental lithosphere, combined with the much lower porosity of continental crust, the continental plate is likely to be much less hydrated (Zheng, 2009). However this topic has been long debated. Continental drilling shows the crust to be relatively dry, with most hydration occurring along fractures, rather than occupying grain boundaries (Yardley, 2009). Hence, this suggests that tectonic activity does allow the hydration of the crust to some extent, but only in localised areas. Ultra-high pressure rocks also provide useful information, as they record the same range of pressures that the oceanic slab experiences during subduction, and so can provide information about the similarities and differences in fluid flow at these depths (Hermann et al., 2013). Petrological studies, metamorphic veins and fluid inclusions within these rocks can all reveal information about this potential fluid flow; however, using petrography alone can be difficult, as minerals can react whilst the crust is being exhumed towards the surface, overprinting minerals that were formed at the peak metamorphic conditions (Hermann et al., 2013; Li et al., 2014). Despite these complexities, these observations indicate the presence of some fluid within the continental crust, although the extent of hydration is unclear.

It has been suggested that the main hydrous minerals within the continental crust are stable much deeper than 100 km and that it is unlikely that thermally weakened, buoyant crust would be able to subduct considerably deeper than this (Ernst, 1999; Ernst et al., 1998). Therefore, continental crust may be unable to dehydrate in the same manner as the oceanic crust during subduction. There is very little evidence to suggest the occurrence of fluid release during prograde and peak metamorphic conditions, although some examples do exist of dehydration metamorphism and hydration anatexis during continental subduction from ultra-high pressure metagranites within the Sulu Orogen (Li et al., 2014). Most observations from ultra-high pressure metamorphic (UHPM) rocks instead record the release of fluid and dehydration melting during exhumation of the continental crust (i.e. during the return of the

buoyant crust to the surface) (Xia et al., 2008; Zheng, 2009; Zheng et al., 2011, 2007). At this time, the release of water can occur through decompression of hydrous minerals, and also through decompressional exsolution of water from nominally anhydrous minerals (NAMs) (Zheng, 2009). NAMs can contain significant amounts of water in the form of molecular $H_2O$ and structural OH (Chen et al., 2011). Two factors mean that this water is more likely to be released during exhumation; firstly, high temperatures are preserved within the crust coincident with a decrease in pressure, and secondly, the fluid solubility of NAMs decreases with depth (Zheng, 2009; Zheng and Hermann, 2014). Therefore, the exhumation of continental crust may provide a means by which any fluid bound within the crust can be released, but the timing and location of this flow is likely to result in a very different style of melting than the flow that produces mantle wedge melting and arc volcanism, as observed at oceanic subduction zones (Hermann et al., 2013; Zheng, 2009, 2012).

#### 1.1.2.2 Key observations from post-collisional areas

Despite these differences, post-collisional igneous rocks are common in collision orogens (Zhao et al., 2013). Below, the main volcanic observations along the Alpine-Himalayan collision belt are summarised. Whereas in subduction zones the style of melting is generally similar globally, across post-collisional areas this can vary considerably. Some features are consistently observed across different collision zones, whilst others are unique, and magmatic observations can even vary significantly within the same area.

A variety of different sources for this melting have been suggested based on geochemical observations. Melts characteristic of a lithospheric mantle source are observed in most collisional zones (von Blanckenburg and Davies, 1995). These lithospheric melts often appear to have a signature of a subduction modified component, which has been suggested to be the result of the melting of lithospheric mantle that has been previously metasomatised during oceanic subduction processes (e.g. Chen et al., 2014; Davies and von Blanckenburg, 1995; Keskin et al., 2008; Kheirkhah et al., 2009; Maury et al., 2000). von Blanckenburg and Davies (1995) did not observe any melts with asthenospheric components within the Alps, but there have since been numerous observations elsewhere. OIB-type melts (i.e. with a similar enrichment in trace elements as ocean-island basalts, indicating an asthenospheric source) are a common feature in post-collisional areas, which are often suggested to be the result of an upwelling of asthenospheric mantle (e.g. Altunkaynak and Genç, 2008; Coulon et al., 2002; Dilek and Altunkaynak, 2007; Ji et al., 2016; Pang et al., 2012; Walker et al., 2009; Xu et al., 2008). One characteristic feature that has been noted is a change from a subduction modified lithospheric source to OIB-type melts over time, sometimes with an

intervening quiescent period (Altunkaynak and Genç, 2008; Coulon et al., 2002; Dilek et al., 2010; Keskin et al., 2008). Some studies have suggested a limited crustal signature, whilst others observe extensive crustal contamination (Kheirkhah et al., 2015; Maury et al., 2000). It is unclear whether these signatures originate from a crustal source, or by contamination from within the overlying plate as mantle melts migrate into the crust. Signatures possibly from the subducting continental crust have also been recorded (Hou et al., 2012; Ji et al., 2009; Kohn and Parkinson, 2002), along with melting of the lower crust of the overriding plate (Chen et al., 2014; Chung et al., 2009; Lee et al., 2012; Ma et al., 2014). Melting of the oceanic crust after collision may also occur (Mo et al., 2008; Omrani et al., 2008). Adakitic magmas have been observed after calc-alkaline subduction-related magmatism has ceased (Chiu et al., 2013; Chung et al., 2009; Omrani et al., 2008). These may possibly be a result of the melting of mafic material at depth under unusually high temperatures, which could be induced by a change in thermal conditions after collision, melting either the oceanic or lower continental crust. However, fractional crystallisation processes can also produce adakite-like signatures, which should hence be interpreted with caution (Castillo, 2012; Macpherson et al., 2006).

One common feature in post-collisional areas is the onset of renewed magmatism following a longer quiescent period, with little or no magmatic activity (e.g. Chiu et al., 2013; Kheirkhah et al., 2009; Mo et al., 2007; Neill et al., 2013; Wen et al., 2008). Post-collisional magmas form from much lower degrees of melting than previous arc volcanism, ranging from very low to moderate degrees of partial melts (Ahmadzadeh et al., 2010; Ernst, 1999; Kheirkhah et al., 2013; Pearce et al., 1990; von Blanckenburg and Davies, 1995), but short-lived pulses of more intense magmatic activity also occur (Lee et al., 2012, 2009; Mo et al., 2007; Wen et al., 2008; Zhu et al., 2011). Magmatism extends over a much wider area than more narrowly confined subduction-related melting (Neill et al., 2013; Pearce et al., 1990) (Fig. 1.2). Most magmatism is observed within the overriding plate, although some does occur around the suture or even within the foreland (Allen et al., 2013; Davies and von Blanckenburg, 1995; Kheirkhah et al., 2009; Pearce et al., 1990). Magmas often show no age progression, although some patterns both parallel to the subduction trench (Maury et al., 2000) and migrating towards the subduction trench (Chung et al., 2005; Lee et al., 2009) have been observed. Linear belts of magmatism have also been recorded across the Alpine-Himalayan collisional belt, including: a 200 km long magmatic belt in Algeria (Maury et al., 2000); the Pediatric Lineament in the Alps (Davies and von Blanckenburg, 1995; von Blanckenburg and Davies, 1995); within Anatolia (Keskin et al., 2008); the Urumieh–Dokhtar magmatic arc in Iran, mostly interpreted as a result of arc volcanism, but also as post-collisional

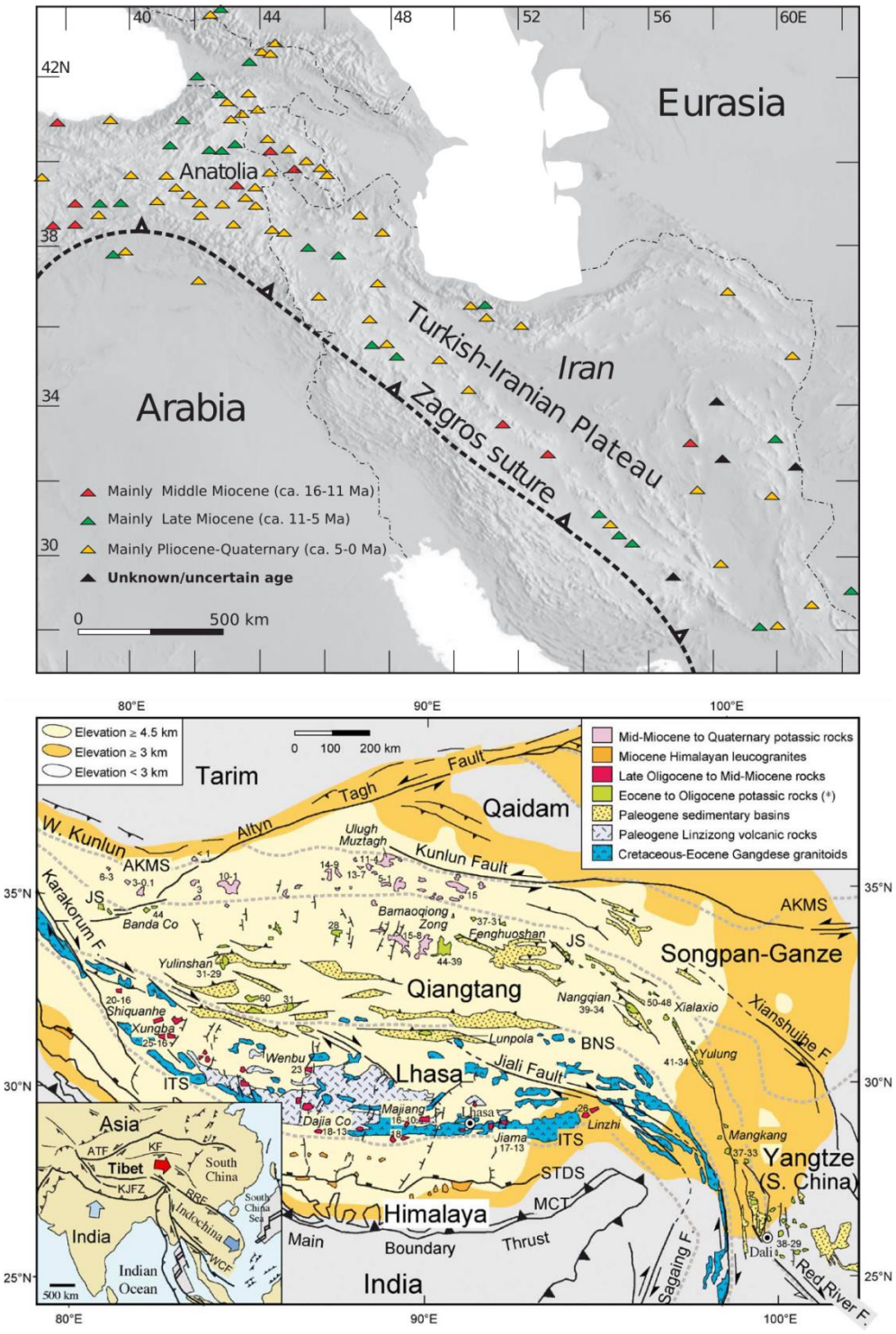


**Figure 1.2: The nature of magmatism across collisional zones.** Top - the Arabia-Eurasia collision zone (volcanic centres represented by triangles), and bottom - the India-Asia collision. Magmatism is widespread in both cases, distributed 100s of kms from the suture zone within the overriding plate, and prolonged over Myrs (from Kaislaniemi et al. (2014) (top) and Chung et al. (2005) (bottom)).

(Ghasemi and Talbot, 2006); and a 150 km long granitoid belt in Tibet (Guo et al., 2013; Hou et al., 2012).

This variety in the source, timing and locality of melting is most likely the result of a number of different mechanisms at work along the length of the Alpine-Himalayan belt (Allen et al., 2013; Lee et al., 2009). One common interpretation that is used to explain some of these observations is the detachment of previously subducted oceanic lithosphere from the incoming continental plate.

## 1.2 Slab breakoff

### 1.2.1 The dynamics of breakoff

Slab breakoff (also commonly referred to as 'slab detachment') was first hypothesised after the analysis of significant gaps in the distribution of earthquake hypocentral depths in subducting slabs (Chatelain et al., 1992; Isacks and Molnar, 1969; Yoshioka and Wortel, 1995). Subsequently, seismic tomographic imaging of the mantle showed decreases in P-wave velocities to normal mantle values along the inferred planes of these slabs, suggesting detachment in these regions (Wortel and Spakman, 2000) (Fig. 1.3).

It was suggested that subducting slabs may become stagnated when the slab pull force driving subduction is no longer large enough to overcome the buoyancy forces resisting it. The introduction of buoyant material into the subduction trench increases these resisting forces and may result in a decrease in subduction velocity (Davies and von Blanckenburg, 1995) (Fig. 1.4). The slab may become weaker as subduction continues, due to heating and an increasingly higher proportion of weaker continental material. Extensional stresses may be generated between the continental and denser oceanic lithosphere, resulting in breakoff when these exceed the strength of the slab (van Hunen and Allen, 2011). This separation results in the formation of a 'slab window'; an area of hotter asthenospheric mantle intervening between the upper and lower detached sections of the slab, which grows in area over time, due to the continued descent of the dense lower part of the slab and the upwelling of mantle asthenosphere to replace this.

Early analytical studies confirmed the plausibility of slab breakoff occurring in the mantle. Yoshioka et al. (1994) studied the process of slab necking and detachment by observing the development of a descending cold plume ('slab') using 2D convection models, and found the process to be initiated by heterogeneities in the viscosity field within the slab. A more

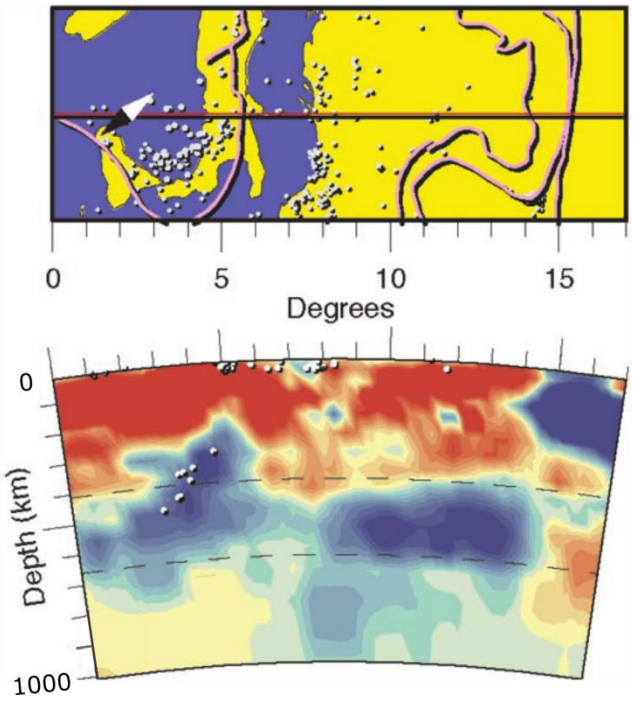


**Figure 1.3: Seismic tomographic imaging of P-wave velocities across the southern Apennines.** White circles represent earthquake locations. Pink lines represent the tectonic outlines. Red colours represent negative seismic wave velocity anomalies and blue colours positive anomalies. Slab breakoff within the subducted slab below Italy is identified by the decrease in seismic wave speeds and lack of earthquakes along the profile of the slab (from Wortel and Spakman (2000)).

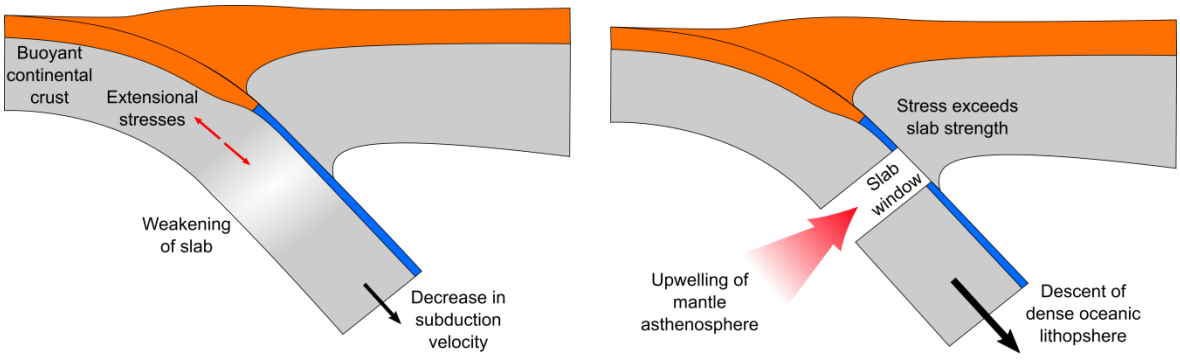


**Figure 1.4: The dynamics of continent-continent collision and slab breakoff.** The introduction of buoyant continental crust into a subduction zone can generate extensional stresses within the subducting slab, resulting in a decrease in (and possible cessation of) subduction velocity. Thermal heating can further weaken the slab, leading to slab breakoff where the stress exceeds the strength of the slab. The opening of a slab window at this location may lead to the upwelling of asthenospheric mantle, to replace the descending detached slab.

quantitative approach was taken by Davies and von Blanckenburg (1995), who calculated the change in buoyancy force expected during a change in subduction from oceanic to continental lithosphere, and evaluated an upper bound for the strength of the lithosphere at increasing depths. They defined breakoff to occur when the force exceeds the strength, and showed that for a convergence velocity of 1 $cmyr^{-1}$ this is likely to occur between a depth of 50 and 120 km. This can occur in a number of settings, such as when spreading ridges or oceanic plateaus approach a subduction zone, but this study focuses on the change from the subduction of oceanic lithosphere to continental.

### 1.2.2 Slab breakoff-induced melting

The generation of magmatism following slab breakoff may occur through a number of different mechanisms (Fig. 1.5). Firstly, breakoff may result in a thermal perturbation of the overlying mantle wedge material (Davies and von Blanckenburg, 1995). Mantle material directly overlying the subducted slab is likely to be hydrated as a result of slab dewatering throughout oceanic subduction, and will hence have a lower solidus temperature than dry material. However, this material is unlikely to have already exceeded the solidus and undergone partial melting, and will hence be more fertile than if hydration had previously induced melting (Thorkelson, 1996). Therefore, hot lithospheric mantle that is already near the solidus will likely melt following any increase in temperature induced by slab breakoff. Secondly, if the mantle underlying the subducting slab is hotter and hence less dense, this may flow upwards into the slab window that is formed (Thorkelson, 1996). Decompression melting of this upwelling asthenosphere may occur if shallow depths are reached (van de Zedde and Wortel, 2001). Thirdly, partial melting at the edges of the subducted crust may occur whilst it is exposed to hotter mantle material after breakoff

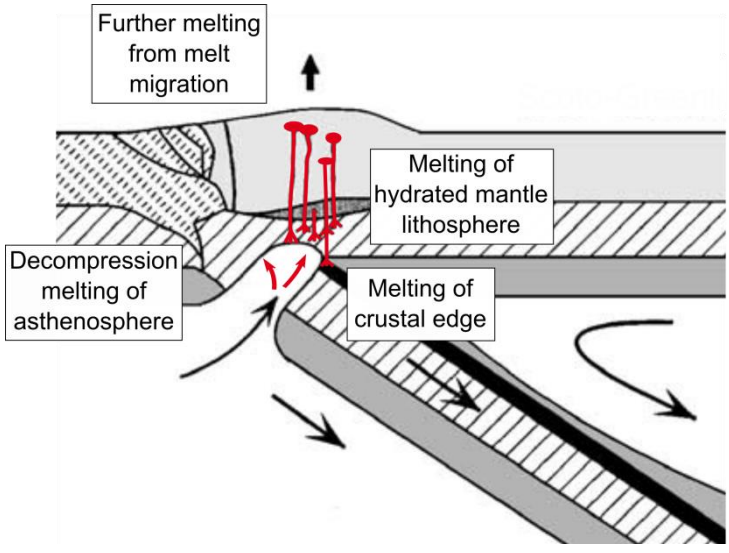


**Figure 1.5: Possible means by which slab breakoff could induce post-collisional magmatism.** Melting shown in red (modified after Ghasemi and Talbot (2006)).

(Davies and von Blanckenburg, 1995). Additionally, any melt generated may penetrate upwards into the overriding continental lithosphere, resulting in further heating and melting (van de Zedde and Wortel, 2001).

Some observations from post-collisional areas could be well explained by the above mechanisms. Melting interpreted to have originated from a metasomatised lithospheric mantle may be the result of an upwelling of asthenospheric mantle after breakoff, causing a thermal perturbation in the overriding plate perhaps previously modified by a flux of fluid during subduction. A breakoff-induced cause of these melts has been suggested across the Alpine-Himalayan collision, from Algeria in the west (Coulon et al., 2002; Maury et al., 2000), in Anatolia and Iran (Ahmadzadeh et al., 2010; Altunkaynak and Genç, 2008; Dilek et al., 2010; Dilek and Altunkaynak, 2007; Ghasemi and Talbot, 2006; Neill et al., 2013), and also in Tibet in the east (Kohn and Parkinson, 2002; Lee et al., 2009; Mahéo et al., 2002). A change from a calc-alkaline to alkaline signature and the appearance of OIB-type melts may be the result of decompressional melting of the asthenosphere within the slab window. Transitional basalts, which are sometimes observed between the calc-alkaline and alkaline signatures, may be the result of the melting of the boundary between the lithosphere and asthenosphere (e.g. Coulon et al., 2002). Some studies suggest an observed signature that represents a mixing of subduction modified lithospheric mantle and undepleted mantle flowing in from behind the slab (Lee et al., 2012; Li et al., 2014; Xu et al., 2008). Adakitic signatures could also be the result of melting of the crustal tips within the detached slab (Omrani et al., 2008). Magmatism that shows an age progression along a narrow belt parallel to the subduction trench, and occurs following a quiescent period (e.g. Maury et al., 2000; Nemcok et al., 1998), is consistent with numerical models that show breakoff is not synchronous with initial collision and propagates as a slab tear (van Hunen and Allen, 2011). However, the results of Davies and von Blanckenburg (1995) imply that breakoff can only induce magmatism if the depth of breakoff is shallower than the overriding lithosphere. Similarly, Allen et al. (2013) suggest melting through the above mechanisms seems unlikely to account for magmatism in parts of Iran where the lithosphere is between 150 and 200 km thick.

## 1.3 Other interpretations for post-collisional magmatism

Several other interpretations have been suggested to account for the generation of post-collisional magmatism, which are summarised in Fig. 1.6. Below the processes of delamination and exhumation are further considered, in addition to toroidal mantle flow in three dimensions.

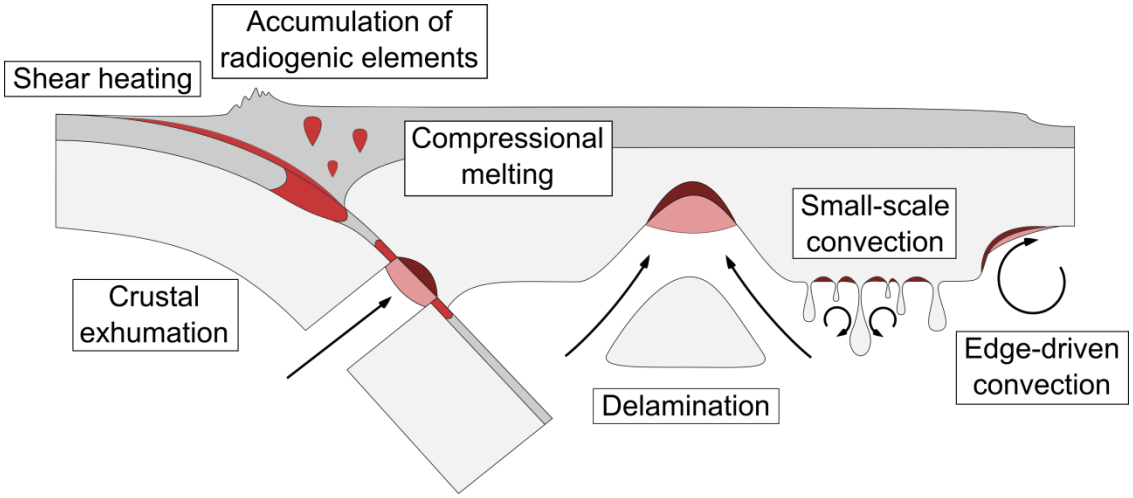


**Figure 1.6: Mechanisms which may induce post-collisional magmatism.** Including those involving solely crustal melting (red), to the melting of the asthenospheric mantle (pink) and lithospheric mantle (brown).

### 1.3.1 Delamination

Both removal of the subducting lithospheric mantle from the crust and complete detachment of sections of thickened lithospheric roots are commonly termed delamination, and have been suggested as a cause for melting following collision. The former is that as proposed by Bird (1978; 1979), whereby the more buoyant continental crust is peeled away from the denser mantle lithosphere. This could be initiated within a continental plate, but also following the introduction of continental lithosphere into a subduction zone. Recent numerical studies have found that a significant rheological difference between the crust and mantle is critical to initiating slab delamination, which may be present during continental collision (Duretz and Gerya, 2013; Magni et al., 2013; Schott and Schmeling, 1998). The detachment of lithospheric roots is also known as convective removal of the lithosphere or lithospheric 'dripping', and is not a direct result of collision. The mantle lithosphere may not be removed entirely in this case.

The removal of the lithospheric mantle may lead to the upwelling of hot asthenosphere, which may cause an increase in heat flow. This has been suggested as a cause of melting, both through the heating of the lower crust which is put into direct contact with hot asthenosphere, and through the decompression melting of upwelling asthenosphere (Dilek and Altunkaynak, 2007; Keskin, 2003). Numerical models have shown the potential of delamination to cause melting of the lower crust over a wide area (Ueda et al., 2012) (Fig. 1.7). Göğüş and Psyklywec (2008) find that delamination, as compared to lithospheric

dripping, is significantly more efficient as a means of heating the lower crust, as the temperature increase occurs more rapidly and persists for a longer period of time. A time delay between collision and melting induced through delamination would be expected, as for slab breakoff. However, unlike breakoff, delamination would be expected to produce large-scale crustal melting over a significantly wider area.

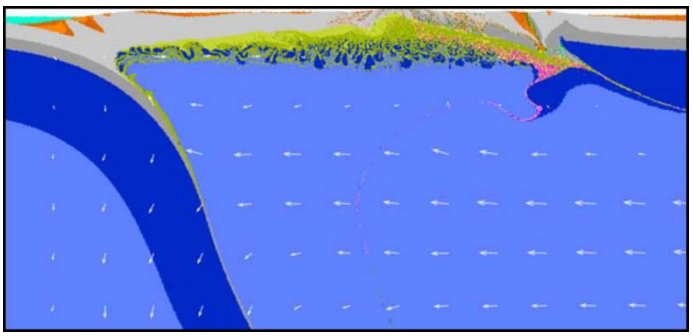

**Figure 1.7: Numerical modelling of delamination.** Delamination of the continental crust (grey) and lithospheric mantle (dark blue) following collision, showing significant partial melting of the crust, depicted in green/yellow colours (after Ueda et al. (2012)).

### 1.3.2 Toroidal mantle flow

Toroidal mantle flow around the edges of detached slabs has been suggested based on seismic and geochemical observations, and is consistent with the numerical modelling results of 3D mantle flow patterns (Piromallo et al., 2006; Sternai et al., 2014). Anisotropic orientations from shear wave splitting studies show mantle flow patterns do not correlate with the overall plate motion at subduction zones, but instead form circular patterns around the edges of subducting oceanic plates (Jadamec and Billen, 2012; Zandt and Humphreys, 2008). This flow may be induced at the ends of horizontally propagating slab tears or around sub-vertical detachments caused by along-trench variations, such as differing rollback velocities or the introduction of more buoyant material at certain localities along the trench (Faccenna et al., 2005; Govers and Wortel, 2005; Magni et al., 2014b; Rosenbaum et al., 2008; Wortel and Spakman, 2000). Uplift is observed at the edges of these detached slabs, indicating the presence of continuous upwelling mantle at these localities (Faccenna et al., 2011). The observed anomalous volcanism displaying transitional signatures between arc-type and OIB-type may be a result of decompression melting of hot inflowing asthenosphere from behind the slab, upwelling at the slab edge due to the effect of both toroidal and poloidal mantle flow (Faccenna et al., 2011, 2005; James et al., 2011; Rosenbaum et al., 2008). This mechanism has been suggested to account for the volcanism observed at Mt. Etna and Mt. Vulture, along the Calabrian subduction zone (Faccenna et al., 2011, 2010; Rosenbaum et al., 2008), and for areas of the Snake River Plain/Yellowstone volcanic province and the Basin and Range province in the western U.S. (James et al., 2011; Zandt and Humphreys, 2008).

### 1.3.3 Exhumation

The exhumation of continental crust was first suggested based on the evidence of ultra-high pressure (UHP) metamorphic rocks observed in collision zones (Chopin, 1984; Smith, 1984). It was inferred that this material must have been transported to depths greater than 100 km and then brought back to the surface. Observations of exhumed crust globally are diverse in nature, revealing differing timings, depths and duration of exhumation events. This suggests that exhumation doesn't necessarily occur as the detachment and upward movement of a single crustal slice, but a variety of mechanisms may be at work, such as ductile channel flow of the continental crust, whole slab eduction, trans-mantle diapirs and relamination of the crust (Hacker et al., 2013). Results from numerical modelling suggests that breakoff is not required to initiate crustal exhumation (Warren et al., 2008). Instead weakening mechanisms, such as that induced by increased strain and temperature during continental crustal subduction, may be sufficient to trigger this process.

In addition to the dynamic possibility of crustal exhumation, it has been suggested that this process could also result in the melting of the continental crust, either through fluid-saturated melting at UHP conditions or through dehydration reactions which occur along the prograde path. Direct observations of partial melting and rock compositions consistent with previous melt extraction events have been observed across a number of collisional belts, including: the Dabie Shan; the Kokchetav Massif, Kazakhstan; the Bohemiam Massif, the Western Gneiss Region, Norwegian Caledonides; the North Eastern Greenland eclogite province; and the Sulu Orogen (see Labrousse et al., 2015 and references therein). Both Whitney et al. (2009) and Labrousse et al. (2015) have modelled the occurrence of partial melting during crustal exhumation, showing not only the possibility of melting, but also the effect this has on the buoyancy and continued exhumation of the crust.

## 1.4 Thesis outline

### 1.4.1 Aims of this thesis

Melting in collision zones is diverse in many respects, with variations in the source, timing, amount, age, and location of this melting. Despite this range in melting characteristics, post-collisional magmatism is a phenomenon that is observed across many continental collision zones. As such, a single mechanism is often sought to account for the geochemical observations from these areas. Slab breakoff is perhaps the mechanism that is most regularly

proposed as being capable of producing the magmatic effects in collision zones, when interpreting the observations from geochemical analyses of magmatic rocks (e.g. Coulon et al., 2002; Mahéo et al., 2002; von Blanckenburg and Davies, 1995). Breakoff is an event that is expected to occur within all types of collisional environments, and within this one event a variety of mechanisms are perhaps capable of generating relatively diverse magmatic effects (see Section 1.2.2). There have been many numerical studies to investigate the dynamics of breakoff, which provides a means of investigating the process of slab breakoff through time, and observing how this progresses 100's kilometres deep within the Earth. Although the depth, timing, and location of breakoff within the slab may vary, breakoff itself has been found to be a consistent phenomenon across a range of collisional conditions (see Section 3.1 and 4.1 for further details). However, the suggested link between slab breakoff and magmatism has not been systematically investigated through the use of numerical models.

The objective of this thesis is to investigate more thoroughly the possible link between slab breakoff and post-collisional magmatism through numerical modelling. Specifically, there are three main aims of this work:

***1) To investigate whether the process of slab breakoff is capable of generating any significant post-collisional melting.***

Numerical models will be designed which in addition to running spontaneous collisional experiments, also determine the melting of different compositional materials through time.

***2) If breakoff is found to induce melting, to assess the specific collisional conditions which can produce melting.***

The range of breakoff dynamics will be investigated through varying the geodynamical conditions of continental collision, and these results will be used to examine whether the melting processes are a widespread feature, or limited to certain collisional and breakoff dynamics.

***3) To investigate the processes through which slab breakoff induces melting.***

A number of different mechanisms have been previously proposed to account for the melting of different source materials, which would likely produce a variety of different melting styles in terms of timing, amount, and location. The specific processes through which breakoff generates melt within these models will be investigated, and compared with these suggested mechanisms and observations from collision zones.

### 1.4.2 Structure of this thesis

This thesis aims to assess to what extent slab breakoff may be a viable mechanism for inducing post-collisional magmatism. Below is a summary of the included chapters:

*Chapter 2* - outlines the governing equations and techniques used within the numerical studies, along with a description of the initial model setup. The development of the hydration and melting implementation is described, as this will be shown to be crucial in modelling the generation of post-collisional melts.

*Chapter 3* - includes a systematic parametric study, with the aim to explore thoroughly a wide range of parameters which could have a significant control on the breakoff dynamics, as these are likely to significantly affect the generation of breakoff-induced melting. The depth of breakoff is specifically explored, as shallow breakoff has been suggested to be vital in generating melting, but the timing of breakoff and any induced flow patterns are also studied, as these may also have a control on the melting processes. It is considered whether both deep and/or shallow breakoff could induce magmatism of the lithospheric and/or asthenospheric mantle through the use of a parameterised solidus, specifically focussing on the possibility of mantle hydration as a means of reducing the solidus during breakoff.

*Chapter 4* - analyses the viability of slab breakoff to generate post-collisional melts. The geodynamical conditions that were found to promote favourable conditions for melting are investigated through a multi-dimensional parametric study, and a thermodynamic database applied to the results to accurately determine the state of hydration across the site of collision, by calculating the timing and location of any (de)hydration reactions occurring. This database also determines where melt is present as a stable phase in a number of different materials, including the asthenospheric mantle, depleted lithospheric mantle and crustal lithologies. For each material the conditions that are required for breakoff to induce any melting are assessed, along with the processes by which this melting occurs.

*Chapter 5* - summarises the results from these studies and suggests further advancements within the hydration and melting implementation which would improve the accuracy of the results. Recommendations for future work are given, specifically focussing on other dynamical processes which are found to be either dominant in these results, or which these results indicate may have a significant effect on post-collisional melting.

# Chapter 2

# Methods

## 2.1 Governing equations

Over long time scales the mantle can be considered to flow as a fluid. Hence, the equations for fluid dynamics can be implemented when considering the dynamics of the Earth. The governing equations to describe this flow are the conservation of mass, momentum and energy. The conservation of mass, which for a fixed volume defines the rate of change of mass, based upon the rate of fluid flow out of the volume (Ismail-Zadeh and Tackley, 2010), can be described as:

$$\frac{\partial \rho}{\partial t} + \nabla \cdot (\overrightarrow{\rho u}) = 0 \tag{2.1}$$

where ρ is the density, t the time, and u the velocity (Table 2.2, at the end of Section 2.3, shows all the parameters described in Chapter 2). It is assumed that the mantle is incompressible; meaning that, for this equation, the density of any material point can be assumed to remain constant, and therefore Eq. (2.1) can be simplified to:

$$\nabla \cdot \vec{u} = 0 \tag{2.2}$$

This assumption is valid where the pressure and temperature changes are small and no phase transformations involving changes in density occur (Gerya, 2010). The Navier-Stokes equation describes the conservation of momentum for a fluid within a gravitational field. When modelling the flow of the Earth, this can be simplified to give the Stokes equation by ignoring those terms which describe the effect of inertial forces, as these are negligible

Where appropriate, every effort has been made to acknowledge the work of others for their contributions to the design and development of the numerical code, and to highlight the sections that are unique to this study. B. Maunder should be acknowledged for his training and support throughout the development of the numerical model.

compared to viscous resistance and gravitational forces when considering high viscosity materials such as the mantle:

$$\nabla \cdot \left(\eta \dot{\varepsilon}_{ij}\right) - \nabla \mathrm{p} + \rho g = 0 \tag{2.3}$$

where η is the dynamic viscosity, $\dot{\varepsilon}$ the strain rate, p the deviatoric pressure and $g$ the gravitational acceleration. The conservation of energy can be described by:

$$\frac{\partial T}{\partial t} + \vec{u} \cdot \nabla \mathrm{T} = \kappa \nabla^2 \mathrm{T} + H \tag{2.4}$$

where T is the temperature, κ the thermal diffusivity, and H the rate of internal heat production.

The flow within the mantle is generated by differences in buoyancy, which can result from variations in temperature, pressure, and chemical and mineralogical composition. Buoyancy differences resulting from phase transitions are not considered, but varying values for material density dependent upon the material composition are defined (see Section 2.4.1.3). Hence, the buoyancy force is described by:

$$\Delta\rho(T, i) = \Delta\rho_i - \alpha\rho_o(T - T_0) \tag{2.5}$$

The composition C is considered to be conserved and non-diffusive, and is advected with the mantle flow:

$$\frac{\partial C}{\partial t} + \vec{u} \cdot \nabla \mathrm{C} = 0 \tag{2.6}$$

The Boussinesq approximation is applied, which ignores the effects of viscous and adiabatic heating and differences in density, except when calculating the buoyancy within Eq. (2.13), and assumes incompressibility of the fluid. Although adiabatic heating is neglected when considering the mantle flow, it is important when determining the melting of material, particularly deeper within the mantle. To compensate for this, a temperature correction to the material is added when determining the melt fraction.

The governing equations are non-dimensionalised using the following definitions:

$$x = x'h \tag{2.7}$$

$$t = t'h^2/\kappa \tag{2.8}$$

$$\eta = \eta'\eta_0 \tag{2.9}$$

$$T = T'\Delta T \tag{2.10}$$

$$p = p'(k/h^2)\eta_0 \tag{2.11}$$

This gives the final non-dimensional equations, where x, t, η, T and p represent the non-dimensional values (x', t', η', T' and p' in Eqs. (2.7) - (2.11)), with the primes removed for clarity:

$$\nabla \cdot \vec{u} = 0 \tag{2.12}$$

$$-\nabla p + \nabla \cdot \left(\eta(\nabla\vec{u} + \nabla\vec{u}^T)\right) + (RaT - \sum_{i=1}^{N} Rb_i C_i)e_z = 0 \tag{2.13}$$

$$\frac{\partial T}{\partial t} + \vec{u} \cdot \nabla T = \nabla^2 T + H \tag{2.14}$$

where x is the distance, h is the depth of the model domain, $\eta_0$ is the reference viscosity, $\Delta T$ is the reference temperature difference (defined as the difference between $T_m$, the temperature at the bottom of the model domain, which is equivalent to the mantle potential temperature in this case, and $T_0$, the temperature at the top of the model domain), C is the compositional function, i a given composition, and $e_z$ vertical unit vector. The Rayleigh numbers (Ra and $Rb_i$), which control the vigour of the convection based on the thermal and compositional conditions, are defined respectively as:

$$Ra = \frac{\alpha\rho_0 g\Delta T h^3}{\kappa\eta_0} \tag{2.15}$$

$$Rb_i = \frac{\Delta\rho_i g h^3}{\kappa\eta_0} \tag{2.16}$$

where α is the thermal expansion coefficient, $\rho_0$ the reference density, and $\Delta\rho_i$ the intrinsic density of a composition relative to the mantle.

## 2.2 Numerical methods

The Cartesian version of the code Citcom is used (Moresi et al., 1996; Moresi and Gurnis, 1996; Moresi and Solomatov, 1995), to solve the equations for the conservation of mass, momentum and energy using an Eulerian finite element technique. This employs a fixed grid, divided into a number of elements, for which velocity and temperature are defined at the nodes. The model domain consists of 512 x 128 elements in the x and z directions respectively. The element size is defined so as to achieve the highest resolution of 3.3 x 3.3 $km^2$ at the top of the model, specifically around the location of the weak zone, where the high viscosity contrasts require a smaller element size in order to solve the governing equations accurately and avoid numerical error. The governing equations are discretised in order to be used with the finite element technique, and Eqs. (2.12) and (2.13) transformed into the following matrix form:

$$B^T u = 0 \tag{2.17}$$

$$Au + Bp = f \tag{2.18}$$

where B is the discrete gradient operator, u is a vector of unknown velocities, A is the stiffness matrix, p is a vector of unknown pressures, and f is a vector of the body and boundary forces (Moresi and Gurnis, 1996). The equations are combined to eliminate u, giving:

$$B^T A^{-1} B p = B^T A^{-1} f \tag{2.19}$$

which is then solved using an Uzawa algorithm (Moresi and Gurnis, 1996). An iterative conjugate gradient scheme is used to solve for the pressure. The conservation of energy is solved through a standard Petrov-Galerkin scheme (Moresi and Solomatov, 1995). Although Citcom is designed to be used with the multigrid approach, this is not the method taken in these calculations, and instead a conjugate gradient iterative solution method is used. This approach leads to an increase in calculation time, but helps increase the stability when high viscosity gradients are present.

A particle tracer method is also used, both to track the composition and in the migration of free water through the model domain (see Section 2.5.1.2). The composition affects a number of different properties, including the rheology, buoyancy, mineral-bound water content, and composition used when calculating stable mineral assemblages. A number of composition functions are used to describe the different materials used (upper continental crust, lower continental crust, sediments, oceanic crust and lithospheric mantle), and for each particle are defined a value of 1 or 0. This method was used rather than a single composition function with different values for each material, in order to prevent inaccuracies when particle values are interpolated to the element grid. Particles are initially distributed at random locations to give a homogenous density distribution and are subsequently advected with the velocity field. Particles are advected every timestep according to velocity values interpolated from the calculated nodal values, using a second order Runge-Kutta scheme. The particles located in elements along boundaries where material is allowed to flow in and out of the model domain, are replaced at each timestep with new randomly distributed particles. This ensures no gaps in the tracer distribution are formed through flow away from the boundaries. These particles inherit the initial values of the particles along these boundaries with flow in or out of the model.

## 2.3 Rheology

Rheology describes how a material flows or deforms when exposed to stress, which can occur through a number of different mechanisms (Bürgmann and Dresen, 2008). Within the Earth's mantle, diffusion and dislocation creep are predominant. Diffusion creep results from the diffusive transport of atoms between crystal grains and is active when rock is subjected to low amounts of stress (Karato and Wu, 1993). At higher stress or where crystal grains are large, dislocation creep occurs through the migration of imperfections or 'dislocations' within the crystal. This results in a preferred orientation of minerals, which is observed both from seismic anisotropy, as well as rocks that have been extracted from the upper mantle, providing evidence for the active nature of this mechanism within the Earth (Karato and Wu, 1993). However, this is unlikely to be dominant throughout the whole mantle. Below 200-300 km, a reduction in anisotropy suggests a change in the active deformation mechanism from dislocation creep. This suggests that dislocation creep is probably confined to a layer within the mantle below the cooler lithospheric mantle, but not extending deep into the upper mantle. The composite viscosity of these mechanisms can be described by:

$$\frac{1}{\eta_{visc}} = \frac{1}{\eta_{diff}} + \frac{1}{\eta_{disl}} \tag{2.20}$$

where $\eta_{diff}$, the viscosity resulting from diffusion creep, and $\eta_{disl}$, that resulting from dislocation creep are both defined as:

$$\eta = A^{\frac{1}{n}} \dot{\varepsilon}^{\frac{1-n}{n}} exp\left(\frac{E^* + pV}{nRT}\right) \tag{2.21}$$

where A is the pre-exponential exponent, n the power-law exponent, E* the activation energy, V the activation volume, and R the gas constant. The values assigned to A, n, and E* are different for diffusion and dislocation creep (see Table 2.1). In addition to these mechanisms, rocks can also deform through brittle failure at low temperatures (Byerlee, 1978):

$$\eta_y = \frac{\min(\sigma_0 + \mu p, \sigma_{max})}{\dot{\varepsilon}} \tag{2.22}$$

where $\eta_y$ is the viscosity resulting from brittle yielding, $\sigma_0$ the cohesion, $\mu$ the friction coefficient, and $\sigma_{max}$ the maximum yield stress. The effective viscosity ($\eta_{eff}$) is defined as the minimum of $\eta_{visc}$, $\eta_y$, and $\eta_{max}$, where $\eta_{max}$ is an upper limit placed on the viscosity which helps with numerical stability:

$$\eta_{eff} = \min(\eta_{visc}, \eta_y, \eta_{max}) \tag{2.23}$$

### 2.3.1 Rheological flow laws

Flow laws have been determined experimentally to describe how different materials deform under stress. A certain amount of uncertainty is associated with these, owing to the difficulty in replicating the high pressures found deeper within the Earth, and the extrapolation from high stresses over short timescales produced in the laboratory to low stresses over long timescales which are active in the Earth (Karato and Wu, 1993). This deformation is primarily dependent upon the pressure and temperature, but is also affected by a number of other factors, such as water content and grain size. The pressure dependence is described by the activation volume of the material, and due to the uncertainty for high pressures, estimates of activation volume can vary significantly (Section 2.3.2). Hirth and Kohlstedt (2003) show

the significant effect that water can have on mantle rheology, particularly at sites of oceanic subduction where there is a constant flux of water through the mantle wedge due to continual subduction of hydrated basaltic rock. This could result in a decrease in viscosity by a factor of 500 ± 300 (Hirth and Kohlstedt, 1996). Even studies of asthenospheric mantle away from subduction zones show the mantle to hold small amounts of water, leading Karato and Wu (1993) to suggest that a flow law between that for a dry and hydrated material probably best describes the asthenospheric mantle.

To obtain flow laws which describe a range in mantle rheology between dry and hydrated material, Maunder et al. (2016) took a number of commonly used mantle flow laws (Hirth and Kohlstedt, 2003; Karato and Wu, 1993; Ranalli, 1995) and from these calculated the viscosity for a range of temperatures and strain rates. Using the method developed by Maunder et al., (2016), the mean and the ±1 SD viscosities are determined from these values and a best fit flow law calculated (Table 2.1). In addition to this, ±0.5 SD flow laws are also determined, to investigate more thoroughly the effect of mantle rheology on breakoff dynamics (Chapter 3). The -0.5 and -1 SD flow laws both lie within the range of the hydrated flow laws, whilst the mean and +0.5 SD are considered as intermediate rheologies between hydrated and dry, and the +1 SD as representing a dry mantle (Fig. 2.1).

| Mantle flow law | $A_{diff}$ ($Pa^{-n}s^{-1}$) | $E^*_{diff}$ ($Jmol^{-1}$) | $n_{diff}$ | $A_{disl}$ ($Pa^{-n}s^{-1}$) | $E^*_{disl}$ ($Jmol^{-1}$) | $n_{disl}$ |
|---|---|---|---|---|---|---|
| +1 SD | $3.97 \times 10^{9}$ | $3.66 \times 10^{5}$ | 1 | $5.92 \times 10^{15}$ | $5.42 \times 10^{5}$ | 3.48 |
| +0.5 SD | $1.23 \times 10^{10}$ | $3.43 \times 10^{5}$ | 1 | $9.31 \times 10^{15}$ | $5.18 \times 10^{5}$ | 3.48 |
| Mean | $3.79 \times 10^{10}$ | $3.20 \times 10^{5}$ | 1 | $1.47 \times 10^{16}$ | $4.96 \times 10^{5}$ | 3.48 |
| -0.5 SD | $1.17 \times 10^{11}$ | $2.96 \times 10^{5}$ | 1 | $2.30 \times 10^{16}$ | $4.73 \times 10^{5}$ | 3.47 |
| -1 SD | $3.61 \times 10^{11}$ | $2.73 \times 10^{5}$ | 1 | $3.62 \times 10^{16}$ | $4.50 \times 10^{5}$ | 3.47 |

**Table 2.1: Calculated mantle flow law values for dislocation and diffusion creep.**

### 2.3.2 Activation volume

An increase in depth acts to raise the viscosity of the mantle, through an increase in pressure, but also to lower it, as a result of adiabatic heating which causes an increase in temperature (Turcotte and Schubert, 2002) (Fig. 2.2A - dashed, grey lines). These two effects counteract

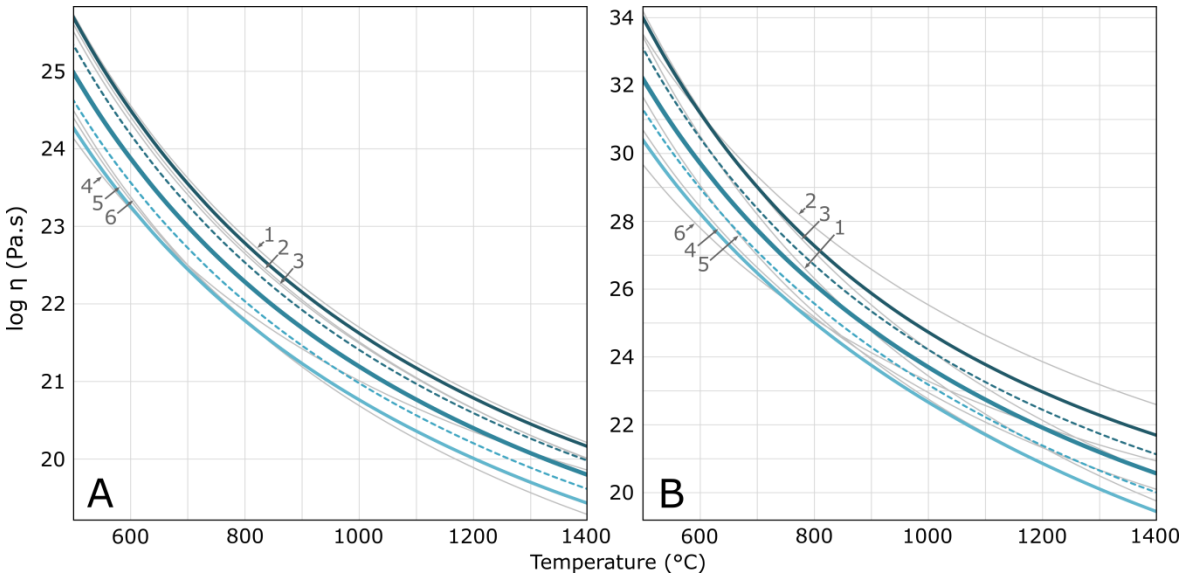


**Figure 2.1: Viscosity as a function of temperature for a range of flow laws.** Showing experimental flow laws (grey lines) and the calculated -1 SD to +1SD flow laws (blue lines) for dislocation creep (A, plotted for a strain rate of 1 x 10-15 s-1) and diffusion creep (B). Experimental flow laws: Dry (lines 1-3) and hydrated (lines 4-6): 1 & 4 - Ranalli (1995), 2 & 6 - Karato and Wu (1993), 3 & 5 - Hirth and Kohlstedt (2003). Calculated flow laws: +1 SD (dark blue), +0.5 SD (dashed dark blue), mean (blue), -0.5 SD (dashed light blue), -1SD (light blue). See Maunder et al. (2016) for further details on the method used to calculate the lines of best fit.

each other; however, the effect of pressure is greater than that of temperature, resulting in an increase in viscosity of around an order of magnitude within the upper mantle (Fig. 2.2A - dark blue line). The lack of adiabatic heating within the models is compensated for by using a reduced value of activation volume, which controls the viscosity increase as a function of pressure. If activation volume were to be neglected or experimentally derived mantle values used in the calculations, this would result in variations in the viscosity, on an order of magnitude scale, from values expected according to typical mantle flow laws.

The activation volume with depth required to produce a typical mantle viscosity profile is determined, based on experimental flow laws, when adiabatic heating is neglected.

Viscosity can be described by:

$$\eta = \beta exp\left(\frac{E^* + pV}{nR(T + \Delta T)}\right) \tag{2.24}$$

where β is defined by:

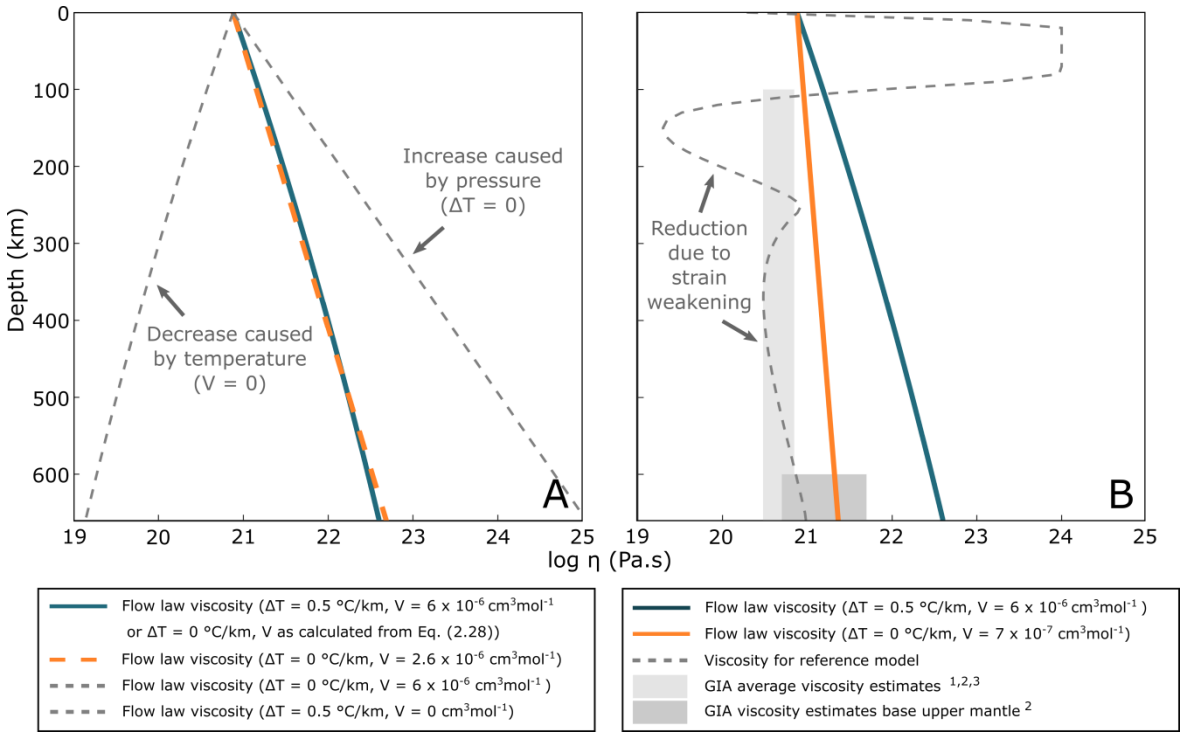


**Figure 2.2: A comparison of viscosity profiles when considering activation volume.** A - The viscosity profiles as a result of diffusion creep (according to the mean mantle flow law), showing the effect of pressure and temperature increase with depth (dashed, grey lines), along with the calculated profiles where an adiabatic temperature increase is negated and the activation volume is altered accordingly (blue & orange lines). B - A comparison of the viscosity profiles based upon the mantle flow law (blue & orange lines), GIA estimates for viscosity (grey rectangles), and the resulting viscosity profile from a model result from within a typical section of oceanic lithosphere after steady-state subduction has been established (dashed, grey line). 1 - Kaufmann and Lambeck (2002), 2-Mitrovica and Forte (2004), 3 - Lambeck (1998).

$$\beta = A^{\frac{1}{n}}\dot{\varepsilon}^{\frac{1-n}{n}} \tag{2.25}$$

and ΔT taken to be the difference between the temperature increase that would be caused by an adiabatic temperature increase. (In this case, T in Eq. (2.24) includes no adiabatic component, as the Boussinesq approximations are used). If there is no adiabatic temperature increase (i.e. ΔT = 0), the viscosity is equal to:

$$\eta = \beta exp\left(\frac{E^* + p(V + \Delta V)}{nRT}\right) \tag{2.26}$$

where ΔV is the change in activation volume from the standard value to give the same viscosity as calculated from Eq. (2.24). By equating Eqs. (2.24) and (2.26):

$$\beta exp\left(\frac{E^* + pV}{nR(T + \Delta T)}\right) = \beta exp\left(\frac{E^* + p(V + \Delta V)}{nRT}\right) \quad (2.27)$$

$$\frac{E^* + pV}{T + \Delta T} = \frac{E^* + p(V + \Delta V)}{T} \quad (2.28)$$

These can be rearranged to give:

$$\Delta V = \frac{T}{p}\left(\frac{E^* + pV}{T + \Delta T}\right) - \frac{E^*}{p} - V \quad (2.29)$$

ΔV is calculated for a range of pressures, from the surface down to the base of the upper mantle assuming a constant mantle density of 3330 $kgm^{-3}$, and using a mantle potential temperature for T of 1350°C, a value for ΔT of 330°C (assuming an adiabat of 0.5 °C/km), an activation energy, E*, of 3.20 x $10^5$ $Jmol^{-1}$, and a typical value for the activation volume of diffusion creep for V of 6 x $10^{-6}$ $cm^3mol^{-1}$ (Karato and Wu, 1993). This yields an adjusted value for the activation volume (V + ΔV) of between 2.5 and 2.9 x $10^{-6}$ $cm^3mol^{-1}$ (Fig. 2.2A - blue line). From this range a value for activation volume of 2.6 x $10^{-6}$ $cm^3mol^{-1}$ is chosen which best represents the viscosity profile expected from the flow laws (Fig. 2.2A - orange line). The same analysis is also carried out for dislocation creep, using an activation energy of 4.96 x $10^5$ $Jmol^{-1}$ and a typical value for the activation volume of dislocation creep for V of 20 x $10^{-6}$ $cm^3mol^{-1}$ (Karato and Wu, 1993), to give a best fit value of 13.4 x $10^{-6}$ $cm^3mol^{-1}$.

#### 2.3.2.1 Confrontation of experimental values with geophysical observations

Observations of changes in gravity and sea level resulting from the glacial isostatic adjustment (GIA) process can also be used to infer an estimate of the mantle viscosity. From this data, the upper mantle in certain locations has been suggested to have an average viscosity of between 3-7 x $10^{20}$ Pa.s (Kaufmann and Lambeck, 2002; Lambeck, 1998; Mitrovica and Forte, 2004; Paulson et al., 2007) (Fig. 2.2B - light grey rectangle). The results of Mitrovica and Forte (2004) suggest the viscosity at the base of the upper mantle could be between 5 x $10^{20}$ and 5 x $10^{21}$ Pa.s (Fig. 2.2B - dark grey rectangle). In comparison to this, typical mantle flows for diffusion creep seem to yield values that are too high towards the base of the upper mantle (Fig. 2.2B - blue line). Based upon this information, further reduced values of activation volume are implemented to bring the mantle viscosity profile in line with these studies (Fig. 2.2B - orange line). A value of 0.7 x $10^{-6}$ $cm^3mol^{-1}$ is used for diffusion creep, giving a value of viscosity of 2.4 x $10^{21}$ Pa.s for the reference mantle rheology at the base of the upper mantle, and a value of 8.0 x $10^{-6}$ $cm^3mol^{-1}$ for

dislocation creep, consistent with that used in other numerical studies of subduction (e.g Duretz et al., 2011). The viscosity profile calculated using this adjusted value for diffusion creep yields slightly higher values than those from GIA estimates (Fig. 2.2B - blue line). However, a typical viscosity profile generated within the model during subduction provides a good fit with these estimates, due to the effect of strain rate dependent viscosity within the mantle (Fig. 2.2B - dashed, grey line).

#### 2.3.2.2 Real-world implications of variations in activation volume

Changes in activation volume may affect the nature of subduction of both the oceanic and continental plates, and could also have significant consequences for the dynamics of any breakoff event and the generation of breakoff-related magmatism. A higher activation volume would result in a more viscous mantle towards the base of the upper mantle, which could lead to slower subduction and less vigorous plate tectonics. For breakoff specifically, this may result in a more diffuse style of breakoff, whereby the plate is supported by the strong, lower part of the upper mantle, and becomes stagnated and heats up gradually. A high value of activation volume for dislocation creep would also reduce the effectiveness of this mechanism to aid breakoff deeper within the upper mantle. A sudden, sharp breakoff event would not be expected in this case, but slow viscous necking may lead to an eventual breakoff event within the slab. This may prevent a rapid influx of mantle through the slab window, and may reduce the amount of heating within the overriding plate and of the slab itself, and prevent any adiabatic decompression melting.

Conversely a lower activation may result in faster, more vigorous subduction, and a shallower, more rapid breakoff event, as there would be less support for the slab due to the weaker nature of the lower part of the upper mantle. Necking and breakoff may also be more dominant around the site of breakoff, leading to faster breakoff. This may increase the amount of breakoff-induced magmatism that could be generated. Therefore, studies that do ignore the effect of activation volume on viscosity within the mantle may over-estimate the potential that slab breakoff has to induce post-collisional magmatism. The values chosen here are in line with other numerical studies, and provide upper mantle viscosities and oceanic subduction dynamics that are representative of the real-world.

| Symbol | Parameter | Units | Default value |
|---|---|---|---|
| A | pre-exponential exponent | $Pa^{-n}s^{-1}$ | - |
| C | compositional function | - | - |
| $C_p$ | specific heat capacity | $Jkg^{-1}K^{-1}$ | 1171 |
| E* | activation energy | $Jmol^{-1}$ | - |
| $e_z$ | vertical unit vector | - | - |
| g | gravitational acceleration | $ms^{-2}$ | 9.8 |
| H | rate of internal heat production | $Wm^{-3}$ | - |
| $H_c$ | average crustal radiogenic heat production | $Wm^{-3}$ | 0/0.7 |
| h | depth of model domain | km | 660 |
| i | a given composition | - | - |
| k | thermal conductivity | $Wm^{-1}K^{-1}$ | - |
| n | power-law exponent | - | - |
| p | pressure | Pa | - |
| R | gas constant | $J\ K^{-1}\ mol^{-1}$ | 8.3 |
| Ra | thermal Rayleigh number | - | $2.8x10^6$ |
| $Rb_i$ | compositional Rayleigh number | - | - |
| T | temperature | °C | - |
| $T_m$ | mantle potential temperature | °C | 1350 |
| $T_0$ | surface temperature | °C | 0 |
| $T_c$ | temperature within the continental crust | K | - |
| $T_{lm}$ | temperature within the lithospheric mantle | K | - |
| $\Delta T$ | reference temperature difference | °C | 1350 |
| t | time | s | - |
| u | velocity | $ms^{-1}$ | - |
| V | activation volume | $cm^3mol^{-1}$ | 0.7(df.)/8.0(dsl.) |

| | | | |
|---|---|---|---|
| $x$ | distance | m | - |
| $z$ | depth | m | - |
| $z_c$ | depth to the base of the continental crust | m | - |
| $z_l$ | depth to the base of the lithosphere | m | - |
| $\alpha$ | thermal expansion coefficient | $K^{-1}$ | $3.5x10^{-5}$ |
| $\dot{\varepsilon}$ | strain rate | $s^{-1}$ | - |
| $\eta$ | dynamic viscosity | Pa s | - |
| $\eta_0$ | reference viscosity | Pa s | $2x10^{20}$ |
| $\eta_{visc}$ | composite viscosity | Pa s | - |
| $\eta_{disl}$ | viscosity from dislocation creep | Pa s | - |
| $\eta_{diff}$ | viscosity from diffusion creep | Pa s | - |
| $\eta_y$ | viscosity from brittle yielding | Pa s | - |
| $\eta_{max}$ | upper viscosity limit | Pa s | $1x10^{24}$ |
| $\eta_{eff}$ | effective viscosity | Pa s | - |
| $\kappa$ | thermal diffusivity | $m^2\ s^{-1}$ | $8x10^{-7}$ |
| $\mu$ | friction coefficient | - | 0.2 |
| $\rho$ | density | $kgm^{-3}$ | - |
| $\rho_0$ | reference density | $kgm^{-3}$ | 3330 |
| $\Delta\rho_i$ | relative density to mantle | $kgm^{-3}$ | - |
| $\sigma_y$ | yield stress | Pa | - |
| $\sigma_0$ | cohesion | MPa | 40 |
| $\sigma_{max}$ | maximum yield stress | MPa | 400 |

**Table 2.2: Parameter symbols and units, and the equations in Chapter 2 that refer to these.**

## 2.4 Model setup

The model simulates the subduction of an oceanic plate before the introduction of a continental plate into the subduction zone (Fig. 2.3). This setup allows for a natural

progression from oceanic to continental subduction, in which the development of the subduction angle, plate speed and subduction depth of the continental plate during this transition are not controlled by external forcing. The continental plate is initially positioned at the far left edge of the model (extending to x=100 km), and is introduced into the subduction zone after the subduction of a finite length of oceanic lithosphere. 'Collision' is defined as the moment in time when the continental lithosphere first reaches the edge of the subduction trench and begins its descent below the overriding plate. 'Breakoff' is defined as the moment in time when the 1000 °C isotherm within the subducting slab ceases to be continuous. The timing and location of the separation of the 1000 °C isotherm is generally concurrent with the time and area of the highest strain rate around the location of breakoff (for example see Fig. 3.2 and 4.4). The weakest part of the slab at this time is used to define the depth of breakoff, which in almost all cases is at the same location as the separation of the 1000 °C isotherm. The model domain represents a total width of 1980 km, and a depth of 660 km. Below, the variations in temperature, rheology and density across the model are outlined, which are implemented initially for the reference model.

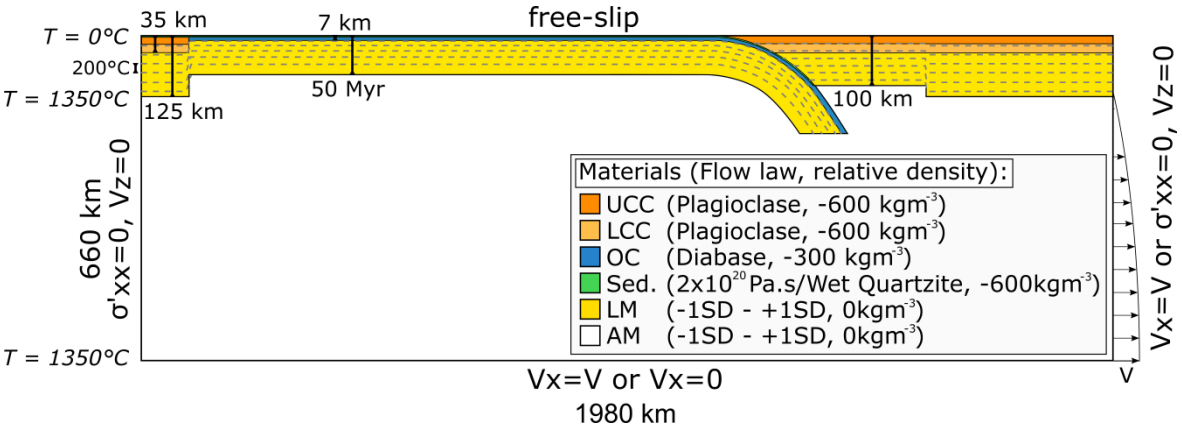


**Figure 2.3: Initial setup for the reference model.** Showing the: compositional differences across the model domain, including the rheology, density and geometry; the temperature profile; and the thermal and dynamical boundary conditions.

## 2.4.1 Initial conditions

### 2.4.1.1 Temperature

The asthenospheric mantle initially has a constant temperature of 1350°C. The temperature of the lithosphere is determined by the thickness, increasing from 0°C at the surface to 1350 °C at the base of the lithosphere, linearly for the continental lithosphere (except where

crustal radiogenic heating is implemented, as described later in Section 2.4.1.1) and according to the half space cooling model for a given age for the oceanic lithosphere. The oceanic plate has an initial age of 50 Myr. Although 50 Myr is young for both oceanic lithosphere located furthest from a mid-ocean ridge and for a typical subduction zone, the oceanic plate continues to age and grow in lithospheric thickness for some period of time, ranging from 10-50 Myr, before continental collision begins. Geotherms of real oceanic plates begin to deviate significantly from the half space cooling model at around 70-80 Myrs and do not continue to decrease in temperature significantly beyond this time (Stein and Stein, 1992; Turcotte and Schubert, 2002). As the process of collision and breakoff is the focus of this work, the state of the oceanic plate adjacent to the continental lithosphere is of most concern, as this section will have the greatest control on the breakoff dynamics. Hence, an initial age of 50 Myr is considered reasonable for the purpose of modelling collision and breakoff. The oceanic plate initially extends to a depth of 250 km below the overriding continental plate, which provides a sufficient force to initiate oceanic subduction.

The subducting continental lithosphere has a thickness of 125 km, and although this is significantly thinner than old cratonic lithosphere (Priestley and McKenzie, 2006), it is more representative of lithosphere found nearer a passive margin and that most likely to be involved in subduction. An initially abrupt passive margin is used in the model setup for simplicity and to avoid considering the complexity of these structures. The implementation of this feature would be unlikely to make a significant difference to the model results. In this setup, heat diffusion over time before the subducting plate reaches the subduction zone results in a more gradual lithospheric thermal gradient between the oceanic and continental lithospheres. Initial tests were also conducted to investigate the effect that a passive margin may have on the collision and breakoff dynamics, whereby a linear thermal gradient between the oceanic and continental lithospheres and an increasing thickness of continental crust was implemented within a passive margin. This was found to have no observable effect on the breakoff depth, and only a small effect on the timing of breakoff.

A slightly thinner overriding lithosphere is implemented, of thickness 100 km. This is to partially replicate the dynamic and thermal effect that fluids and melts would have in this area, which would raise the temperature of the lithosphere above the mantle wedge region (Currie and Hyndman, 2006), without the need to implement hydration and melt weakening into the rheology nor the migration of melts. During subduction, the thinner overriding plate is maintained by the mantle corner flow induced by the downgoing slab, whilst upon subduction of the continental lithosphere, the area around the subduction trench and overriding lithosphere subsequently cool as this flow ceases. As the corner flow also acts to

reduce the thickness of the overriding plate in real subduction zones, this approach still does not replicate the full amount of weakening that is present from fluids and melts, but does allow us to study the extent to which the pre-collisional thickness of the overriding plate determines the collision and breakoff dynamics.

Within the studies presented in Chapters 3 and 4 the effect of radiogenic heating within the continental crust on the breakoff dynamics and melting is also considered. Although the amount of radiogenic heat producing elements in the crust is thought to decrease with depth (Turcotte and Schubert, 2002), for simplicity a uniform heat source is implemented throughout the whole continental crust of 0.7 $\mu Wm^{-3}$ (Fowler, 2005), and an initially altered continental lithospheric geotherm to account for long-term radiogenic heat production within the crust. The initial altered geotherm within the continental crust ($T_c$) and continental lithospheric mantle ($T_{lm}$) can be defined by:

$$T_c = T_0 + \left(\frac{T_m - T_0}{z_l} + \frac{H_c z_c}{k} - \frac{H_c {z_c}^2}{2kz_l}\right) z - \frac{H_c z^2}{2k} \tag{2.30}$$

$$T_{lm} = T_m + \left(\frac{T_m - T_0}{z_l} - \frac{H_c {z_c}^2}{2kz_l}\right)(z - z_l) \tag{2.31}$$

where $T_0$ is the surface temperature, $T_m$ the temperature at the base of the lithosphere, k the thermal conductivity$\left(k = \kappa \rho C_p\right)$, z the depth, $z_l$ the depth to the base of the lithosphere, and $z_c$ the depth to the base of the crust. $T_{lm}$ is defined so as to increase linearly from the base of the crust to $T_m$ at the base of the mantle lithosphere. Appendix A.1 describes the derivation of Eqs. (2.30) and (2.31).

The numerical solution for the reference model including radiogenic heating implemented over time is compared with the expected temperature profile from Eqs. (2.30) and (2.31) (Fig. 2.4). After 13 Myr of oceanic subduction, the temperature profile clearly represents that of the ideal radiogenic profile up to a depth of ~ 80 km, below which point the base of the lithosphere has become cooler due to heat diffusion.

#### 2.4.1.2 Rheology

Flow laws for the mantle are implemented as described in Section 2.3.1. For other materials within this study, those from Ranalli (1995) are used: a diabase flow law for the oceanic crust; a wet quartzite flow law for the sediments; and a plagioclase flow law for the whole

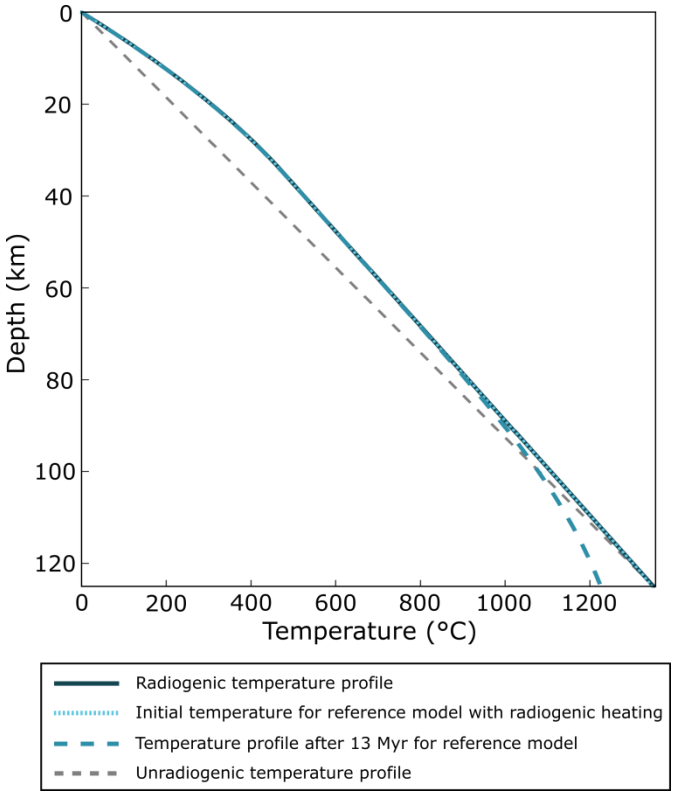


**Figure 2.4: Temperature profiles for radiogenic heating within the continental crust.** Shown are the ideal temperature profile (dark blue line), the model results at 0 Myr and 13 Myr (dotted, light blue and dashed blue lines), and also the profile with no radiogenic heating (dashed, grey line).

continental crust (Table 2.3) The effect of using a rheologically layered crust is explored in Chapter 3, which implements a combination of wet quartzite, dry quartzite, and plagioclase flow laws to the upper and lower continental crusts. In addition to the flow laws, a maximum viscosity of $1x10^{24}$ Pa s is also implemented.

To decouple the subducting oceanic lithosphere from the overriding plate, a thin layer of weaker material, of thickness 1.3 km, is positioned at the top of the subducting plate. This is assigned a constant viscosity of $2x10^{20}$ Pa s down to the base of the overriding lithosphere, after which the viscosity of this material is determined based upon the rheological flow law of sediment. This layer is required to be as thin as possible so as to prevent any artificial extension between the plates, whilst being sufficiently thick so as to decouple the two plates. In order to reduce the sharp viscosity contrast between the weak zone and surrounding stronger lithosphere, the viscosity is logarithmically interpolated from the weak zone viscosity to the background viscosity over a distance of 13 km, on either side of the weak zone (see Maunder et al., 2016). The viscosity of this layer determines the speed of subduction, and is chosen so as to represent typical convergence velocities (~2-10 cm/yr (Lallemand et al., 2005)), considering both the rollback of the overriding plate and the subduction of the oceanic plate.

| Material | Flow law | $A_{disl}$ ($Pa^{-n}s^{-1}$) | $E^*_{disl}$ ($Jmol^{-1}$) | $n_{disl}$ |
|---|---|---|---|---|
| Oceanic crust | Diabase | $1.26 \times 10^{24}$ | $2.60 \times 10^{5}$ | 3.40 |
| Sediments | Wet Quartzite | $1.97 \times 10^{17}$ | $1.54 \times 10^{5}$ | 2.30 |
| Continental crust | Plagioclase | $4.80 \times 10^{22}$ | $2.38 \times 10^{5}$ | 3.20 |
| | Dry Quartzite | $3.75 \times 10^{19}$ | $1.56 \times 10^{5}$ | 2.40 |
| | Wet Quartzite | $1.97 \times 10^{17}$ | $1.54 \times 10^{5}$ | 2.30 |

**Table 2.3: Flow law values for non-mantle material.**

#### 2.4.1.3 Density

The density of material is particularly important when considering the potential for breakoff, as this will affect the depth that the continental lithosphere is able to be subducted to as well as the magnitude of the tensile stresses existing between the oceanic and continental lithospheres. A reference density, $\rho_0$, is used for the mantle of 3330 $kgm^{-3}$ at $T=T_0$. Other reference values of density are described relative to this value: $\Delta\rho$=-600 $kgm^{-3}$ for the continental crust and sediments, and $\Delta\rho$=-300 $kgm^{-3}$ for the oceanic crust (e.g. Sizova et al., 2014; van Hunen and Allen, 2011; Vogt et al., 2012). At a depth of 80 km, the transition from basalt to eclogite is implemented by assigning a value of $\Delta\rho$=+200 $kgm^{-3}$ for the oceanic crust (Hacker, 1996; Ito and Kennedy, 1971).

### 2.4.2 Boundary conditions

Fixed temperature boundary conditions are implemented on both the top and bottom boundary, maintaining the surface at a temperature of 0 °C and the base of the model at 1350 °C. Fixed temperature boundary conditions are also used on the sides boundaries, for reasons as explained in Section 2.4.2.2.

Chertova et al. (2012) show that using closed side boundary conditions can lead to the development of forced return-flows within the mantle from these boundaries. To avoid any unnatural flow, which may prove significant during the process of slab necking and breakoff, and to allow subduction and collision to develop more freely, open boundary conditions are implemented on both sidewalls of the model. These zero horizontal deviatoric stress conditions allow material to freely flow both in and out of the model domain. Using these boundaries also means a freely migrating subduction trench can be implemented without the

need for mid-ocean ridges or weak zones at the model boundaries (e.g. Holt et al., 2015; Magni et al., 2012; Nakakuki and Mura, 2013).

The top boundary is defined as free-slip, whilst the bottom boundary is assigned a no-slip boundary condition, acting as a point of reference for the entire model. The bottom boundary is also closed to vertical flow; hence it is assumed that subducted slabs stagnate at the base of the upper mantle, and do not subduct unhindered into the lower mantle. This is in accordance with seismic tomography from some subduction zones, which show slabs flattening within the vicinity of the 660 km discontinuity (Bijwaard et al., 1998; Fukao et al., 2009, 1992; Fukao and Obayashi, 2013; Li et al., 2008b; van der Hilst et al., 1991). Material is also unable to flow vertically across the top boundary, and the model does not accommodate for variations in topography that might arise from the dynamics of the tectonic plates and flow within the mantle. Previous numerical studies have shown that breakoff can result in significant uplift around the subduction zone, leading to a potential increase in topographic elevation of around 2-6 km (Buiter et al., 2002; Duretz et al., 2011). Any topographic variations could be determined either through adding a thin layer on top of the crust, which takes the viscosity of either air or water and allows for vertical movements of the tectonic plates (Gerya and Yuen, 2003), or through calculations involving the normal stresses acting on the top boundary of the model (e.g. Bottrill et al., 2012). Allowing for topographic variations within the model may enhance the amount of mantle upwelling observed and result in asthenospheric flow to shallower depths; however, upwelling that is generated in the models presented in this thesis appears to be accommodated through reworking of the weaker continental crust and extension around the collision zone. Hence, it is expected that allowing for topographic variations is unlikely to have significant consequences for the overall pattern of observed breakoff dynamics and the generation of post-collisional magmatism, particularly for breakoff at greater depths, which has little effect on the dynamics of the near-surface (in accordance with the correlation between topographic variations and breakoff depth as observed by Duretz et al. (2011)).

A small width of continental lithosphere is initially positioned towards the left hand side of the model, and subsequently more lithospheric material flows in through the right hand boundary throughout the model calculation. As the subduction trench is not fixed in location and is able to freely retreat or advance, a sufficiently wide box is required so that the slab does not leave the model domain. By initially positioning only a small section of continental lithosphere within the model, the width of the box required is able to be reduced and the model resolution increased.

#### 2.4.2.1 Initial slab roll-back force

Observations of subducted slabs today from seismic tomography show that a wide variety of subduction morphologies exist, including variations in the slab dip and the style of interaction with the 660 km mantle discontinuity (Fukao and Obayashi, 2013; Li et al., 2008b; van der Hilst et al., 1991). Despite this wide variety, it appears that slabs do not tend to overturn within the mantle so as to develop a bent-over shape (Garel et al., 2014). Due to the initially cold and strong nature of the slab in this study, it would always overturn, as it is unable to unbend sufficiently before reaching the base of the model (such as in Di Giuseppe et al., 2008). The presence of a higher viscosity lower mantle is not modelled, which may help develop a more natural subduction morphology (Garel et al., 2014). To overcome this, a velocity out of the right hand side boundary is imposed throughout the initial period of subduction. This is defined so as to increase from 0 $cmyr^{-1}$ at the base of the lithospheric mantle to a fixed velocity at the base of the model. The bottom boundary is also assigned a fixed velocity during this period. This right hand side velocity profile follows the form of a quadratic, increasing more rapidly at shallower depths and less so deeper in the mantle, as this was found to be most efficient in providing the correct pull on the plate to generate slab roll-back which subsequently continues unaided. As a range of slab densities and mantle viscosities are present across this study, the magnitude of this initial velocity profile had to be varied in order to achieve the best roll-back geometry, from 2.5 to 15 $cmyr^{-1}$ at the base of the model. When the slab reaches a depth of ~600 km (0.9x the depth of the model), the boundary condition is changed to a zero horizontal deviatoric stress condition and a non-slip condition in the z direction is imposed.

#### 2.4.2.2 Difficulties when using open boundary conditions

In order to improve the numerical accuracy in the calculation of the pressure field, the large values of the isostatic pressure are negated. This is normally done by determining the average buoyancy value for each row of finite elements and subtracting this from the buoyancy of each element in that row. This works well when using closed boundary conditions; however, when using open boundary conditions, this may result in unnatural flow patterns at the boundaries. In the case of an open boundary, a zero pressure is imposed, instead of a zero velocity gradient. By subtracting the row average buoyancy, the pressure of the column adjacent to the boundary may not equal the zero pressure along the boundary, resulting in a pressure gradient and flow into or out of the model. Hence, instead of the row averaged buoyancy value, the buoyancy value of the column adjacent to the boundary is

subtracted from every element in each row, ensuring the pressure on the boundary and within the adjacent element are both zero. When two open boundaries are implemented, the same problem again arises, as the pressures on the boundaries may not be equal. To overcome this, the same pressure profile is imposed on both boundaries, by defining the same lithospheric and crustal properties within both the subducting plate at the left hand boundary and the overriding plate at the right hand boundary. In order to maintain this throughout the model calculation, fixed temperature boundary conditions are also implemented. This ensures the pressure is not altered by small changes in the temperature profiles of the two plates, which could be caused by differences in the magnitude of the underlying mantle flow. The feature of interest (i.e. the location of subduction, collision and breakoff) is also positioned far away from the boundary conditions, so as not to have any artificial effect on the dynamics.

## 2.5 Melting implementation

The generation of melt is a complex process, dependent upon a number of factors that can change through time, including the temperature and pressure of the material. The presence of water can also significantly reduce the temperature required for melting at a given pressure. In order to determine the timing and location of melting, it is important to consider the initial hydration state of each material, when and where dehydration occurs, the nature of the flux of water, and any rehydration. Additionally, the presence and amount of melt is dependent upon the composition of the material, which can change as melt is extracted away from the source location, leading the material to become increasingly depleted. Below the development of the melting implementation within this study is outlined, focussing particularly on how material hydration and depletion is considered. Some of these techniques are used in Chapters 3 and 4, whilst others are provided as stages within the model development and as different approaches that could be taken. The more technical details of these implementations are summarised in Appendix B.

### 2.5.1 Implementation in numerical code

Essentially two different approaches have been implemented to calculate (de)hydration and the melting of material in the calculations: 1) Using a parameterised solidus (Section 2.5.1.1), and 2) using a pre-calculated lookup table of mineral assemblages, hydration states, and amounts of melt (Section 2.5.1.2). Each of these methods are discussed below.

#### 2.5.1.1 Parameterised solidi

Parameterised solidi can give an estimation of the amount of melting, as a function of the temperature, pressure, and water content of the material, and can also consider other factors, such as the extraction of certain phases upon melting. In order to determine the amount of melting that could be induced by slab breakoff, the parametrisation of Katz et al. (2003) is applied to the results in Chapter 3 after model calculations are performed (see Appendix B.1 for further details). In this case, material across the model is considered to be dry, and the decrease in temperature or increase in water content that would be required for the mantle to reach conditions to melt is calculated.

In order to account for the depletion of material, this same parameterised solidus can be implemented within the model calculations. Particles can be used to track the amount and timing of melting across the model, which are advected with the flow field. The total amount of previous melting that has occurred (i.e. the depletion) can be stored for each particle and used to control the amount of subsequent melting for that particle. This method can also take into the account the effect of latent heat due to melting (see Kaislaniemi and van Hunen (2014) for further details).

The parameterised solidus is also dependent upon the hydration of the material, and in turn affects the hydration state of the material. As a first order approximation of the hydration state of the mantle, the asthenospheric mantle located above the crust can be considered hydrated, as oceanic lithospheric material is the primary source of mantle hydration within a subduction zone (see Appendix B.2 for further details of the implementation of this hydration method). Appendix Fig. B.1 shows an example of a model calculation during breakoff using this hydration method and including melt depletion. This method assumes an inexhaustible supply of water is available to be released from crustal material, as the hydration is refreshed after each timestep. During ongoing subduction, whilst the presence of hydrated material is constantly being replenished, this may be considered a reasonable approximation. However, upon collision, subduction slows and then terminates; hence the mantle wedge cannot be considered to be perpetually hydrated.

#### 2.5.1.2 Thermodynamic databases

An alternative method, which is capable of more accurately determining the hydration state of the mantle, is to use a thermodynamic database to calculate the stable mineralogy, including the bulk and free water content. Therefore, the dehydration and rehydration of material can be determined depending upon the stability of water within a given

composition. In Chapter 4, 'lookup tables' are pre-determined using the thermodynamic software Perple_X (Connolly, 2005), which store the stable mineralogy at a range of pressures, temperatures and bulk-water contents, and help to reduce the model calculation time (see Table 2.4, 2.5 and Magni et al., 2014 for further details). A number of different material compositions are considered in Chapter 4: sediments, oceanic crust, continental upper and lower crust, depleted mantle, and primitive mantle. The crust, sediments, and part of the oceanic lithospheric mantle are defined to be initially hydrated. Following the release of free water from a material, this is modelled to migrate vertically upwards until it reaches under-saturated material that is able to reabsorb this water (see Appendix B.3 for further details of this water migration implementation). The thermodynamic database used also shows whether melt is present as a stable phase for each given pressure-temperature conditions, allowing the determination of the presence of melting for the materials considered in the models in Chapter 4.

The asthenospheric solidus determined from the thermodynamic database is significantly higher than the parameterised solidus of Katz et al. (2003) (Appendix Fig. B.3). To assess the effect that this may have on the results, Appendix B.5 compares the use of the thermodynamic database and the use of the parameterised solidus (Appendix B.4 summarises the technical details of implementing the same hydration scheme with both solidi).

Within a natural system, the preferential partitioning of elements into a partial melt results in a change in composition of the source rock, which decreases the likelihood that this material will melt again. The implementation of the parameterised solidus within the calculations has been designed to account for the reduction in melt generation for more depleted material (see Kaislaniemi (2015) for full details). However, when using 3D lookup tables, which only consider variations in temperature, pressure and water content, the material is assumed to maintain the same composition throughout the calculation. To account for a change in composition, an 11-D lookup table could, in theory, be implemented, which includes the variations in all eight components of the composition (see Table 2.4), along with variations in the pressure, temperature and water content. Alternatively, directly calculating the petrological data with Perple_X, instead of using a pre-determined lookup table, could also determine the new composition of the material upon melting. However, such a calculation is too computationally expensive and would result in very long model calculation times, whilst using a large lookup table is both impractical and computationally expensive to create. In Chapter 4, as an alternative approximation to account for the decrease in fusibility of material upon melting, particles that have exceeded a melting threshold are depleted (hence

| Material | | AM[1] | LM[2] | UCC[3] | LCC[3] | OC[4] | Sed.[5] |
|---|---|---|---|---|---|---|---|
| Composition | $SiO_2$ | 46.48 | 45.21 | 66.72 | 53.96 | 52.59 | 65.65 |
| | FeO | 7.64 | 8.27 | 5.05 | 8.66 | 9.77 | 5.84 |
| | MgO | 38.19 | 39.16 | 2.48 | 7.32 | 7.38 | 2.78 |
| | $Al_2O_3$ | 4.1 | 4.02 | 15.43 | 17.08 | 16.93 | 13.35 |
| | CaO | 3.25 | 3.21 | 3.6 | 9.69 | 10.12 | 6.67 |
| | NaO | 0.33 | 0.13 | 3.28 | 2.68 | 3.21 | 2.72 |
| | $K_2O$ | - | - | 2.81 | 0.62 | - | 2.29 |
| | $TiO_2$ | - | - | 0.64 | - | - | 0.69 |

**Table 2.4: Compositions of materials used in lookup tables.** Abbreviations used: AM = asthenospheric mantle, LM = lithospheric mantle, UCC = upper continental crust, LCC = lower continental crust, OC = oceanic crust, Sed. = sediments. References: 1 - Hart and Zindler (1986), 2 - Workman and Hart (2005), 3 - Rudnick and Gao (2003), 4 - Schmidt and Poli (1998), 5 - Plank and Langmuir (1998). The database of Holland and Powell (2002) is used in Chapter 4 (a revised version of Holland and Powell (1998)).

| Lookup table limits | | | |
|---|---|---|---|
| | Max | Min | Interval |
| Pressure (GPa) | 9.0 | 0.6 | 0.2 |
| Temperature (K) | 1950 | 350 | 10 |
| $H_2O$ (wt%) | 9.00 / 5.00* | 0.00 | 0.05 |

**Table 2.5: Minimum and maximum values and value interval used in the lookup tables for pressure, temperature and $H_2O$.** *9.00 wt% is used for mantle material, and 5.00 wt% for crustal material, as above this value the material is water-saturated.

assuming that when the melt amount exceeds this threshold it can be extracted away from the source rock), and the lookup tables are no longer referred to for these particles (see Appendix B.6 for further details of implementation). A similar, but slightly more sophisticated method for considering this depletion is also considered in Appendix B.6, but a comparison of results shows the difference between these to be minimal, and hence the first method is implemented in Chapter 4 as a simpler way to approximate the melt depletion.

### 2.5.2 Limitations of the hydration and melting implementation

Many of the limitations contained within the methods used for calculating the melting and hydration have tried to be assessed throughout the development of the implementation. However, some still remain which should be addressed in further studies:

*Composition of residue* - Although the depletion of material has been accounted for when using the thermodynamic database, this underestimates the amount of melting, as material in nature is still likely to re-melt after initial extraction. To gain a more accurate understanding of the generation of melt and amount of total extracted melt, the stable mineralogy needs to be determined, taking into account the changing composition with melt extraction.

*Melt migration* - The melt is considered to be extracted instantaneously to the surface once a threshold amount is reached. However, in nature this melt would migrate upwards, transferring heat to shallower material and also possibly reacting with this material. This may lead to further melting at shallower depths within the models, and provide sufficient heat to melt phases that would otherwise remain below the solidus. If the composition of materials were changed, this may also affect the melt generation of material and would affect the signature of melt observed at the surface. The development of melt migration within numerical models may help provide a much more realistic idea of the signatures of melts that may be observable at the surface.

*Flux of water* - Two assumptions have been made when considering the movement of water. Firstly, water is allowed to move only vertically upwards, and secondly, water is assumed to migrate significantly faster than the flow field. Free water would instead flow according to local pressure gradients, which are not necessarily vertically upwards, and also may be carried with the overall flow field, which may affect the area of hydration and locus of melting. Quinquis and Buiter (2014) show that using different water migration schemes has little effect on the distribution of fixed water (i.e. the location where water is absorbed and stored) when using a thermodynamic database to determine the release and absorption of

water. However the distribution of free water can become broader for migration schemes that are not simply calculated in an element-wise fashion. Conversely, Wilson et al. (2014) find that the effect of pressure gradients on the fluid flow can result in a localisation of fluids toward the sub-arc region. The results in Chapter 4 find that melting of the mantle is in most cases a result of a sudden lowering of the solidus temperature upon the release of water, and hence the area of mantle melting could differ if these other migration schemes were implemented. On the contrary, melting of crustal material may be little affected, as this generally occurs as a result of decompression melting of previously hydrated areas. In addition, the effect of hydration on the rheology is not considered, which may result in a weaker mantle wedge. If this were to be included in the model calculations, the effect of melt on the rheology, leading to material weakening, and of melt extraction, most likely leading to material strengthening due to a removal of water with the melt, should also be considered.

*Supercriticality of fluids and melt* - The second critical endpoint defines the pressure-temperature conditions at which fluids and melt do not co-exist as separate phases but become completely miscible (Bureau and Keppler, 1999; Zheng et al., 2011). In the model setup, the water saturated solidus is extrapolated to pressures which may exceed this point, especially so for crustal material. Hence, at depths greater than the lithosphere (and even perhaps shallower than this), the results for melt generation may not be completely reliable.

# Chapter 3

# A systematic parametric study to investigate the control on the depth of slab breakoff and possible implications for post-collisional mantle melting

## 3.1 Introduction

### 3.1.1 The depth of breakoff and consequences for melting

Slab breakoff has been suggested based on seismic and tomographic data and can be initiated by the subduction of buoyant continental lithosphere (Wortel and Spakman, 2000). Observations of magmatism in post-collisional areas have often been interpreted as a result of the breakoff process. However, early numerical studies suggest that this magmatism is only viable when breakoff occurs at depths shallower than the base of the overriding lithosphere, in order to induce lithospheric melting, and at depths shallower than around 50 km, to generate decompression melting of dry asthenosphere (see Chapter 1.2.2 and Fig. 1.5) (Davies and von Blanckenburg, 1995; van de Zedde and Wortel, 2001).

Many numerical studies have since been carried out, investigating the effect of a wide range of parameters on the breakoff dynamics and show a variation in breakoff depth from 25 to over 550 km. The strength of the oceanic plate has been found to have a significant control on this depth, whereby a weaker slab results in necking and breakoff at shallower depths. A

younger oceanic plate (Baumann et al., 2010; Duretz et al., 2011; Gerya et al., 2004) and a slower subduction velocity (Davies and von Blanckenburg, 1995; Li et al., 2002, 2013; Wong A Ton and Wortel, 1997) both result in a hotter and weaker slab, and therefore result in shallower breakoff. However, the relative strength of the oceanic and continental lithosphere also controls the location of breakoff, and may have a more prominent influence on the depth. For example, a strong oceanic lithosphere attached to a weak continental lithosphere may lead to shallow breakoff within the continent, despite the strong nature of the oceanic slab. The thickness of the oceanic and continental lithosphere, as well as the crustal thickness, rheology, and density, will all have an effect on relative strength of the slab and the final breakoff location. Van Hunen and Allen (2011) found that the relative density of the oceanic and continental lithospheres determines the depth of continental subduction, which also influences the breakoff depth. The mechanism through which slab detachment occurs has in some cases been found to have a greater control on the breakoff depth than the strength or density. Brittle failure, either of the whole or solely crustal part of the slab, causes shallower breakoff and is encouraged by older, denser slabs (Andrews and Billen, 2009). Similarly, the effect of Peierl's mechanism, a low-temperature viscous deformation mechanism (Kameyama et al., 1999), within the colder parts of the slab greatly reduces the breakoff depth (Duretz et al., 2011). Hence, despite the increase in slab strength brought about by an older or colder oceanic plate, some studies have found a decrease in breakoff depth with factors which result in a strong slab.

Despite early model calculations predicting breakoff at depths as shallow as 26 km (Wong A Ton and Wortel, 1997), studies have since found breakoff to mostly occur below the base of the overriding lithosphere (e.g. Baumann et al., 2010; Duretz et al., 2011; van Hunen and Allen, 2011). If the majority of continental collision events do not result in very shallow breakoff, this has significant consequences for the interpretation of the generation of post-collisional magmatism.

### 3.1.2 Aims of this study

The depth of slab breakoff, and the consequences for the mantle flow and temperature changes, may all play an important role in determining the potential for breakoff related magmatism. Therefore, the aim of this parametric study is to explore the effect of a number of parameters on the breakoff dynamics. Those already considered in previous studies will be investigated, but other less examined parameters will also be looked at, such as the mantle rheology, temperature of the overriding plate and radiogenic heating.

The effect of each parameter is considered independently of any other parameters. This is perhaps less representative of a typical subduction zone, where certain parameters may be dependent upon each other. However, due to the variations that are observed in subduction zones worldwide and the uncertainty in some parameters, it may be hard to identify precisely how parameters would be dependent upon one other. By varying each parameter independently, a wider variety of parameters can be investigated in this study than would be possible if the dependencies of certain parameters were to be explored. This also allows us to identify which parameters have the greatest effect on the breakoff dynamics. However, in some cases varying parameters inter-dependently may act together to produce more complex and unexpected dynamics. A more thorough multi-parameter study is implemented in chapter 4, for a sub-set of the parameters varied here which are found to have the greatest effect on the breakoff dynamics. This leads to a wider range in observed breakoff dynamics, and other post-collisional dynamical behaviours that are not observed in this study, which are discussed further in chapter 4. In future studies it may also be beneficial to consider more thoroughly and precisely a wider range of properties for certain materials. For example, the properties of the continental crust, including the rheology, density, radiogenic heat production and thickness, and their relation to each other could be explored, and the influence on continental subduction and breakoff dynamics could be investigated.

This study specifically focuses on how the breakoff depth is affected, but the timing of breakoff and the pattern of mantle flow during and after breakoff are also considered. The possible consequences for mantle melting are briefly considered by applying a parameterised solidus to the results. In Chapter 4, the causes of and style of melting that breakoff may induce are thoroughly explored.

## 3.2 Methods

### 3.2.1 Model setup

The governing equations, initial and boundary conditions are as described in Chapter 2. An extensive number of parameters are varied independently of each other over a wide range of possible values, to investigate which factors pose the greatest control on the breakoff dynamics. These include the: upper and whole crustal rheology; mantle rheology; continental crustal thickness; subducting continental lithospheric thickness; radiogenic heating of the continental crust; overriding lithospheric thickness; oceanic plate age; parameters affecting the brittle deformation including the maximum yield strength, cohesion, and friction

coefficient; and the viscosity of the weak zone that separates the converging lithospheres, which controls the convergence velocity. Details of the whole parametric study and the values assigned to each parameter for each model are given in Table 3.1. The initial and boundary conditions for the reference model are defined as described in Chapter 2.4 (Fig. 2.3). The breakoff depth is defined as the weakest point within the slab when the 1000 °C isotherms separate, and the breakoff time as measured from the start of continental subduction up to this point.

### 3.2.2 Application of parameterised solidus

The parameterised solidus of Katz et al. (2003) is applied to the results to calculate the amount of melting that could be produced. Further details of this implementation can be found in Chapter 2.5 and Appendix B.1. As the solidus is for undepleted mantle, this estimation will be ignored for areas of crustal material and act as an upper bound for the amount of melting that could be expected within the more depleted lithospheric mantle. This parameterisation is based upon the pressure, temperature, water content and modal clinopyroxene (cpx): lithostatic pressure is assumed across the models; the effect of adiabatic heating is included within the temperature profile by adding an adiabatic gradient of 0.5 K/ km to the ambient temperatures; the bulk water content across the model is defined to be 0 wt%, but the increase in water content that would be required to produce melting is calculated; and a value of 0.15 for the modal cpx is used.

## 3.3 Results

The breakoff dynamics are outlined for the reference model (Model 1 in Table 3.1), before the key features that are observed when varying a number of parameters are summarised and analysed, to assess which pose the biggest control on the breakoff dynamics. A simple parameterised mantle melting solidus is then applied to key results to assess the potential for melting following slab breakoff, and to calculate any further increase in temperature or hydration that would be required to produce melting.

### 3.3.1 Development of reference model

Fig. 3.1 shows the evolution of the reference model, which has a setup as described in Section 2.4. Throughout the period of oceanic subduction, subduction is sustained at a steady rate through both the descent of the oceanic plate into the subduction zone and the roll-back of the overriding plate (Figs. 3.1A, 3.1I, and 3.1Q). The rate of subduction slows down as the

| Model | Flow law | | Continental lithospheric thickness (km) | Continental crustal thickness (km) | Radiogenic heating ($\mu Wm^{-3}$) | Overriding lithospheric thickness (km) | Oceanic plate age (Myr) | Brittle deformation | | | Weak zone viscosity (Pa.s) |
|---|---|---|---|---|---|---|---|---|---|---|---|
| | Continental crustal (upper/lower) | Mantle | | | | | | Max. yield strength (MPa) | Friction coefficient | Cohesion (MPa) | |
| 1 | Plag./Plag. | Mean | 125 | 35 | 0 | 100 | 50 | 400 | 0.2 | 40 | $2x10^{20}$ |
| 2 | Dry Qz./Plag. | Mean | 125 | 35 | 0 | 100 | 50 | 400 | 0.2 | 40 | $2x10^{20}$ |
| 3 | Wet Qz./Plag. | Mean | 125 | 35 | 0 | 100 | 50 | 400 | 0.2 | 40 | $2x10^{20}$ |
| 4 | Dry Qz./Dry Qz. | Mean | 125 | 35 | 0 | 100 | 50 | 400 | 0.2 | 40 | $2x10^{20}$ |
| 5 | Wet Qz./Dry Qz. | Mean | 125 | 35 | 0 | 100 | 50 | 400 | 0.2 | 40 | $2x10^{20}$ |
| 6 | Wet Qz./Wet Qz. | Mean | 125 | 35 | 0 | 100 | 50 | 400 | 0.2 | 40 | $2x10^{20}$ |
| 7 | Plag./Plag. | +1.0 SD | 125 | 35 | 0 | 100 | 50 | 400 | 0.2 | 40 | $2x10^{20}$ |
| 8 | Plag./Plag. | +0.5 SD | 125 | 35 | 0 | 100 | 50 | 400 | 0.2 | 40 | $2x10^{20}$ |
| 9 | Plag./Plag. | -0.5 SD | 125 | 35 | 0 | 100 | 50 | 400 | 0.2 | 40 | $2x10^{20}$ |
| 10 | Plag./Plag. | -1.0 SD | 125 | 35 | 0 | 100 | 50 | 400 | 0.2 | 40 | $2x10^{20}$ |
| 11 | Plag./Plag. | Mean | 100 | 35 | 0 | 100 | 50 | 400 | 0.2 | 40 | $2x10^{20}$ |
| 12 | Plag./Plag. | Mean | 150 | 35 | 0 | 100 | 50 | 400 | 0.2 | 40 | $2x10^{20}$ |
| 13 | Plag./Plag. | Mean | 175 | 35 | 0 | 100 | 50 | 400 | 0.2 | 40 | $2x10^{20}$ |
| 14 | Plag./Plag. | Mean | 125 | 20 | 0 | 100 | 50 | 400 | 0.2 | 40 | $2x10^{20}$ |
| 15 | Plag./Plag. | Mean | 125 | 25 | 0 | 100 | 50 | 400 | 0.2 | 40 | $2x10^{20}$ |
| 16 | Plag./Plag. | Mean | 125 | 30 | 0 | 100 | 50 | 400 | 0.2 | 40 | $2x10^{20}$ |
| 17 | Plag./Plag. | Mean | 125 | 40 | 0 | 100 | 50 | 400 | 0.2 | 40 | $2x10^{20}$ |
| 18 | Plag./Plag. | Mean | 125 | 45 | 0 | 100 | 50 | 400 | 0.2 | 40 | $2x10^{20}$ |

| | | | | | | | | | | | |
|---|---|---|---|---|---|---|---|---|---|---|---|
| 19 | Plag./Plag. | Mean | 125 | 50 | 0 | 100 | 50 | 400 | 0.2 | 40 | $2x10^{20}$ |
| 20 | Plag./Plag. | Mean | 125 | 35 | 0.7 | 100 | 50 | 400 | 0.2 | 40 | $2x10^{20}$ |
| 21 | Plag./Plag. | Mean | 125 | 35 | 0 | 60 | 50 | 400 | 0.2 | 40 | $2x10^{20}$ |
| 22 | Plag./Plag. | Mean | 125 | 35 | 0 | 100 | 30 | 400 | 0.2 | 40 | $2x10^{20}$ |
| 23 | Plag./Plag. | Mean | 125 | 35 | 0 | 100 | 80 | 400 | 0.2 | 40 | $2x10^{20}$ |
| 24 | Plag./Plag. | Mean | 125 | 35 | 0 | 100 | 100 | 400 | 0.2 | 40 | $2x10^{20}$ |
| 25 | Plag./Plag. | Mean | 125 | 35 | 0 | 100 | 50 | 200 | 0.2 | 40 | $2x10^{20}$ |
| 26 | Plag./Plag. | Mean | 125 | 35 | 0 | 100 | 50 | 800 | 0.2 | 40 | $2x10^{20}$ |
| 27 | Plag./Plag. | Mean | 125 | 35 | 0 | 100 | 50 | 400 | 0.1 | 40 | $2x10^{20}$ |
| 28 | Plag./Plag. | Mean | 125 | 35 | 0 | 100 | 50 | 400 | 0.6 | 40 | $2x10^{20}$ |
| 29 | Plag./Plag. | Mean | 125 | 35 | 0 | 100 | 50 | 400 | 0.2 | 0 | $2x10^{20}$ |
| 30 | Plag./Plag. | Mean | 125 | 35 | 0 | 100 | 50 | 400 | 0.2 | 100 | $2x10^{20}$ |
| 31 | Plag./Plag. | Mean | 125 | 35 | 0 | 100 | 50 | 400 | 0.2 | 40 | $5x10^{19}$ |
| 32 | Plag./Plag. | Mean | 125 | 35 | 0 | 100 | 50 | 400 | 0.2 | 40 | $1x10^{20}$ |

**Table 3.1: Parameters used in each calculation of parametric study.** The parameter values different to those of the reference model (Model 1) are highlighted in grey. For the continental crustal flow laws: Plag. represents Plagioclase, and Qz. represents Quartzite.

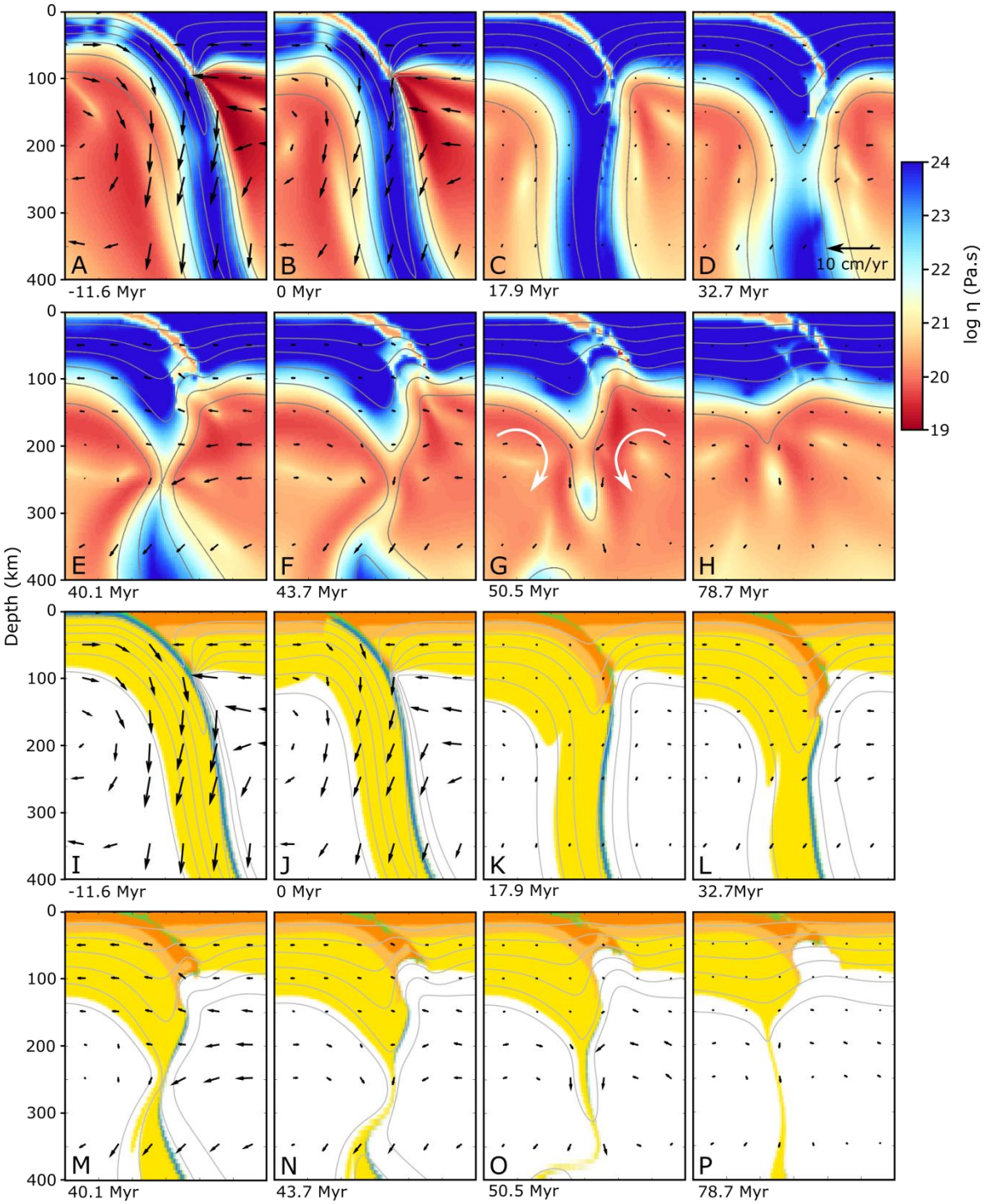
Depth (km)
0
100
200
300
400
A
B
C
D
E
F
G
H
I
J
K
L
M
N
O
P
-11.6 Myr
0 Myr
17.9 Myr
32.7 Myr
40.1 Myr
43.7 Myr
50.5 Myr
78.7 Myr
-11.6 Myr
0 Myr
17.9 Myr
32.7Myr
40.1 Myr
43.7 Myr
50.5 Myr
78.7 Myr
10 cm/yr
log η (Pa.s)
24
23
22
21
20
19

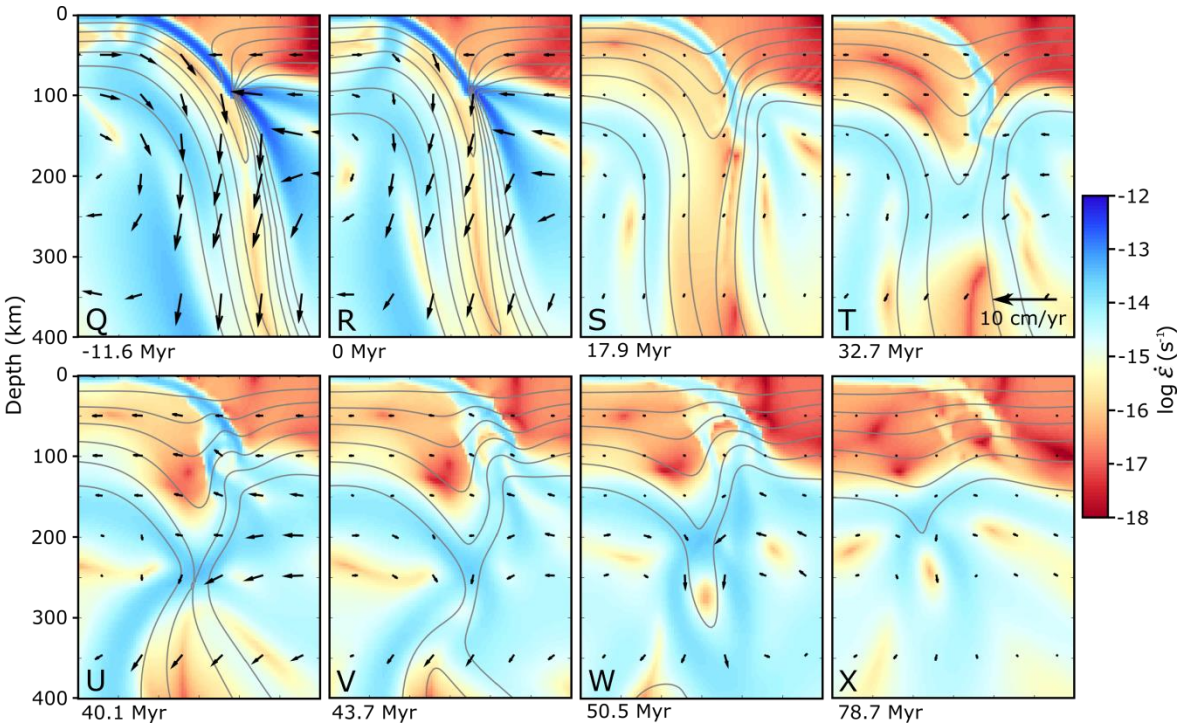


**Figure 3.1: Breakoff dynamics for the reference model (Model 1).** The development of the reference model is shown through subduction of the oceanic plate (Figs. 3.1A, 3.1I, and 3.1Q), initial continental collision (Figs. 3.1B, 3.1J, and 3.1R), slab stagnation (Figs. 3.1C, 3.1K, and 3.1S), slab necking (Figs. 3.1D, 3.1L, and 3.1T), slab breakoff (Figs. 3.1E, 3.1M, and 3.1U), exhumation of the continental crust (Figs. 3.1F, 3.1N, and 3.1V), slab dripping (Figs. 3.1G, 3.1O, and 3.1W) and thermal equilibration after collision and breakoff (Figs. 3.1H, 3.1P, and 3.1X). Figs. 3.1A - 3.1H show the viscosity, 3.1I - 3.1P the position of different compositional materials based upon the locations of tracer particles within the model, and 3.1Q - 3.1X the strain rate. See Fig. 2.3 for a key showing the materials represented in Figs. 3.1I - 3.1P. Temperature contours are in grey and have an interval of 200 °C. The black arrows show the velocity of material from the point where the arrow begins. The scale for these velocity vectors is given in Figs. 3.1D and 3.1T and is representative for all panels. Fig. 3.1G also shows the general pattern of convection on either side of the detached slab with white arrows. Times are given relative to the time of initial collision. Each panel has a width of 300 km.

continental lithosphere enters the subduction zone. The crust continues to be subducted to a maximum depth of 140 km, at which point the slab stagnates (Figs. 3.1C, 3.1K, and 3.1S). Tensional stresses exist within the slab between the buoyant continental crust and the denser oceanic lithosphere; however these alone are not sufficient to cause slab breakoff (Figs. 3.1D, 3.1L, and 3.1T). The slab increases in temperature as it resides within the mantle, weakening the entire slab, and resulting in the slab becoming weakest where the tensional stresses are greatest (Figs. 3.1E, 3.1M, and 3.1U). As the slab necks, warm asthenospheric material flows towards this location of necking, further weakening the surrounding mantle

and accelerating the necking and weakening process. Breakoff is not a rapid process but occurs through thermal weakening, with the entire process from stagnation of the slab to final breakoff taking 19 Myrs. Breakoff occurs at a depth of 245 km and at a time of 40.1 Myr after initial collision, located within the oceanic lithosphere. At shallower depths there is a greater force acting downwards on the slab from the dense oceanic lithosphere, but the slab is also colder due to its proximity to the overriding lithosphere. In this case, the oceanic lithosphere is also thinner than the continental, making it warmer and potentially weaker than the continental lithosphere. Hence breakoff localises at the point where the slab is shallow but also thin and weak. The thermal weakening of the slab also affects the continental crust, which subsequently begins to exhume upwards along its path of subduction, coincident with the necking and breakoff process (Figs. 3.1F, 3.1N, and 3.1V). This results in a small amount of extension around the suture of 15 km (Figs. 3.1H, 3.1P, and 3.1X).

### 3.3.2 Parameters controlling the breakoff dynamics

The depth of breakoff ranges from 170 to 280 km across the study, whilst the timing of breakoff as measured post-collision from 25 to 130 Myr (Fig. 3.2). The biggest range in breakoff depth for any one parameter is 106 km (for variations in the continental crustal thickness), and the range for the breakoff timing is 103.5 Myr (for variations in the mantle rheology). Below the variations in each parameter are summarised, and their effect on the breakoff dynamics. When comparing the following parameters, the relative effect is considered with respect to these values.

#### 3.3.2.1 Continental crustal rheology

Both the whole crustal rheology, and the upper crustal rheology independent of the lower crustal rheology, are varied to account for the more felsic nature of the upper continental crust. The rheology of the upper crust is found to have a small effect on the amount of exhumation, whereby a weaker crust enables a more rapid buoyant crustal flow, which can lead to hotter temperatures underneath the area of crustal exhumation and more extension. However, very little variation is observed in the dynamics of the breakoff process when only the upper crustal rheology is varied (Fig. 3.2).

The amount of coupling between the continental crust and the mantle lithosphere, determined by the strength of the lower crust, has a greater control on the crustal dynamics and consequently on the breakoff process. When a plagioclase flow law is implemented, the

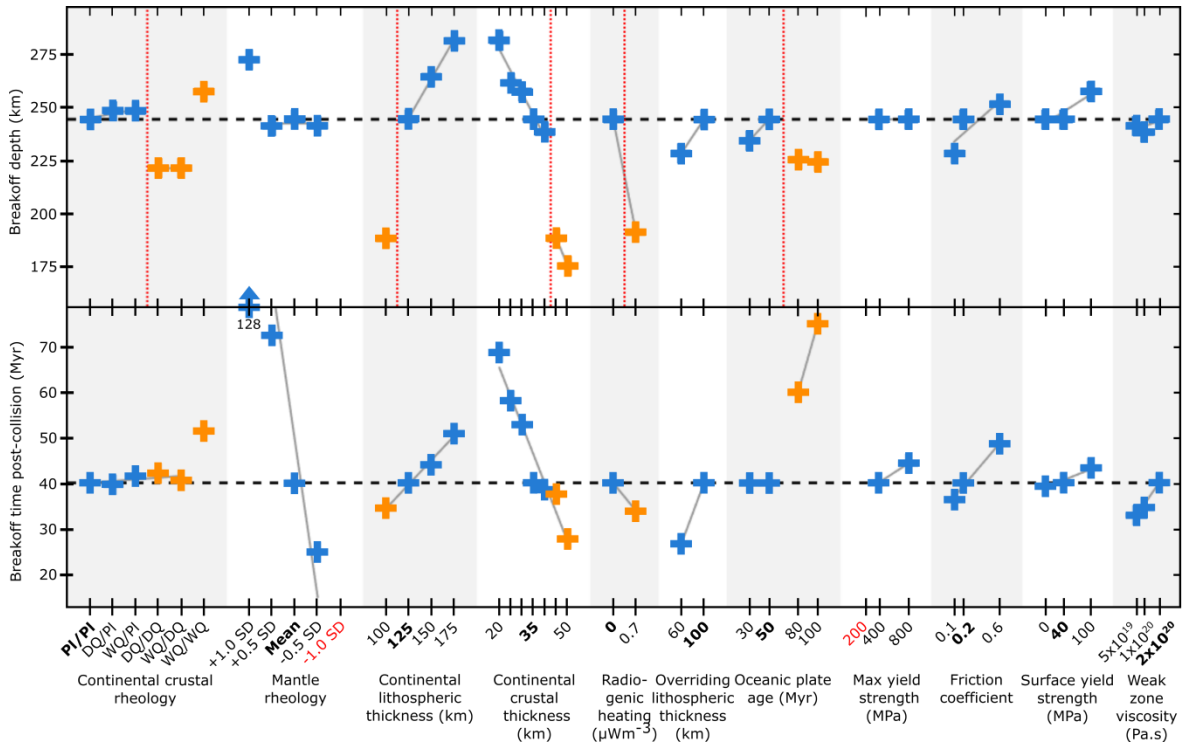


**Figure 3.2: Variations in breakoff depth and time for all studied parameters.** Parameter values in bold show the default value. Values in red were investigated, but stable subduction was not initiated due to early oceanic breakoff. Blue crosses represent a breakoff location within the oceanic lithosphere, whilst orange represents breakoff within the continental lithosphere. Linear lines of best fit are plotted where trends in the depth and timing can be observed. The horizontal black dashed line shows the breakoff depth and time for the reference model. The vertical red lines show where a sudden decrease in breakoff depth occurs, because of a change from breakoff within the oceanic to continental lithosphere. Continental crustal flow law - Pl: plagioclase, DQ: dry quartzite, WQ: wet quartzite.

lithosphere and crust remain strongly coupled (Figs. 3.1C, and 3.1K), whilst a dry quartzite flow law results in a thin layer of weaker material at the Moho (~15 km wide with a minimum viscosity an order of magnitude weaker than the crust and mantle) (Figs. 3.3A, and 3.3E), and a wet quartzite flow law further makes this layer thicker and weaker (~ 25 km with a minimum viscosity over two orders of magnitude weaker) (Figs. 3.4A, and 3.4E).

For a dry quartzite rheology, the stagnated slab initially weakens at a similar depth as for a stronger crust (compare Figs. 3.1K and 3.3E). However, the decrease in coupling between the crust and mantle leads to an upwards flow of the crust, independent of the mantle lithosphere (Figs. 3.3B, 3.3F, and 3.3J). This results in the thinnest and hence weakest section of the slab being located within the continental lithosphere, resulting in a shallower breakoff depth by 25 km (Figs. 3.3C, 3.3G, and 3.3K).

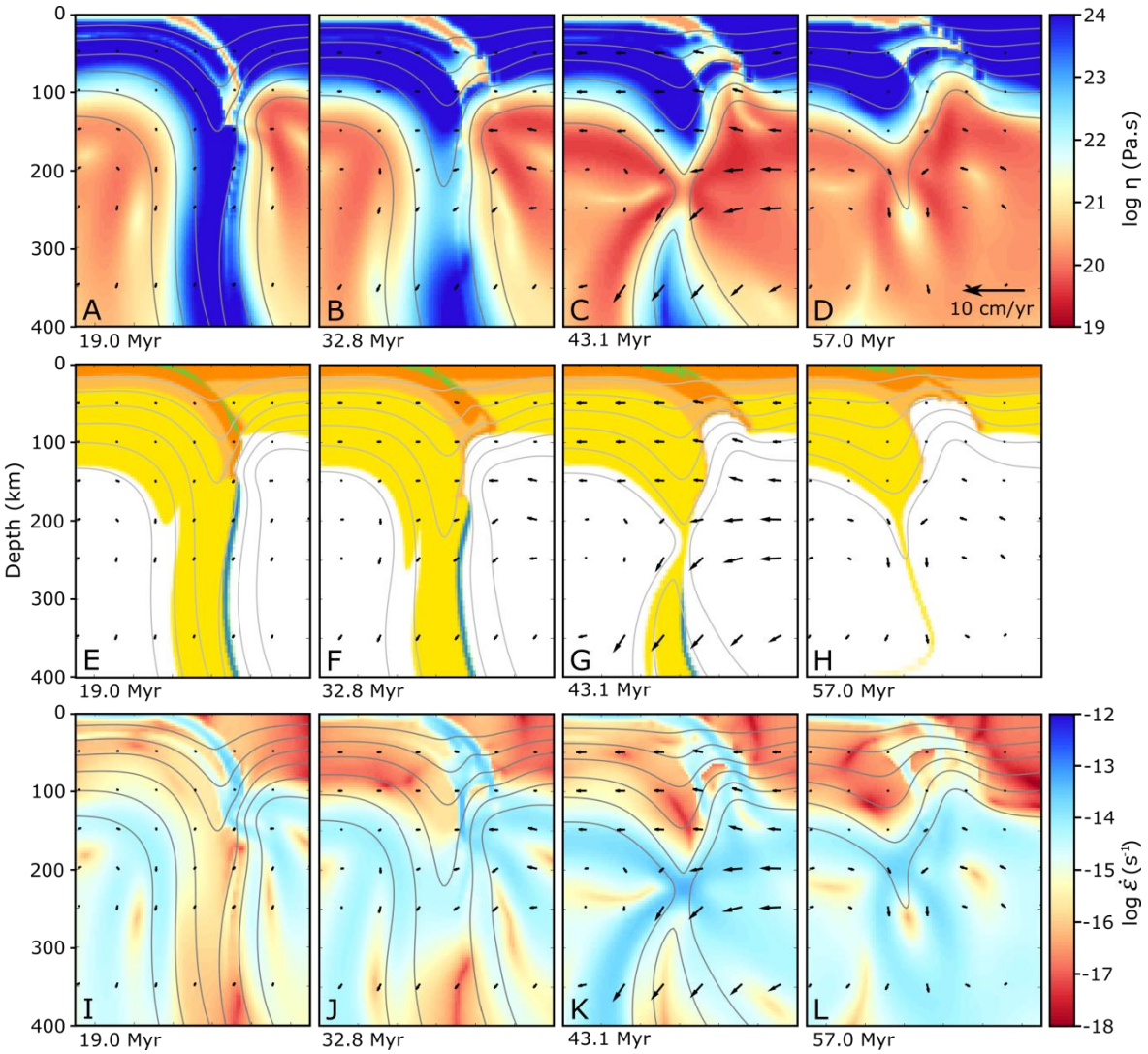


**Figure 3.3: Breakoff dynamics for Model 4 - dry quartzite crustal rheology.** Figs. 3.3A - Fig. 3.3D show the viscosity, 3.3E - 3.3H the position of different compositional materials based upon the locations of tracer particles within the model, and 3.3I - 3.3L the strain rate. See Fig. 2.3 for a key showing the materials represented in Figs. 3.3E - 3.3H. Temperature contours, velocity vectors, and panel width are as in Fig. 3.1.

When a wet quartzite rheology is implemented, significantly more decoupling occurs between the crust and mantle, even before necking of the slab initiates (Figs. 3.4A, 3.4E, and 3.4I). The earlier timing of this crustal exhumation means the slab does not reside as long in the asthenospheric mantle, and hence the slab is cooler and stronger. Hence breakoff does not coincide with the exhumation event. Loss of the more buoyant continental crust from the stagnated slab, and the flow of upwelling asthenosphere beneath the crust, initiates rollback of the slab (Figs. 3.4B, 3.4F, and 3.4J). The slab descends further and slab necking localises within the continental lithosphere, but this is at a similar depth as compared to the strongest

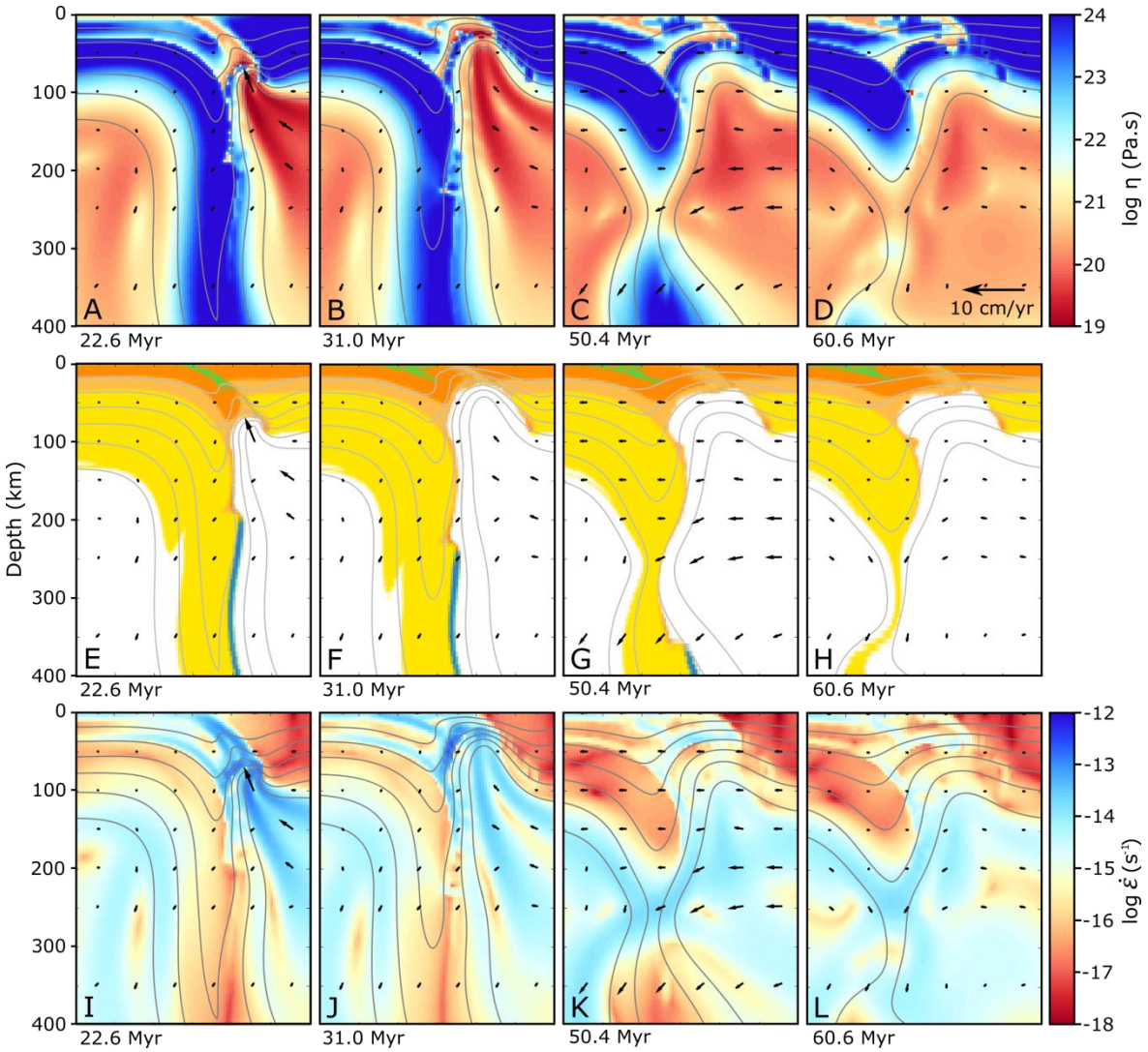


**Figure 3.4: Breakoff dynamics for Model 6 - wet quartzite crustal rheology.** Panels are as in Fig. 3.3.

crustal rheology (compare Figs. 3.1E, 3.1M, 3.1U and 3.4C, 3.4G, 3.4K). Hence breakoff actually occurs 10 km deeper and 10 Myr later.

Therefore, although a weaker crust can result in shallower breakoff by localising slab necking within the continental lithosphere rather than within the oceanic, further weakening can actually lead to deeper and later breakoff due to the early buoyant exhumation of the continental crust.

### 3.3.2.2 Mantle rheology

A range of flow laws are implemented for the mantle rheology, determined from commonly used flow laws (see Chapter 2.3.1 and Maunder et al. (2016) for further details). These are a

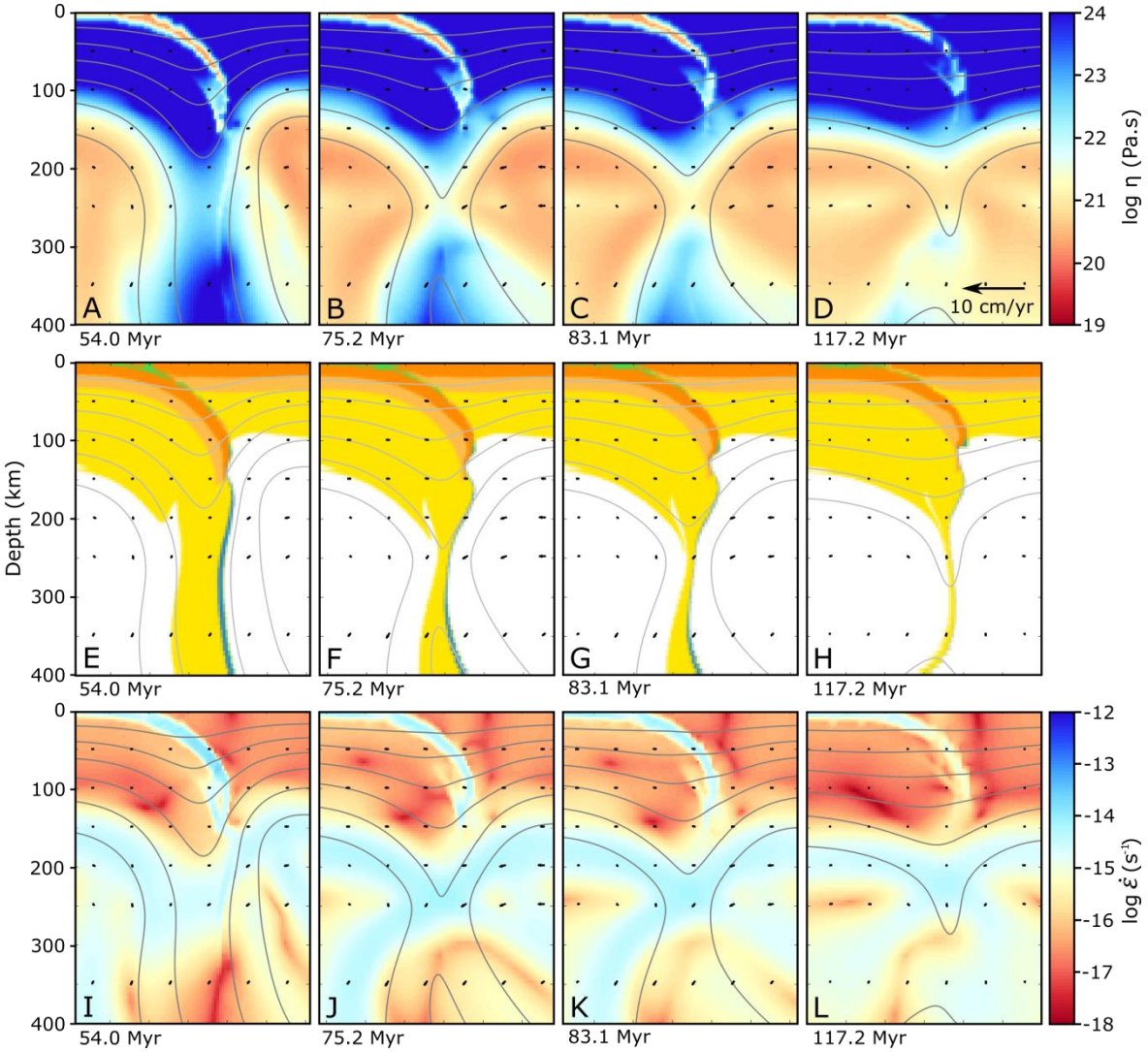


**Figure 3.5: Breakoff dynamics for Model 8 - +0.5 SD mantle rheology.** Panels are as in Fig. 3.3.

mean flow law, representative of an intermediate flow law between a wet and dry rheology, a +1SD flow law, representative of a dry flow law, a +0.5 SD flow law, representative of a slightly weaker dry flow law, and a -0.5 SD flow, representative of a wet flow law. Calculations were also carried out using a -1SD flow, representative of a weaker wet flow law, but the mantle was too weak in this case for oceanic subduction to develop initially.

The results show that the mantle rheology has very little control over the breakoff depth, but significantly affects the timing of breakoff (Fig. 3.2). In each model the weakest location of the slab does not change, and hence slab necking localises at the same point within the slab (compare Figs. 3.1E, 3.1M, 3.5B, 3.5F, 3.6B, and 3.6F). Using a weaker mantle flow law leads to faster breakoff, as it causes the mantle lithospheric part of the slab to be weaker, initiates a stronger mantle flow within the asthenosphere during slab necking, and may also

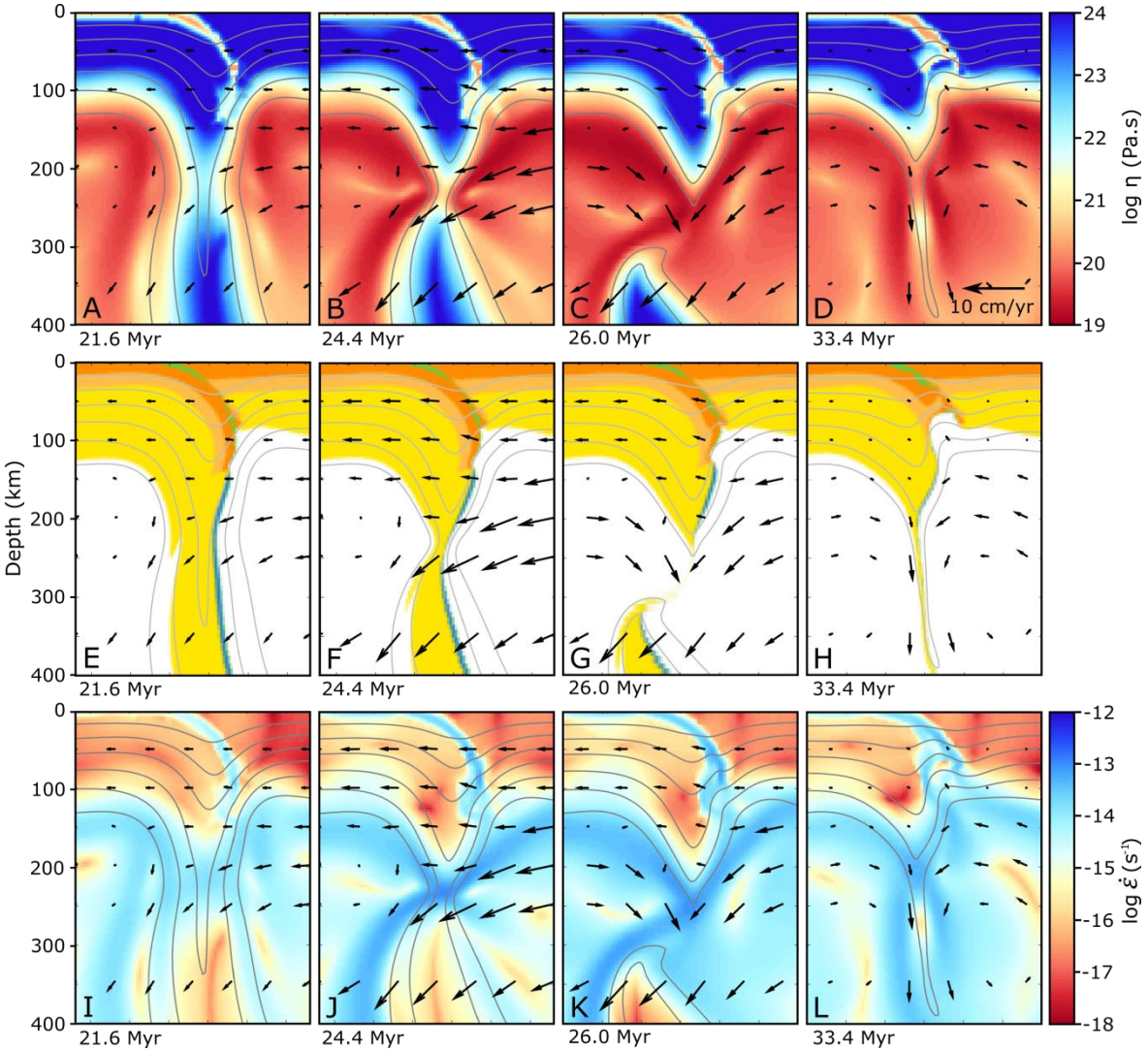


**Figure 3.6: Breakoff dynamics for Model 9 - -0.5 SD mantle rheology.** Panels are as in Fig. 3.3.

provide less support for the stagnated slab leading to greater extensional stresses within the slab (Figs. 3.6B, 3.6F, and 3.6J).

The only exception is for the strongest mantle rheology, for which the slab does not break into two sections as in all other models, but slowly heats up from the base. A breakoff depth is documented as when the thinnest part of the slab exceeds 1000 °C, giving a breakoff depth 30 km deeper than for the mean mantle flow law. The long time scale of this model (180 Myr from initiation to breakoff) and the subsequent cooling of the lithosphere perhaps results in an over-thickening of the lithosphere, which may be reduced by far-field mantle flow patterns which are not modelled. However, we suggest that for a mantle rheology as strong as the +1 SD flow law, 'breakoff' is not a significant event occurring within the mantle and no observable effects would be produced.

### 3.3.2.3 Continental lithospheric thickness

The subducting continental lithospheric thickness is varied between 100 and 175 km, representing a range from the thickness of a continental margin to a thick cratonic lithosphere. The thickness has a significant effect on the breakoff depth, which varies over 90 km, and a relatively smaller but not insubstantial effect on the timing, which varies over 16 Myr (Fig. 3.2). A thicker lithosphere increases the depth of breakoff, as the thinnest and weakest section of the oceanic lithosphere, at which the slab necks, becomes deeper (Fig. 3.7 B, F, J). This is a result of the lithospheric core of the collision zone being cooler, and not because of deeper subduction of the continental lithosphere (Figs. 3.7A, and 3.7E). The maximum continental crust depth actually decreases with increasing lithospheric thickness,

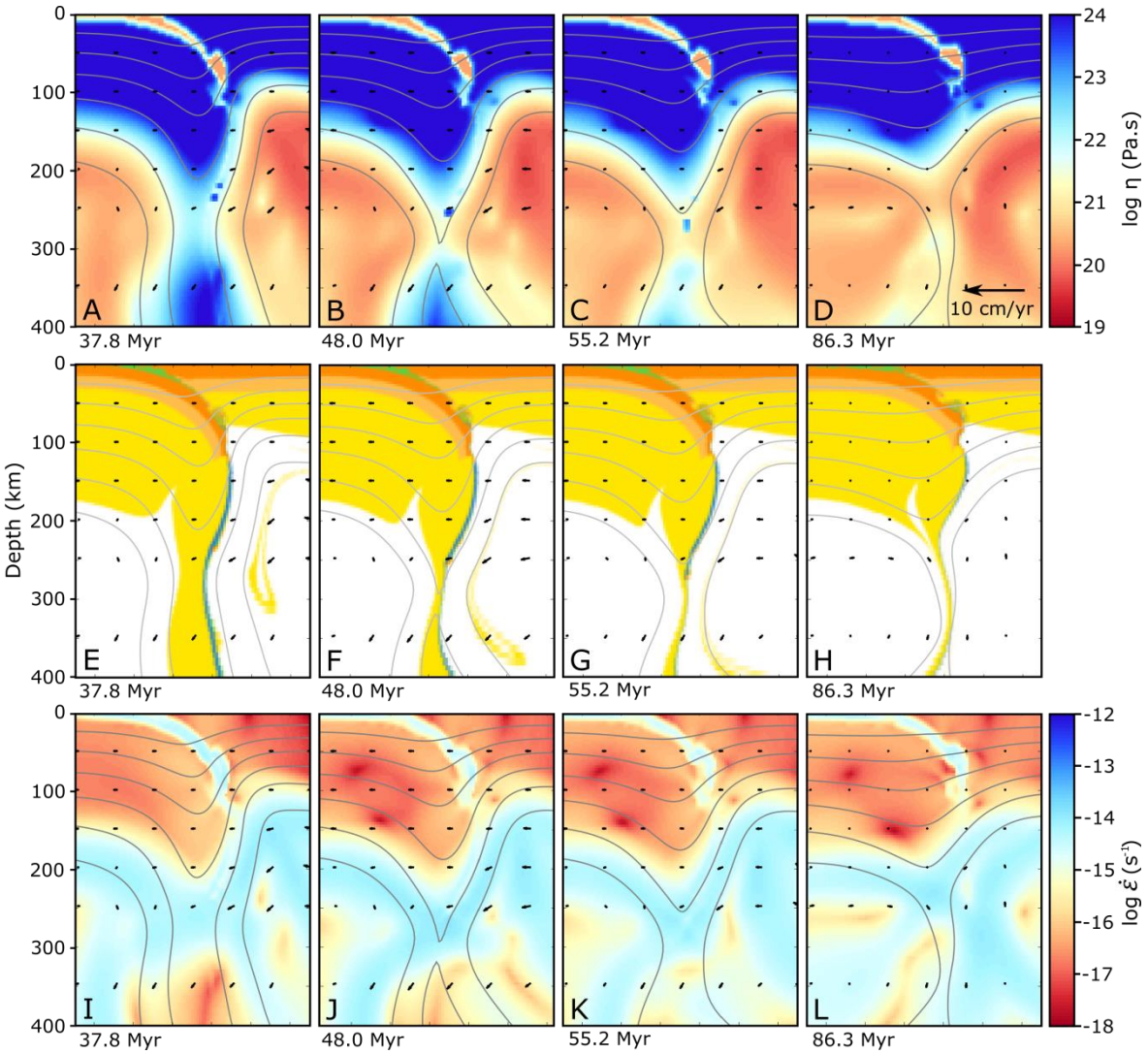


**Figure 3.7: Breakoff dynamics for Model 13 - 175 km continental lithospheric thickness.** Panels are as in Fig. 3.3.

as a thicker lithosphere is unable to bend as easily into the subduction zone. The breakoff depth decreases linearly, at around 20 km per 25 km decrease in lithospheric thickness (Fig. 3.2). However, for a 100 km thick continental lithosphere a further decrease in breakoff depth is observed due to the localising of necking within the continental lithosphere rather than within the oceanic lithosphere (Figs. 3.8B, 3.8F, and 3.8J). The crust is hotter in this case, due to the decrease in lithospheric thickness, and hence the crust undergoes more significant exhumation and faster exhumation when necking begins (Figs. 3.8A, 3.8E, and 3.8I). As with a weaker crustal rheology, this thins the deepest part of the continental lithosphere. This, coupled with a thinner overall lithospheric thickness initially, causes breakoff to localise within the continental lithosphere.

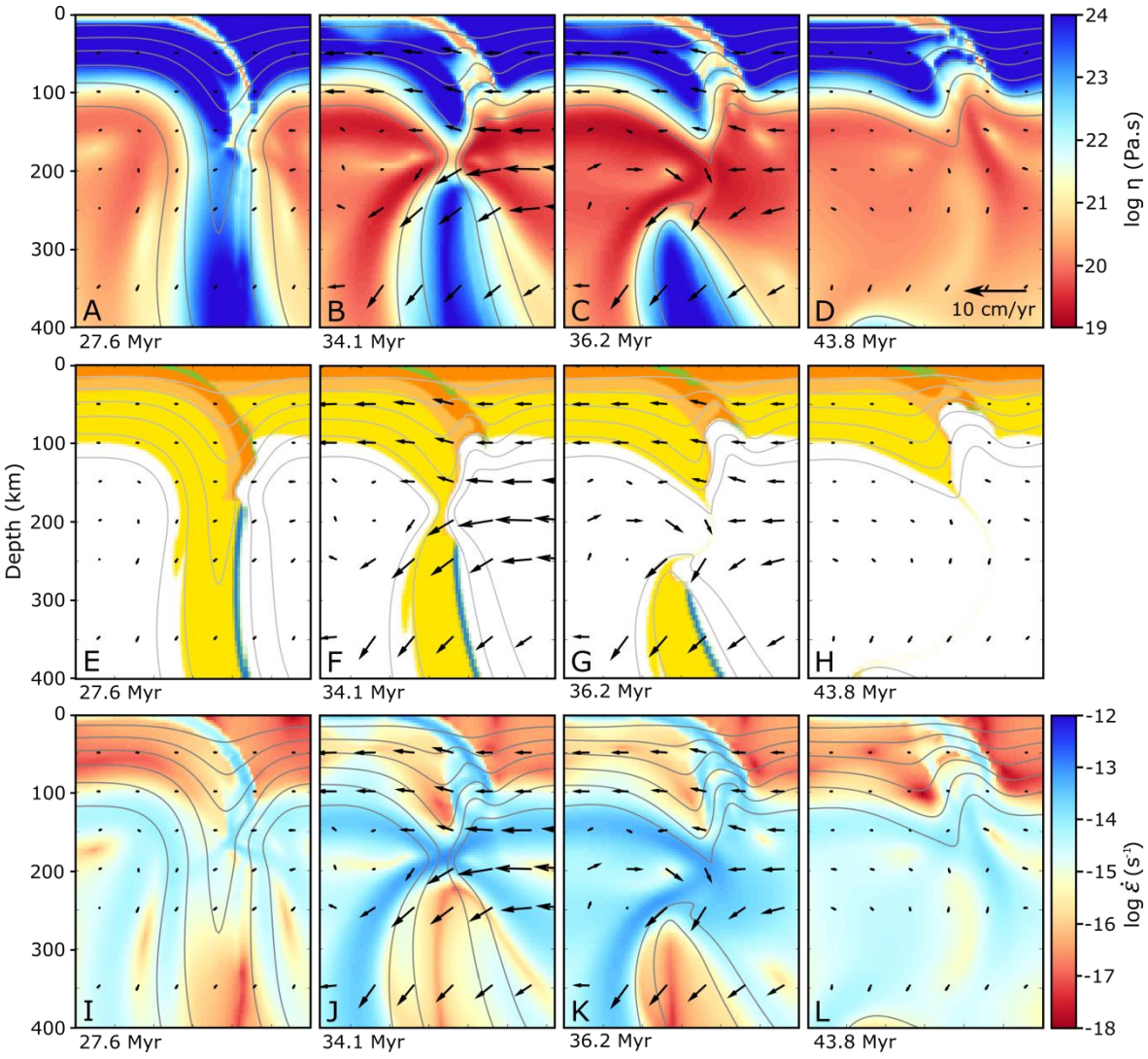


**Figure 3.8: Breakoff dynamics for Model 11 - 100 km continental lithospheric thickness.** Panels are as in Fig. 3.3.

### 3.3.2.4 Continental crustal thickness

Values of 20 up to 50 km are implemented for the thickness of the continental crust. Variations in this parameter have a significant effect on both the depth and the timing of slab breakoff (Fig. 3.2). A thinner continental crust leads to a smaller buoyant force acting on the slab and hence the crust is able to be subducted deeper (Fig. 3.9E). The thinnest and weakest part of the oceanic lithosphere, at which it necks, is therefore located deeper within the mantle (Figs. 3.9B, 3.9C, 3.9J, and 3.9K). Between a crustal thickness of 40 and 45 km, the location of breakoff switches from within the oceanic lithosphere to within the continental lithosphere, leading to a sharp decrease in breakoff depth of 50 km (Figs. 3.2, 3.10B, 3.10F, and 3.10J). The breakoff timing also decreases with increasing crustal thickness, and except

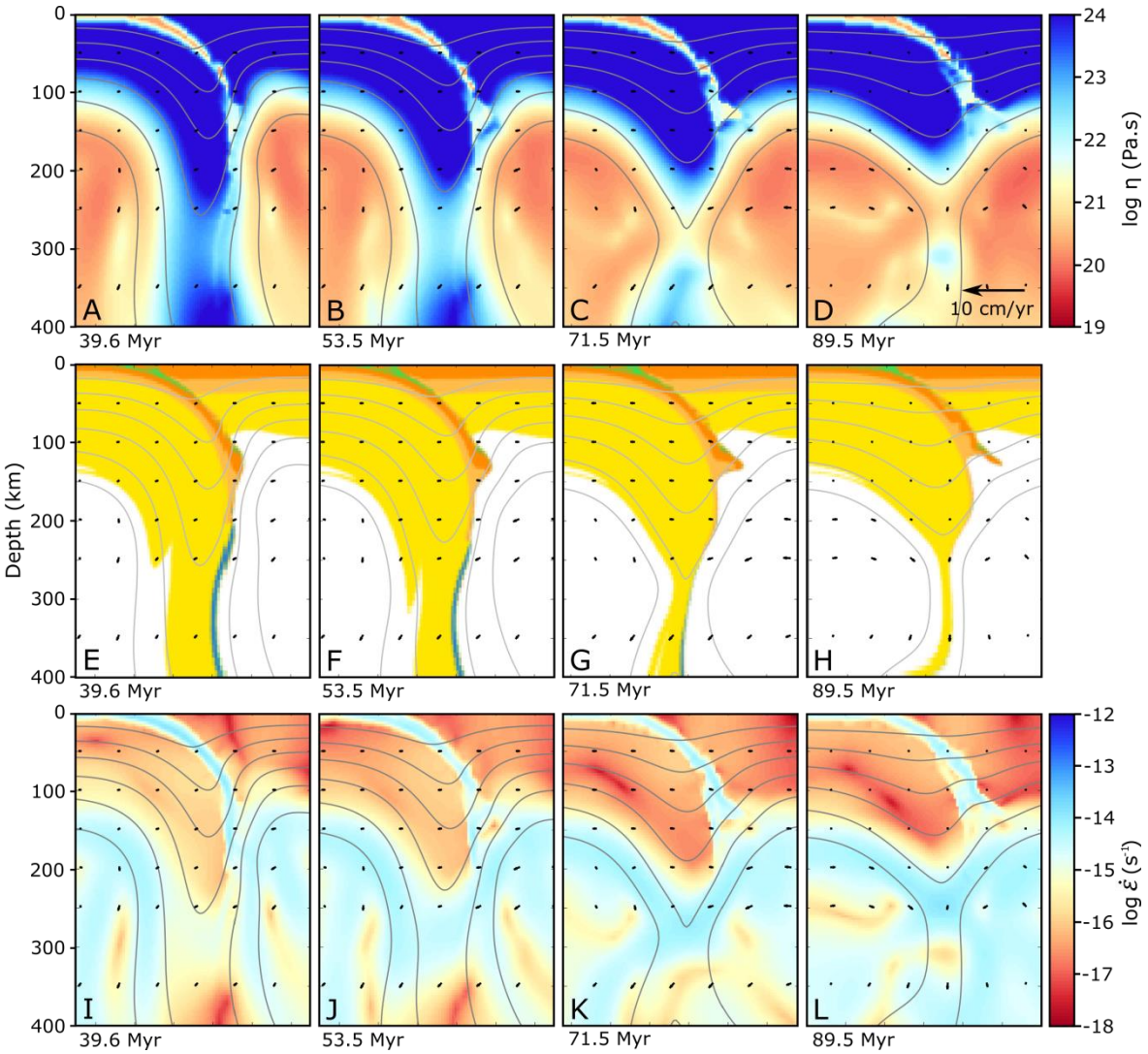


**Figure 3.9: Breakoff dynamics for Model 14 - 20 km continental crustal thickness.** Panels are as in Fig. 3.3.

from the change in thickness from 40 to 45 km, parallels the change in breakoff depth very closely. As a thinner crust is able to be subducted further, a smaller force from the subducted oceanic lithosphere acts downwards on the slab. This, coupled with a smaller upwards buoyancy force from the thinner crust, means more thermal weakening is required before the slab weakens sufficiently to break apart (Figs. 3.9B, and 3.9J).

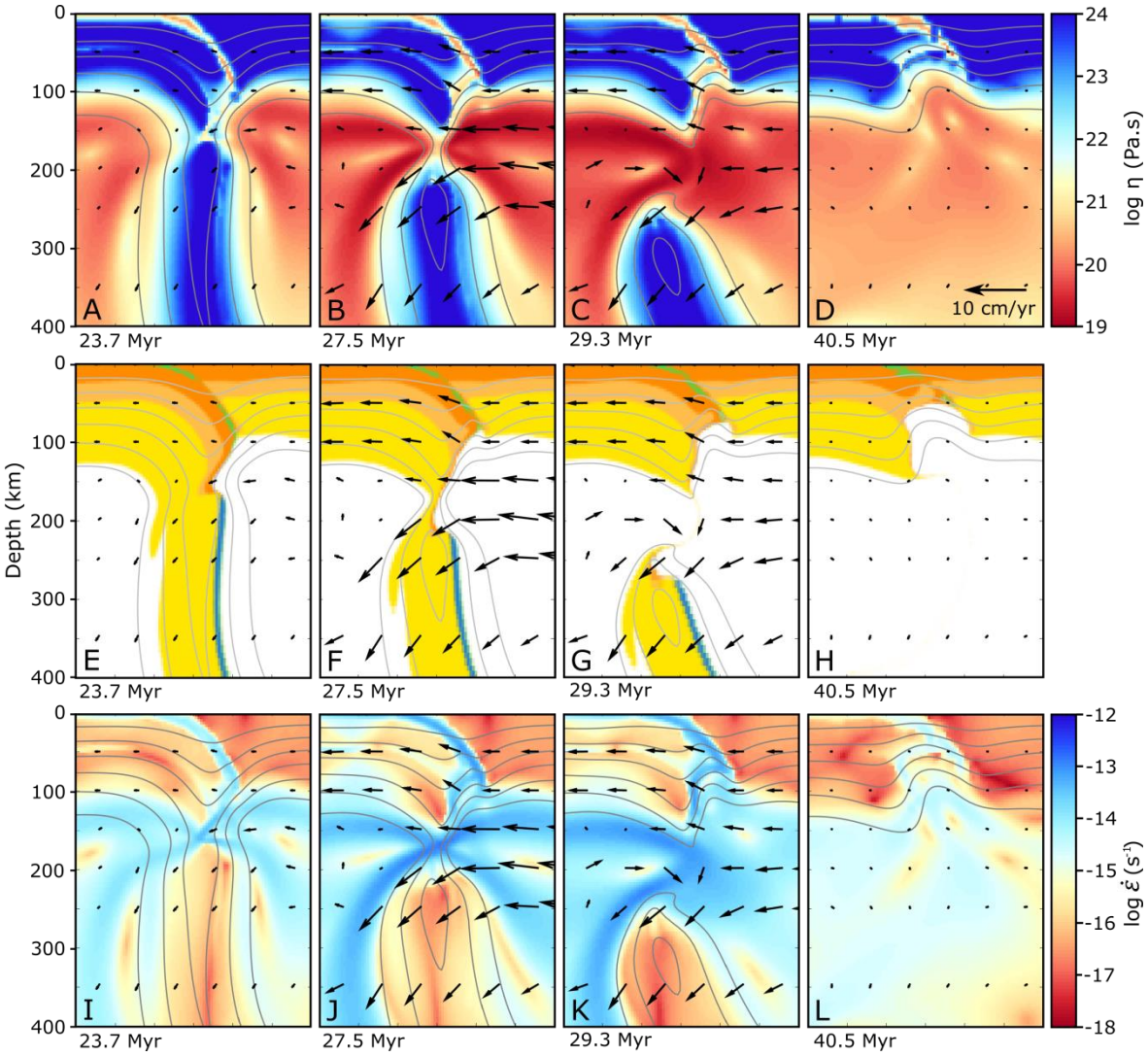


**Figure 3.10: Breakoff dynamics for Model 19 - 50 km continental crustal thickness.** Panels are as in Fig. 3.3.

### 3.3.2.5 Oceanic plate age

The oceanic plate age is both reduced to 30 Myr, and increased to 80 and 100 Myr. Reducing the age results in a slightly shallower breakoff depth by 10 km, as the thinnest part of the slab is shallower (Figs. 3.11B, 3.11F, and 3.11J). However, increasing the age causes an even larger decrease in depth by up to 20 km (Figs. 3.12C, 3.12G, and 3.12K). For these ages, the continental lithosphere is thinner and weaker than the oceanic and hence slab breakoff localises here. The timing of breakoff also increases, as the subducted slab is thicker due to the colder oceanic lithosphere, and the thermal weakening leading to breakoff takes longer to progress.

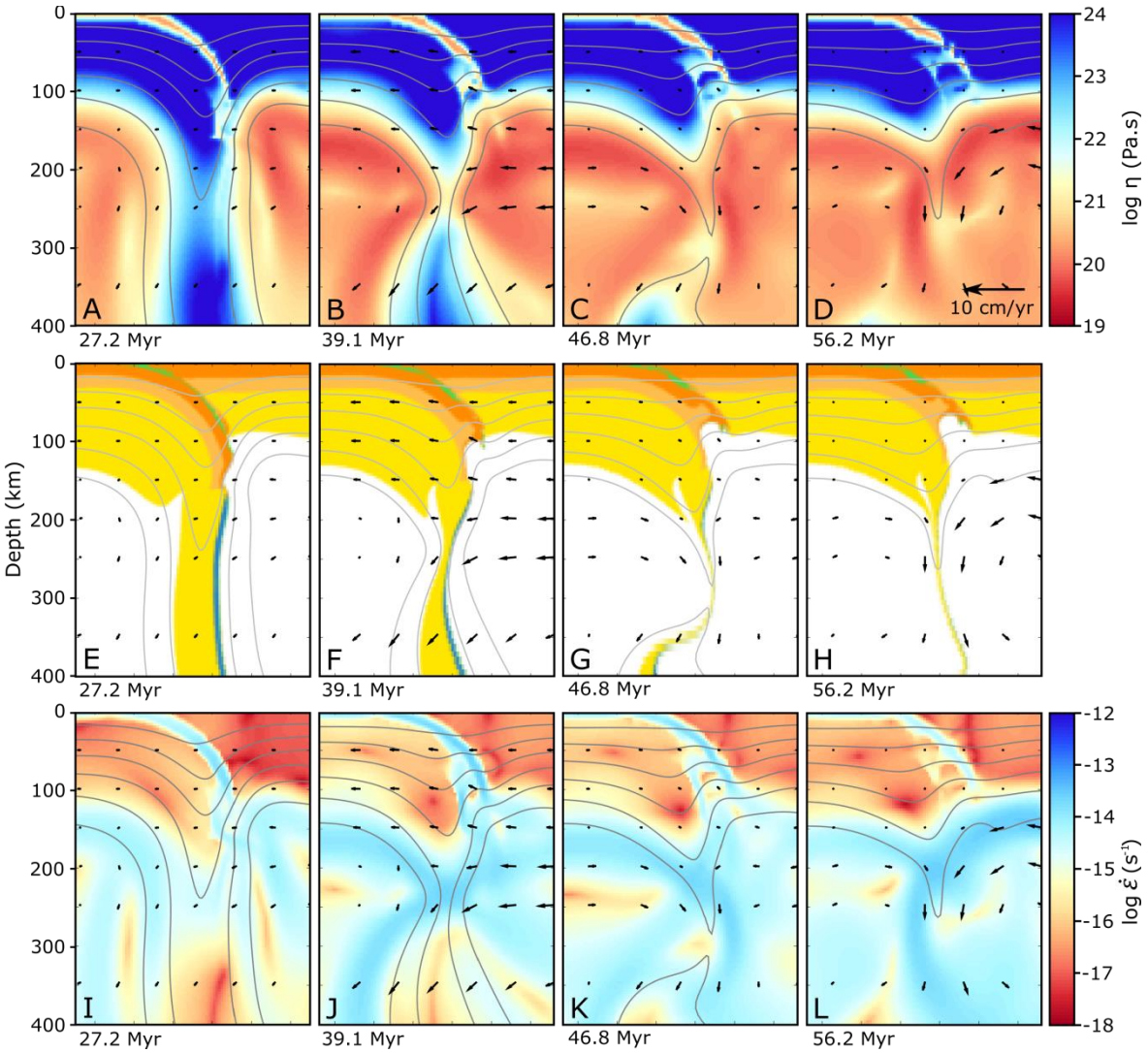


**Figure 3.11: Breakoff dynamics for Model 22 - 30 Myr oceanic lithosphere.** Panels are as in Fig. 3.3.

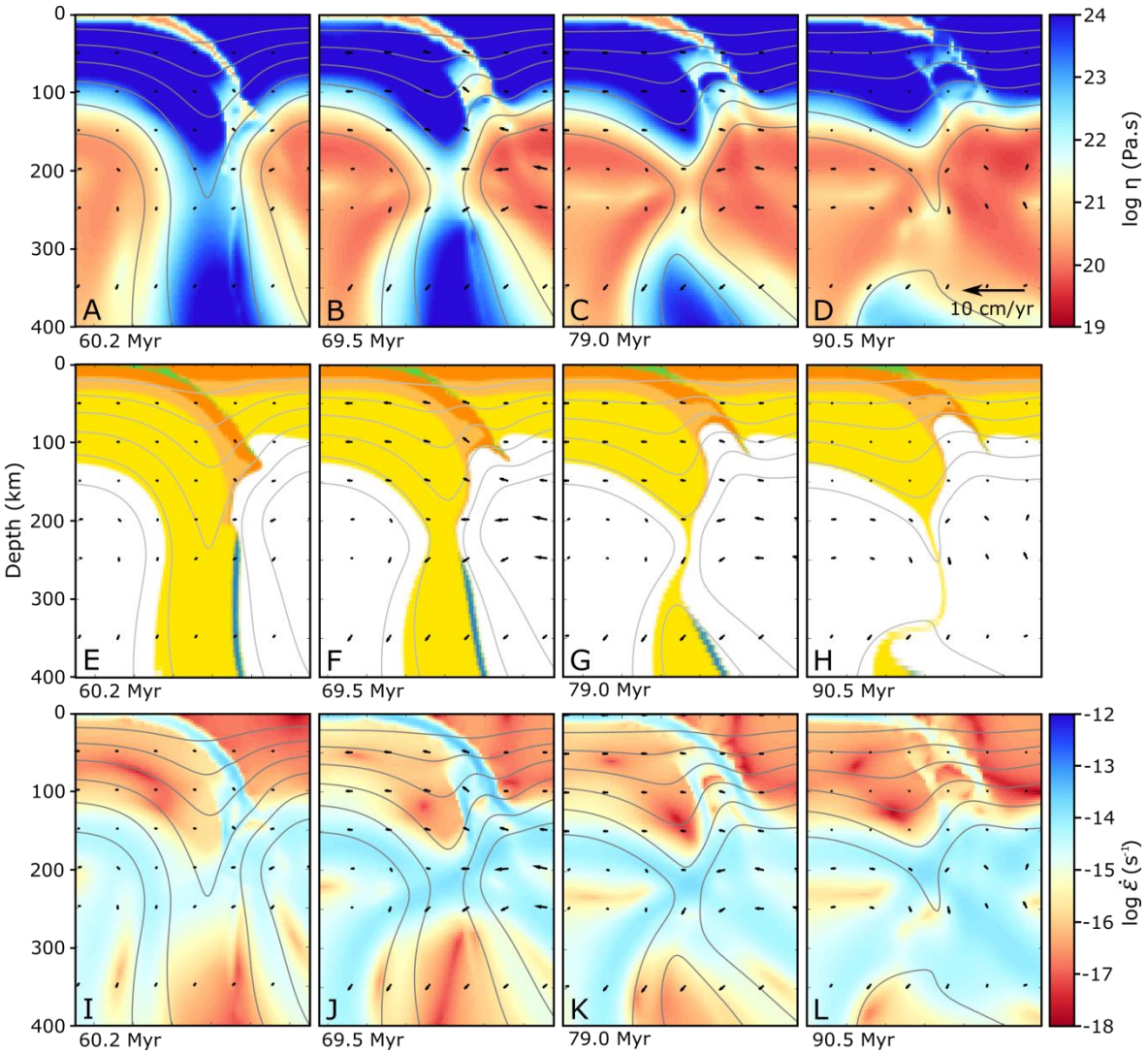


**Figure 3.12: Breakoff dynamics for Model 24 - 100 Myr oceanic lithosphere.** Panels are as in Fig. 3.3.

### 3.3.2.6 Overriding lithospheric thickness

Decreasing the overriding lithospheric thickness from 100 to 60 km slightly reduces both the breakoff depth and timing by 15 km and 13 Myr, respectively (Fig. 3.2). The decrease in thickness results in a reduction in the depth of the hot mantle wedge, and hence necking and weakening of the slab localises shallower within the oceanic lithosphere (Figs. 3.13A, 3.13E, and 3.13I). The mantle adjacent to the slab, being shallower, is also weaker, and a more vigorous mantle flow is generated underneath the overriding lithosphere. This proves more effective at thinning the subducted slab, and, along with the increase in downward force acting on the slab caused by the shallower breakoff depth, decreases the amount of time taken for the slab to break apart (Figs. 3.13B, 3.13F, and 3.13J). A thinner overriding lithosphere also results in a shallower maximum depth of continental crustal subduction, as

the crust reaches higher temperatures at shallower depths compared to when a thicker lithosphere is implemented (Fig. 3.13E).

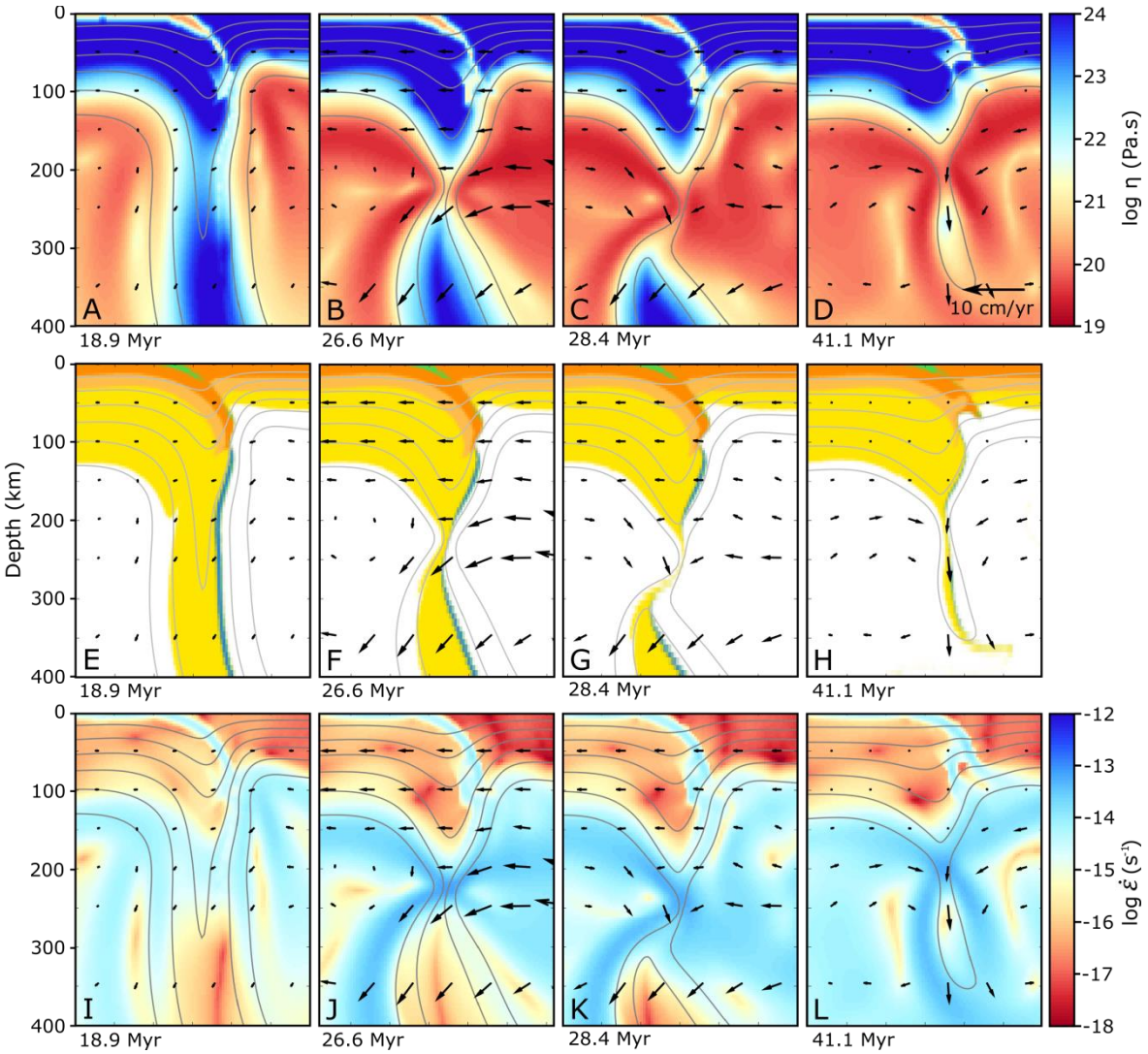


**Figure 3.13: Breakoff dynamics for Model 21 - 60 km overriding lithospheric thickness.** Panels are as in Fig. 3.3.

### 3.3.2.7 Radiogenic heating

Including radiogenic heating of 0.7 $\mu Wm^{-3}$ within the continental crust significantly reduces the breakoff depth by 45 km, but has very little effect on the timing of breakoff (Fig. 3.2). The effect of radiogenic heating leads to significantly hotter crustal material within the subduction zone (up to 100 °C) and material that is up to twice as weak. This results in an earlier exhumation of the continental crust, initiating not after or during, but before the breakoff process (Figs. 3.14A, 3.14E, and 3.14I). The crustal exhumation separates the slab from cooler overlying lithospheric mantle, allowing the hotter asthenospheric mantle to heat

the stagnated slab at a shallower depth. This, combined with the thinner slab due to the removal of the crust, causes breakoff to localise at a shallower depth (Figs. 3.14B, 3.14F, and 3.14J). Breakoff takes place within the continental lithosphere, rather than the oceanic, as the continent is subducted to a greater depth (owing to the removal of the buoyant continental crust from the slab), and becomes situated where the tensile stresses exceed the slab strength. (Note that in this case, the strength profiles of the oceanic and continental lithosphere are similar, as the majority of the continental crust has detached from the mantle lithosphere, affecting both the thermal thickness of the slab and the slab rheology.)

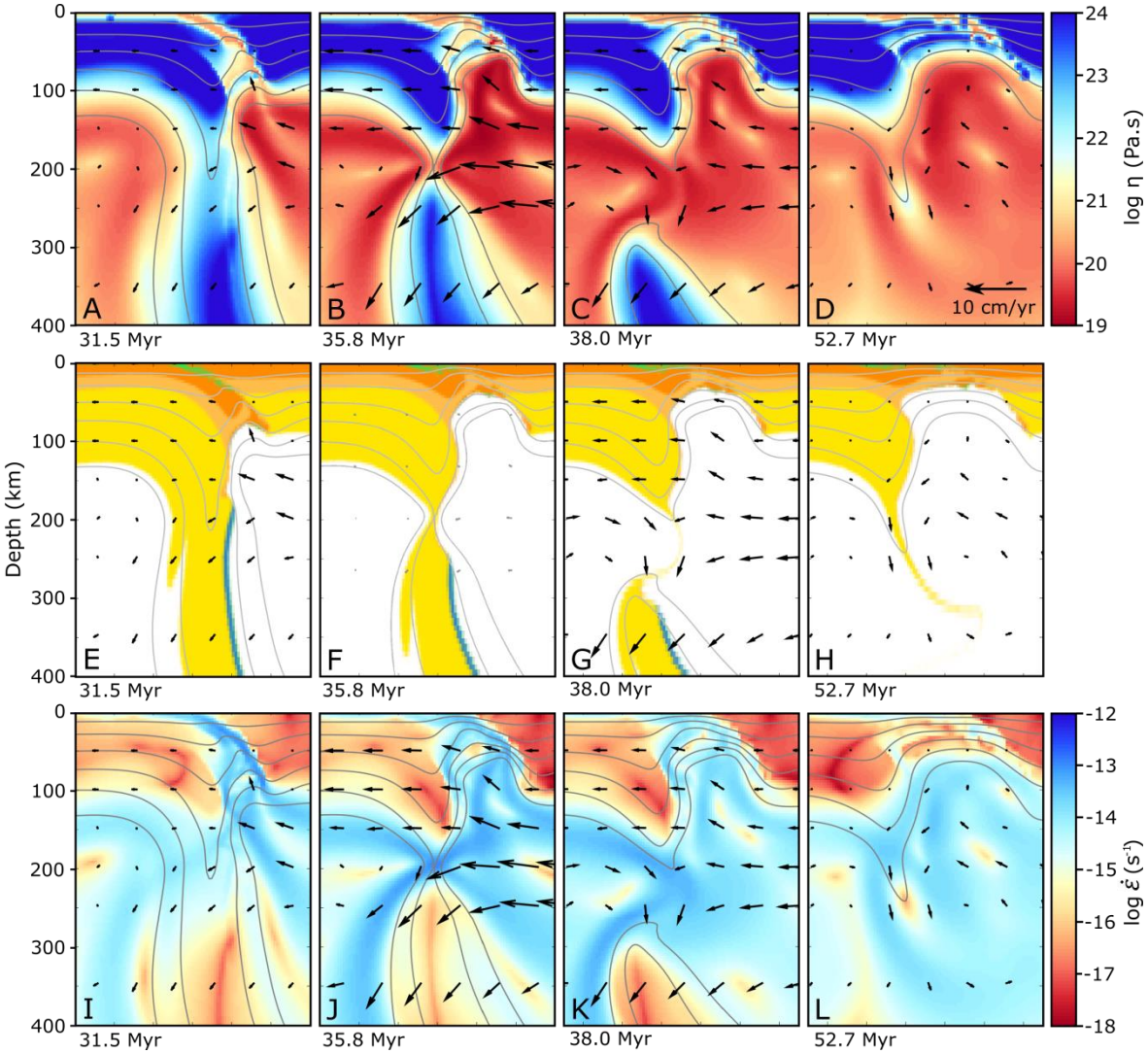


**Figure 3.14: Breakoff dynamics for Model 20 - continental crustal radiogenic heating.** Panels are as in Fig. 3.3.

#### 3.3.2.8 Brittle deformation mechanisms

To observe the effect that the brittle deformation has on breakoff, a number of parameters are varied independently: the cohesion from 0 to 100 MPa, the maximum yield strength from 400 to 800 MPa, the friction coefficient from 0.1 to 0.6. The influence of these parameters is very small compared to other parameters that are tested, but does have some effect on both the breakoff depth and timing (Fig. 3.2). The maximum yield strength has no effect on the breakoff depth, but the breakoff time is slightly increased for a higher yield strength. Increases in the cohesion and friction coefficient both cause a slight increase in breakoff depth and timing. Breakoff for all these models occurs through viscous necking, and brittle failure of the slab is not initiated by varying the above parameters. Hence, the slight variations in breakoff depth and timing are probably a result of small differences in the crustal dynamics and behaviour of the colder, shallower lithosphere, which is affected by brittle deformation.

#### 3.3.2.9 Weak zone strength

Varying the weak zone viscosity by up to an order of magnitude produces a range in convergence velocities of 4 - 8 cm/yr. This has an almost insignificant effect on breakoff depth (< 10 km), but can cause a reduction in breakoff timing by almost 10 Myr for a faster convergence rate (Fig. 3.2).

### 3.3.3 Key model dynamics

#### 3.3.3.1 Breakoff location

When testing the range of values for the parameters within this study, a switch in breakoff location from the oceanic lithosphere to shallower depths either within the continental lithosphere or at the ocean-continent boundary (OCB) is often observed. This occurs when the continental lithosphere becomes the weakest place within the stagnated slab, such as when implementing a weaker crustal rheology, thicker continental crust or older oceanic lithosphere. Increased exhumation of the buoyant continental crust can also promote this switch in location, as this leads to a thinning of the continental lithosphere. This leads to a large jump in breakoff depth for a relatively small change in parameter value. These changes in breakoff location are marked on Fig. 3.2 for each parameter.

#### 3.3.3.2 Thickness of the cold slab core

The thickness and temperature of the cold slab core around the collision zone can have a significant influence on the depth of breakoff. Breakoff localises where the tensile stresses, initiated by subduction of the buoyant continent, exceed the strength of the slab. These stresses are often greater at shallower depths, due to the greater weight of the stagnated slab. However, a thicker slab core results in cold, lithospheric material extending deeper into the mantle, and hence increases the depth to which the weakest part of the slab is located. A thicker continental lithosphere, an older oceanic lithosphere, and a thicker overriding lithosphere all result in a cooler and thicker slab core and a deeper breakoff depth.

#### 3.3.3.3 Mantle flow patterns

During slab necking, the main mantle flow is located below the overriding plate, resulting from the movement of the detached, lower part of the slab away from the overriding plate during this process (Figs. 3.1E, 3.1M, and 3.1U). As breakoff occurs, mantle also flows in from below the subducting plate at a rate of between 0 and 6 cm/yr (Figs. 3.1F, 3.1N, and 3.1V). These two flow patterns (Fig. 3.1G, white arrows) on either side of the descending slab are directed downwards at the locality of breakoff, and asthenospheric mantle does not upwell through the slab window towards the overriding plate. The increase in flow velocity upon necking and breakoff is sustained for a relatively short period of time (<10 Myr), controlled by the rate of viscous slab necking and subsequent descent of the detached slab into the deeper mantle. Using a weaker mantle rheology increases the velocity of this flow, but does not affect this pattern of convection.

### 3.3.4 Partial melting calculations

Using the parameterised solidus of Katz et al. (2003), the amount of melting is determined, assuming a bulk water content of 0 wt%. The increase in temperature or bulk water that would be required to bring the mantle material to the solidus temperature is also calculated. Three models are analysed: the reference model; the model showing the shallowest breakoff at a depth of 175 km, which also has the strongest mantle flow upon breakoff; and the model with the strongest mantle upwelling (Fig. 3.15).

#### 3.3.4.1 Reference model

No melting is produced in the reference model throughout the necking and breakoff process. Breakoff occurs below the base of the overriding lithosphere, and hence melting is not

generated through heating of the overriding lithosphere in direct contact with the slab window, or through decompression melting of dry asthenosphere. Although no mantle upwelling through the slab window occurs as a direct result of breakoff, crustal exhumation and extension within the overriding plate can induce a slight upwards flow of mantle. This area is closest to reaching the solidus, requiring a temperature increase of less than 150 °C, or a bulk water content of 0.08 wt% (Figs. 3.15A.i and 3.15A.ii). The depth to the base of the overriding lithosphere is not significantly reduced by heating during the breakoff event, and requires a temperature increase of over 300 °C to melt, similar to that pre-breakoff (Figs. 3.15A.ii and 3.15A.iv). Following breakoff, a general cooling in the collisional system is observed, rather than a transfer of heat to this area. If the lithosphere were hydrated with a bulk water content of around more than 0.2 wt% (i.e. water-saturated according to the parameterised solidus), it could melt below a depth of 80 km (Figs. 3.15A.i and 3.15A.iii). However, this melting would then be observable throughout collision, as it is not directly induced by breakoff. Additionally, no sustained mantle upwelling is observed, nor any small-scale convection at the base of the lithosphere as a result of breakoff which could heat the

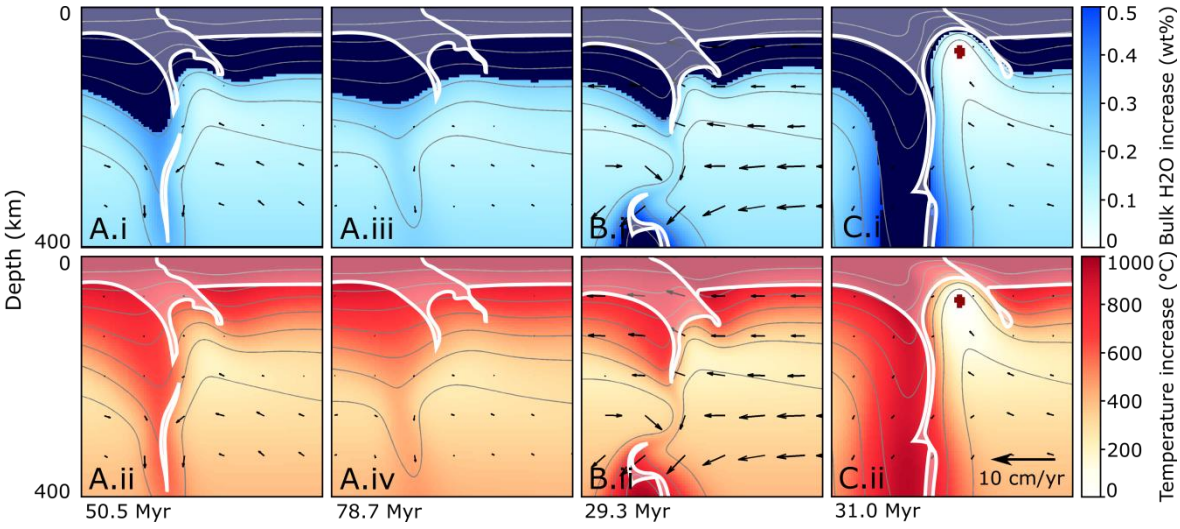


**Figure 3.15: Increase in bulk water content or temperature required for the ambient mantle temperature to exceed the solidus.** Crustal material is shaded and outlined in white, as the parameterised solidus is not applicable for this material. Dark red represents areas of melting. Dark blue on the subplots of bulk water increase show where melting is not possible through hydration, as an increase greater than the saturated water content is required. A - Reference Model 1 for two different model times. No melting nor increase in overriding lithospheric temperature is observed. B - Model 19, with shallowest breakoff and fastest mantle flow. C - Model 6, with strongest mantle upwelling. Asthenospheric decompression melting occurs below the exhumation of continental crust before breakoff.

lithosphere. Around the slab window, a temperature increase of over 500 °C is required to generate melting (Fig. 3.15A.ii). However, if this area was hydrated with a bulk water content of 0.27 wt%, the solidus would be reduced to ambient mantle temperatures (Fig. 3.15A.i).

#### 3.3.4.2 Shallow breakoff and strong mantle flow model

Model 19, with a 50 km thick continental crust (Fig. 3.10), is chosen to assess the viability of melting where breakoff occurs at a shallower depth and also induces the fastest flow through the slab window. Despite breakoff occurring 70 km shallower than for the reference model, no melting during breakoff is observed. The area of mantle below the upward exhumation of the continental crust again requires the lowest temperature increase to exceed the solidus (Fig. 3.15B.ii). The overriding lithosphere can become slightly heated by this crustal exhumation, but, despite the strong mantle flow through the slab window upon breakoff, this cannot produce any further heating. The mantle flow is only transient, and is not directed upwards, and hence is unable to bring a hotter asthenospheric flow in close enough proximity to the overriding lithosphere to generate any thermal perturbation.

#### 3.3.4.3 Strong mantle upwelling model

Model 6 with the weakest continental crust (Fig. 3.4) displays the most crustal exhumation and extension, leading to the most significant mantle upwelling. Small amounts of melting reaching a maximum of 4 wt% over an area of ~ 15 km and sustained for ~5 Myr are produced at a depth of <70 km underneath the extending area (Fig. 3.15C). An area twice as wide would melt if hydrated with a bulk water content of only 0.02 wt% (Fig. 3.15C.i). Despite the inflow of hot asthenospheric mantle into this area, a temperature increase of over 250 °C would be required to melt the adjacent lithospheric mantle (Fig. 3.15C.ii).

## 3.4 Discussion

This study has allowed the systematic investigation of the relative controls on the breakoff dynamics, including parameters which had previously been relatively unexplored, in order to gain an insight into the possibility of the generation of post-collisional mantle melting directly induced by the breakoff process.

### 3.4.1 Modelled versus observed subduction angles

The subduction angle in this study is allowed to develop naturally after the initial period of forced slab roll-back, and is not controlled by imposing any additional forces on the plates. Observations from subduction zones worldwide show a mean slab dip of 32° at shallow depths (≤125 km) and of 58° at deeper depths (> 125 km) (Lallemand et al., 2005). Based upon the temperature profile after subduction has reached a steady-state condition (i.e. retreating at a constant velocity with an unchanging slab dip), the slab in this study has an average dip of ~48° at depths of ≤125 km and of ~76° at depths of 125-400 km. A number of factors may contribute to the slab having a steeper angle than might be expected. The viscosity of the mantle determines the amount of resistance to the rollback of the slab and affects both the shallow and deep slab dip angles. Furthermore, the value of the friction coefficient controls the ability of the slab to bend upon subduction which affects the slab dip at shallow depths. Finally, the possibility of extension or compression within the back-arc is not modelled, which has been found to have a significant correlation with the dip angle (Lallemand et al., 2005). It is not anticipated that this will have a significant effect on the results presented in this study, as the nature of the slab is always to steepen as continental collision progresses, independent of the initial slab dip. However, the possible nature of hydration within the overriding plate could be affected by a different dip angle, which could subsequently alter the amount of melting within this plate. The effect of more global or regional asthenospheric flows are not considered, which may affect the slab dip. This is discussed further in Chapter 5.2.3.

### 3.4.2 Viability of shallow breakoff-induced melting

Early studies suggest that for breakoff to induce melting, breakoff at depths shallower than the base of the overriding lithosphere is required (Davies and von Blanckenburg, 1995; van de Zedde and Wortel, 2001; von Blanckenburg and Davies, 1995). From the range of parameters tested in this study, the continental lithospheric thickness, continental crustal thickness and radiogenic heating were found to have the biggest control on the depth of breakoff. These affect the strength of the subducting continental lithosphere, and can result in a significant decrease in depth when breakoff shifts in location from within the oceanic lithosphere to the continental lithosphere. Despite this, breakoff is not observed at depths shallower than 175 km. The observed range in breakoff depth (175 - 280 km) is compatible with results from other numerical studies (e.g. Andrews and Billen, 2009; van Hunen and Allen, 2011). However, as the shallower or deeper values that some studies show are not observed (Baumann et al., 2010; Duretz et al., 2011), it may be that other parameters need to

be explored (such as other deformation mechanisms or variations in material densities) or variations in parameters need to be modelled synchronously to achieve this wider spectrum. Despite this, this study provides perhaps a range of depths that might be expected in typical collisional environments and suggests that shallow breakoff may only be produced under more unusual conditions. This has implications for interpreting the causes of post-collisional magmatism. Often, when slab breakoff is invoked to account for this melting, it is assumed breakoff can readily occur at depths shallow enough to generate excessive melting, based upon early calculations of breakoff depth, rather than more recent, dynamical models.

### 3.4.3 Viability of deep breakoff-induced melting

The application of a parameterised solidus to the results shows no mantle melting would occur as a direct result of necking and breakoff. The only melting that is observed occurs during exhumation of the continental crust, as a result of upwelling of asthenospheric mantle below this area whilst it undergoes slight extension. However, this is neglecting the possible hydrated state of the mantle material during collision and breakoff. Hydration of the mantle acts to significantly reduce the solidus, which could generate melting even where breakoff does not occur at very shallow depths. In the following sections, a number of different mechanisms through which breakoff, at depths greater than the overriding lithosphere, could melt both the asthenospheric and lithospheric mantle are summarised and discussed in relation to the results (Fig. 3.16):

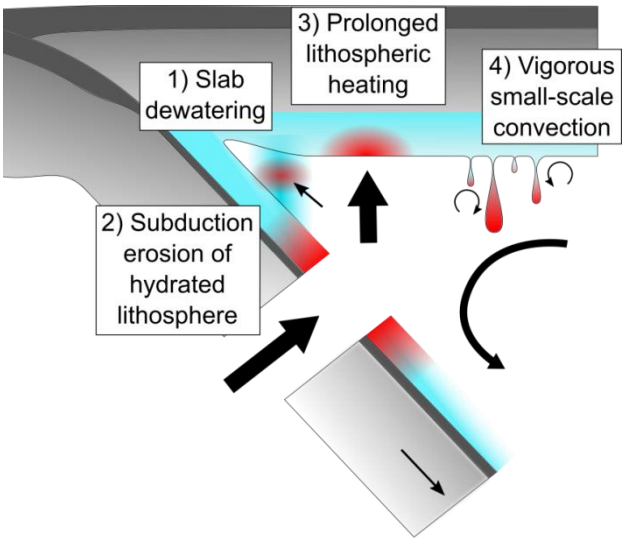


**Figure 3.16: Possible mechanisms for slab breakoff-related melting following breakoff deeper than the overriding lithosphere.** These mechanisms rely upon a hydrated state of the mantle lithosphere and asthenosphere.

#### 3.4.3.1 **Melting of the upwelling asthenosphere through slab dewatering** (Fig. 3.16 - 1) Slab dewatering)

It has been suggested that stagnant slabs may still be capable of releasing fluids after collision, due to increasing temperatures through heat diffusion (Faccenda et al., 2009; Neill et al., 2013). This may provide an effective means of melting the asthenospheric mantle during collision, where the mantle does not upwell to shallow enough depths to melt through dry decompressional processes.

In all models, the area most likely to undergo melting is that underneath the exhuming continental crust. With small amounts of water it seems likely that this area would melt within many of these models. The presence of nominally anhydrous minerals (NAMs) within the continental crust can become unstable upon a decrease in pressure, releasing water (Zheng, 2009). Although only small amounts of water are stored in NAMs, they could provide sufficient amounts to cause mantle melting during exhumation. However, the process of crustal exhumation within an extensional setting is not observed in the major present-day collisional environments such as the ones that followed the closure of the Neo-Tethys (e.g. Arabia-Eurasia and India-Eurasia collision). Where ongoing collision occurs, it seems unlikely that mantle material would be able to upwell in this setting, even where exhumation of the crust occurs. However, even if mantle upwelling was not present, this material could still melt if it became hydrated. It is possible that the slab could release water as it heats up and hydrate the surrounding mantle (Fig. 3.16 - 1) Slab dewatering). The results of this study suggest that the mantle would need to be hydrated with only small amounts of water to reduce the solidus to ambient mantle temperatures (<0.15 wt%). This potential melting may not therefore be a direct result of breakoff, but linked to slab heating after collision.

#### 3.4.3.2 **Melting around the slab window through subduction erosion** (Fig. 3.16 - 2) Subduction erosion of hydrated lithosphere)

Thorkelson (1996) suggest that hydrated material from the overriding lithosphere may be carried down on top of the slab, through subduction erosion during the preceding oceanic subduction, but not reach sufficient temperatures to melt due to the close proximity to the cooler oceanic lithosphere. The opening of a slab window upon breakoff could put hot asthenospheric mantle from underneath the slab in contact with this hydrated area and raise the temperature above the solidus (Fig. 3.16 - 2) Subduction erosion of hydrated lithosphere).

The results show that upon breakoff, the slab window remains the coolest part of the mantle around the depth of breakoff, and increases in temperature until it equilibrises with the surrounding asthenospheric mantle. The breakoff mechanism by itself is unable to generate melting of the mantle around the slab window for breakoff at the depths observed in this study. Melting could be possible if the area around the slab window was hydrated. The results suggest that only a small amount of hydration is required to melt this area, and hence this could be a viable mechanism for generating post-collisional melting, although no subduction erosion is observed within the models. However, we suggest that were this to occur, it may not necessarily coincide with breakoff, but may instead be related to the gradual increase in temperature of the stagnated slab, as necking occurs fairly slowly through viscous deformation.

#### 3.4.3.3 Melting of the overriding lithosphere through prolonged heating and small-scale convection (SSC) (Fig. 3.16 - 3) Prolonged lithospheric heating & 4) Vigorous small-scale convection)

It is possible that the upwelling of the asthenosphere as a result of breakoff could still transfer heat and raise the temperature of the overriding lithospheric mantle above the solidus, particularly if this material were to be hydrated, even where breakoff occurs at depths greater than the overriding plate (Fig. 3.16 - 3) Prolonged lithospheric heating). This flow would both need to be sustained for several million years, with the exact period dependent upon the location of the hydration within the overriding lithosphere (Davies and von Blanckenburg, 1995), and in sufficient proximity to the overriding lithosphere to generate a thermal perturbation. Previous numerical models have observed an upwelling of asthenosphere from behind the detached slab towards the mantle wedge during slab tearing (Li et al., 2013; Menant et al., 2016), although in some cases this is only sustained for very short periods of time (Burkett and Billen, 2010), or is focused deeper within the upper mantle where it is unable to transmit any thermal perturbation into the overriding plate (Andrews and Billen, 2009; Magni et al., 2012).

No significant increase in the temperature of the overriding lithosphere is observed as a result of slab breakoff. The flow within the mantle wedge does increase upon necking and breakoff, and a number of parameters can result in a stronger mantle flow during this period, including a weaker mantle rheology and a thinner overriding plate. Additionally, a faster breakoff (i.e. the period between initial necking and detachment) results in a stronger mantle flow. However, this flow is always short-lived and located relatively deep, and is unable to cause any significant thermal perturbation within the overriding plate. Other numerical

studies that show more upwelling through the slab window apply imposed velocity boundary conditions, which allow the slab to continue converging after collision, and provide an additional driving force for this mantle flow (Li et al., 2013; Menant et al., 2016). This sustained flow may be more representative of the major Neo-Tethyan collision zones today, which display continued convergence. A mantle plume, which could be a cause of this convergence (Cande and Stegman, 2011; Faccenna et al., 2013), would also be hotter than the asthenospheric mantle above the subducting slab and may provide additional heat to raise the overriding lithosphere above the solidus. For example, a plume has been suggested for the signature of the South-Eastern Alps volcanics (Macera et al., 2008). The effects of mantle flow in three dimensions are also not considered. Van Hunen and Allen (2011) show that upon breakoff, the slab tear is likely to propagate away from the initial breakoff location. Hence, mantle flow could be sustained for longer time periods that two dimensional models suggest, due to this prolonged breakoff process parallel to the suture zone.

In addition to heating through conduction, convection might also prove an effective mechanism to melt the overriding lithosphere. Vigorous flow triggered by breakoff could induce small-scale convection at the lithosphere-asthenosphere boundary and melt areas of hydrated lithosphere close in temperature to the solidus (Fig. 3.16 - 4) Vigorous small-scale convection) (similar to the mechanism of melting proposed by Kaislaniemi et al. (2014) within post-collisional areas). However, the deep pattern of mantle flow observed in these models prevents the formation of any small-scale convection at the base of the overriding lithosphere, suggesting that deeper breakoff is unable to trigger any melting of hydrated lithospheric mantle through this mechanism.

## 3.5 Conclusions

The breakoff dynamics, produced by the variety of parameters explored in this study, show the slab strength and the thickness of the cold slab core to have a dominant control on the breakoff depth. The strength of the continental lithosphere in particular can greatly reduce this depth, by leading to a change in breakoff locality from the oceanic lithosphere to the continental lithosphere, accompanied by a significant decrease in the depth of breakoff. However, within this study, the breakoff depth is always significantly deeper than the base of the overriding lithosphere. If this range of depths represents those typically found in nature, post-collisional magmatism may not commonly be the result of dry decompression melting or melting of the overriding lithosphere, although other factors not considered in this study may lead to breakoff at shallower depths. These results show that the mantle flow generated by slab breakoff is both short-lived and located fairly deep within the upper mantle. Mantle

rheology in particular, which has been investigated infrequently in previous studies, has a significant effect on the timing of breakoff and the resulting mantle dynamics. This breakoff-induced flow pattern suggests that melting of the overriding lithosphere, either through prolonged heating or the initiation of small-scale convection at the lithosphere-asthenosphere boundary is unlikely. Despite this, the presence of fluids may be able to generate mantle melting; both of asthenospheric material, potentially hydrated by the release of fluids from the slab, and of potentially hydrated subducted mantle lithosphere, upon the heating of the slab during collision; although these may be a result of continental collision, rather than directly linked to the breakoff process.

# Chapter 4

# Does slab breakoff induce post-collisional melting?

## 4.1 Introduction

The nature and distribution of post-collisional magmas differ markedly from those corresponding to the pre-collisional history of convergence zones. Oceanic subduction creates linear belts of arcs dominated by calc-alkaline series, whereas post collisional magmatism is more diverse chemically, and more widespread spatially. It can extend 100s of kilometres from the suture zone and can be sustained for millions of years after initial collision of the continental plates, although short-lived pulses of more intense melting and longer quiescent periods have been observed, as well as systematic variations in space and time (Chung et al., 2005; Pearce et al., 1990; Wen et al., 2008). Magmatism across these areas appears to originate from a variety of different sources, displaying signatures characteristic of crustal, subcontinental lithospheric and asthenospheric material (e.g. Lee et al. 2012).

Many different mechanisms have been proposed to explain magmatism in continental collisional areas. These include processes involving solely the continental crust: shear heating along crustal faults (Harrison et al., 1998); melting of thickened crust (England and Thompson, 1986); and the exhumation of crust back to the surface (Harris and Massey,

---

This chapter has been submitted as Freeburn, R.J., Bouilhol, P., Maunder, B., Magni, V., van Hunen, J., Numerical models of the magmatic processes induced by slab breakoff, Earth Planet. Sci. Lett. The numerical experiments were conducted and the manuscript produced by R.J. Freeburn. The co-authors have participated in this study by providing training, feedback on the manuscript, and useful discussions on the model development and petrological aspects of this work.

1994). Additionally, processes may involve an influx of heat or melt from the underlying mantle: large scale lithospheric delamination (Bird, 1978); slab breakoff (Davies and von Blanckenburg, 1995); edge-driven convection (Kaislaniemi and van Hunen, 2014) and small-scale convection at the base of the lithosphere (Kaislaniemi et al., 2014b). But of all these processes, slab breakoff after collision is often invoked to explain the changes in the nature and composition of magmas in collisional areas (Coulon et al., 2002; Mahéo et al., 2002; von Blanckenburg and Davies, 1995). Upon continental collision, the subducted slab may weaken due to thermal heating and/or increased extensional stresses between the more buoyant continental and denser oceanic lithospheres, resulting in slab breakoff and the formation of a slab window, and possibly leading to magmatism (van Hunen and Allen, 2011).

The dynamics of slab breakoff has been investigated extensively, and it has been shown that the strength of the subducting oceanic and continental lithospheres, in part influenced by the oceanic slab age, convergence velocity, and continental crustal and lithospheric thicknesses, and the mechanism of detachment, all have a control on the depth of breakoff (Andrews and Billen, 2009; Duretz et al., 2011; Gerya et al., 2004). Models have shown a wide range in this depth, from 40 to over 500 km (Baumann et al., 2010; Duretz et al., 2011), and have shown the importance of a 3D geometry in some cases (Magni et al., 2014b; Menant et al., 2016; van Hunen and Allen, 2011). Slab breakoff may be fairly well constrained dynamically, but its consequences in terms of magmatism remains unclear. Previous studies have suggested that hot asthenosphere, flowing up through the slab window, may have the potential to melt through decompression and/or heat both the subducting crustal material and the overriding continental lithosphere (Davies and von Blanckenburg, 1995; Thorkelson, 1996; van de Zedde and Wortel, 2001). Melting of the overriding lithosphere is viable where breakoff occurs at depths shallower than the base of this layer. However, asthenospheric melting may be less likely, as it requires very shallow breakoff at depths less than 50 km, unless the mantle is volatile rich.

These thermodynamic results are often determined by kinematic models of subduction, which do not focus on the complex dynamics of slab breakoff, the associated mantle flow and the hydration state of the system. Recent numerical studies use coupled petrological-thermomechanical numerical models to study the dynamics of collision and breakoff (Li et al., 2013; Menant et al., 2016); but a systematic investigation of the conditions required to generate breakoff induced melting has not yet been conducted, which is what is undertaken in this study.

Continental collision involves a succession of complex, interacting dynamical and petrological processes, of which the contribution of slab breakoff to post-collisional magmatism is the least well understood and constrained. Therefore, we use coupled petrological-thermomechanical numerical models to examine conditions for post-collisional magmatism, focusing on the magmatic consequences of slab breakoff in particular, so that its effect can be better understood and dissociated from other processes. We will do so by varying a number of key parameters which from the study in Chapter 3 were found to have a significant control on the breakoff dynamics, and by tracking the occurrence of melting of a number of different materials over time. The dynamics in our models are in line with previous numerical studies and replicate many of the features that have been previously observed during collision and breakoff (e.g. Duretz and Gerya, 2013; Ghazian and Buiter, 2013; Warren et al., 2008), and we thus use these models to explore the magmatic processes. We show that slab breakoff by itself is unlikely to explain all of the characteristics of post-collisional magmatism, and that additional processes may play an important role.

## 4.2 Method

This study builds upon that presented in Chapter 3, by using the dynamical results and the inferences made about melting in order to test conditions which are most likely to result in conditions that are favourable for slab breakoff-related melting. The same initial dynamical model setup is used for the reference model, but a multi-dimensional parameter study is employed across the numerical experiments in this chapter. This allows us to study more accurately the sensitivity of certain parameters and combinations of parameters on the breakoff dynamics and potential breakoff-related melting, and to encompass a wider range of breakoff styles, which may be necessary to observe any melting following breakoff. In addition, the results from Chapter 3 suggest hydration may be the key to generating melting following breakoff; in particular where breakoff occurs relatively deep within the upper mantle. A thermodynamic database is therefore used to observe the occurrence of (de)hydration reactions throughout collision and breakoff, and to investigate the link between the pattern of water migration and potential melting that may be induced by this.

### 4.2.1 Governing Equations

We use the Cartesian version of the finite element code Citcom to model oceanic and continental subduction (Moresi and Gurnis, 1996; van Hunen et al., 2005; Zhong et al., 2000). This solves for the conservation of mass, momentum, energy and composition in a fluid, assuming incompressible flow and adopting the Boussinesq approximations. A

standard non-dimensionalisation is applied to the governing equations, with symbols defined in Table 2.2:

$$x = x'h \tag{4.1}$$

$$t = t'h^2/\kappa \tag{4.2}$$

$$\eta = \eta'\eta_0 \tag{4.3}$$

$$T = T'\Delta T \tag{4.4}$$

Giving:

$$\nabla \cdot u = 0 \tag{4.5}$$

$$-\nabla p + \nabla \cdot \left(\eta(\nabla \mathrm{u} + \nabla u^T)\right) + (RaT - \sum_{i=1}^{N} Rb_i C_i)e_z = 0 \tag{4.6}$$

$$\frac{\partial T}{\partial t} + u \cdot \nabla T = \nabla^2 T + H \tag{4.7}$$

$$\frac{\partial C}{\partial t} + u \cdot \nabla C = 0 \tag{4.8}$$

The thermal Rayleigh number, *Ra*, is defined as:

$$Ra = \frac{\alpha \rho_0 g \Delta T h^3}{\kappa \eta_0} \tag{4.9}$$

and similarly the compositional Rayleigh number of a given composition $i$, $Rb_i$:

$$Rb_i = \frac{\Delta \rho_i g h^3}{\kappa \eta_0} \tag{4.10}$$

where $\Delta\rho_i$ is the intrinsic density of composition $i$ relative to mantle material.

The conservation of mass, momentum and energy are solved using a finite element technique, whilst the conservation of composition is solved using a particle-tracking technique (Di Giuseppe et al., 2008; Van Hunen et al., 2002; Hongliang Wang et al., 2015). Model parameters are described in Table 2.2.

### 4.2.2 Model setup

The model domain represents an area of 1980 x 660 km and consists of 512 x 128 finite elements. These have a varying grid size to achieve the highest resolution at the top of the model, with an element size of 3.3 x 3.3 $km^2$ in this area. The development of continental collision and breakoff of the oceanic lithosphere is modelled through the introduction of a continental lithospheric block into a subduction zone (Fig. 4.1) Here, 'collision' is defined as the point when the continental lithosphere first reaches the subduction trench and 'breakoff' as the point when the 1000°C isotherm ceases to be continuous in the slab, at the weakest point within the slab. An oceanic slab is initially positioned down to a depth of 250 km underneath an overriding continental lithosphere. At $x$=100 km a passive margin is initially emplaced, connecting the oceanic lithosphere to continental lithosphere, which subsequently flows in through the left hand boundary. To decouple the subducting and overriding plates a 1.3 km thick layer of sediments with a fixed viscosity of 2 x $10^{20}$ Pa s is positioned at the top of the subducting oceanic and continental lithospheres, which gradually increases to the background viscosity over a length of 13 km (see Maunder et al., 2016). Both oceanic and continental lithospheres are composed of crust and lithospheric mantle (see Table 2.1 and 2.3 for details of the rheological values used for differing compositions). The continental crust is split into an upper and lower crust, which have different rock compositions (affecting its dehydration and melting, see below), but otherwise have the same physical properties. Continental crust and sediments have a fixed relative density of -600 $kg/m^3$ and oceanic crust -300 $kg/m^3$, with respect to a reference mantle density of 3330 $kg/m^3$. At depths greater than 80 km, oceanic crust is prescribed a new density of +200 $kg/m^3$ to represent a simplified transition from basalt to eclogite. Compositional information is stored and advected using particles. Oceanic lithosphere initially obeys the half space cooling thermal profile for a given plate age of 50 Myr. All continental lithosphere has a thermal profile from 0°C at the surface to 1350°C at the base of the lithosphere. A constant initial mantle temperature of 1350°C is defined elsewhere. The rheological effect of adiabatic heating, which is absent in our models, is partly compensated for by using reduced values of the activation volume, $V$, in order to give a background viscosity profile in line with glacial isostatic adjustment data

(Mitrovica and Forte, 2004). A continental crust radiogenic heating of 0.7 $\mu Wm^{-3}$ (Fowler, 2005) is included in some model calculations, along with an initially higher crustal temperature profile.

Top and bottom boundaries have fixed temperatures of 0°C and 1350°C respectively, whilst side boundaries have a fixed continental geotherm (Fig. 4.1). To initially help the development of slab roll-back (as observed for the majority of subducting slabs worldwide (Funiciello et al., 2008)), a horizontal outflow (Fig. 4.1) is applied initially through the right boundary until the slab reaches a depth of 600 km, which has an average velocity of between 3 and 8 $cmyr^{-1}$. Subsequently, both side boundaries impose a zero horizontal deviatoric stress ($\sigma'_{xx}=0$ and $v_z=0$). This allows for a more natural development of flow within the model than when using closed, free-slip boundary conditions (Chertova et al., 2012). Slabs are assumed to stagnate at the base of the upper mantle, and hence a closed bottom boundary is applied, with a fixed velocity boundary during the initial imposed roll-back period, and no-slip following this. The top boundary is free slip to allow the natural movement of the subduction trench.

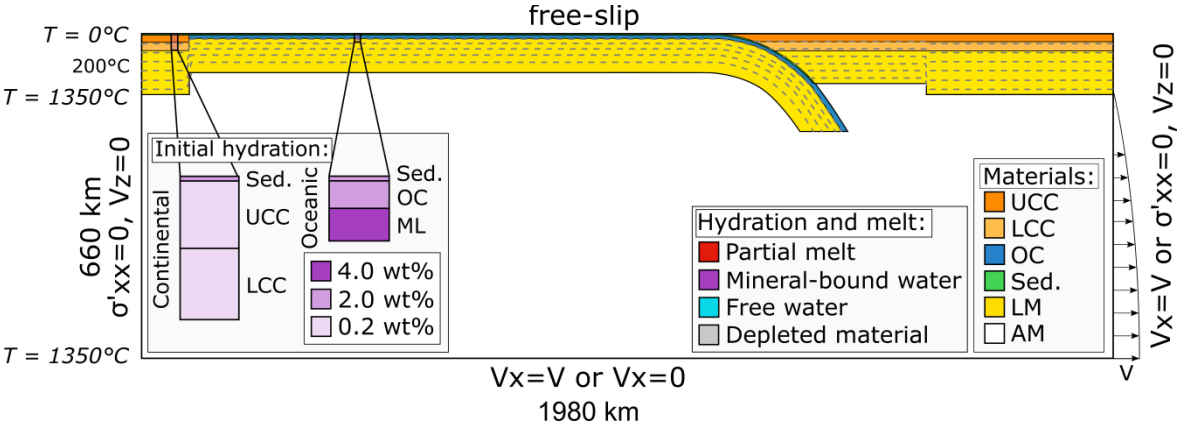


**Figure 4.1: Initial setup for the reference model (Model 1).** Showing initial positioning of materials, boundary conditions and the initial hydration state of both the continental and oceanic lithospheres. Two right hand side and bottom boundary conditions are used: one during the initial forced slab roll-back period, and one following this period. Material colours and name abbreviations apply to all subsequent figures and tables. Abbreviations used: UCC = upper continental crust, LCC = lower continental crust, OC = oceanic crust, sed = sediments, LM = lithospheric mantle, AM = asthenospheric mantle.

### 4.2.3 Hydration and melting implementation

We use a Gibbs free energy minimisation strategy to determine the metamorphic reactions, including (de)hydration reactions and melting reactions, occurring in the subducting slab and mantle. Equilibrium mineral assemblages are calculated beforehand using Perple_X (Connolly, 2009, 2005) for oceanic, upper and lower continental crustal, sediment, and primitive and depleted mantle lithologies for a range of pressures, temperatures and water contents and are stored in lookup tables (see Magni et al. (2014) for details and Table 2.4 and 2.5 for the composition of materials and details of the thermodynamic database used). Since Boussinesq approximations are used, a correction for the mantle adiabat of 0.5$^{o}$C/km is applied to the temperature profiles when determining the stable mineral assemblages. We use passive tracers that hold information about the composition to compute the stable phases at each time step. The presence and amount of melt under any given P-T-$H_2O$ conditions can hence be determined and the variations in water content tracked. An initial hydration profile is defined for the oceanic and continental lithosphere within the subducting plate, which is advected with the flow field (Fig. 4.1). Oceanic crust and sediments are uniformly hydrated with 2 wt% $H_2O$, continental crust with 0.2 wt%, and the upper 8 km of oceanic lithospheric mantle with 4 wt%. If free water is present according to the stable mineral assemblage, this water is allowed to percolate upwards, potentially rehydrating overlying material (see Bouilhol et al. (2015) and Magni et al. (2014) for details). During each timestep any free water is either re-absorbed into new hydrous minerals or is assumed to escape through the top of the model; hence we assume free water is capable of migrating significantly faster than the mantle flow.

To investigate the nature of any magmatism, we record the melting of six different compositions throughout the model calculations; the mantle lithosphere, asthenosphere, sediments, oceanic crust, and upper and lower continental crust. If melt is present and the amount exceeds a threshold, the melt is extracted instantaneously to the surface. Extraction threshold values of 2 and 8 wt% are chosen for mantle and crustal material, respectively, based upon the amount required to form an interconnected melt pathway and ascend to the surface (Brown, 2007; Faul, 1997). Upon melt extraction, the residue will change in composition making it less likely to melt again. Hence to account for this we assume that material that has undergone melt extraction is unable to re-melt. We record post-collisional melting, which is defined as any melting occurring after subduction-related melting has ceased. We also record breakoff-related melting, which is defined as melting which can be clearly linked to the necking and breakoff process, and is not a result of other post-collisional processes.

## 4.3 Results

We aim to analyse if and how breakoff induced melting is generated, and constrain the geodynamic conditions required. We systematically vary a number of parameters that the results from Chapter 3 show to have a significant control on the breakoff depth and/or timing, and record any changes that these dynamical differences produce in the style of melting. Models are conducted within a five-dimensional parameter space, with two values chosen for each of the following parameters; the ratio of continental crust to lithospheric thickness (35:125 km & 40:100 km), the radiogenic heating of the continental crust (0 & 0.7 $\mu Wm^{-3}$), the mantle rheological flow law (mean (partially hydrated) and -0.5 SD (hydrated) (see Chapter 2.3.1 and Maunder et al. (2016)), the crustal rheological flow law (plagioclase & dry quartzite) and the overriding lithospheric thickness (100 km & 60 km) (see Table 4.1, Models 1-32). As will be further discussed below, these values are not intended to cover the full observed parameter range, but instead focus on conditions that are potentially relevant for slab breakoff related melting, which is the key objective of this study.

| Model | Cont. FL | Mantle FL | CC/CL thickness (km) | RH ($\mu Wm^{-3}$) | OP thickness (km) | BO depth (km) | BO time (Myr) | BO location (O/C) |
|---|---|---|---|---|---|---|---|---|
| 1 | Plag. | Partially hydr. | 35/125 | 0 | 100 | 241 | 44.3 | O |
| 2 | Plag. | Partially hydr. | 35/125 | 0 | 60 | 224 | 26.7 | O |
| 3 | Plag. | Partially hydr. | 35/125 | 0.7 | 100 | 191 | 34.0 | C |
| 4 | Plag. | Partially hydr. | 35/125 | 0.7 | 60 | 172 | 25.3 | C |
| 5 | Plag. | Partially hydr. | 40/100 | 0 | 100 | 175 | 24.2 | C |
| 6 | Plag. | Partially hydr. | 40/100 | 0 | 60 | 159 | 16.6 | C |
| 7 | Plag. | Partially hydr. | 40/100 | 0.7 | 100 | 178 | 17.6 | C |
| 8 | Plag. | Partially hydr. | 40/100 | 0.7 | 60 | 149 | 12.3 | C |
| 9 | Plag. | Hydrated | 35/125 | 0 | 100 | 241 | 24.6 | O |
| 10 | Plag. | Hydrated | 35/125 | 0 | 60 | 195 | 14.7 | O |
| 11 | Plag. | Hydrated | 35/125 | 0.7 | 100 | 165 | 17.0 | C |
| 12 | Plag. | Hydrated | 35/125 | 0.7 | 60 | 135 | 10.5 | C |
| 13 | Plag. | Hydrated | 40/100 | 0 | 100 | 169 | 14.8 | C |

| | | | | | | | | |
|---|---|---|---|---|---|---|---|---|
| 14 | Plag. | Hydrated | 40/100 | 0 | 60 | 145 | 9.2 | C |
| 15 | Plag. | Hydrated | 40/100 | 0.7 | 100 | 168 | 10.0 | C |
| 16 | Plag. | Hydrated | 40/100 | 0.7 | 60 | 129 | 5.6 | C |
| 17 | Dry Qz. | Partially hydr. | 35/125 | 0 | 100 | 221 | 44.8 | C |
| 18 | Dry Qz. | Partially hydr. | 35/125 | 0 | 60 | 241 | 33.1 | O |
| 19 | Dry Qz. | Partially hydr. | 35/125 | 0.7 | 100 | 208 | 51.7 | C |
| 20 | Dry Qz. | Partially hydr. | 35/125 | 0.7 | 60 | 231 | 28.0 | C |
| 21 | Dry Qz. | Partially hydr. | 40/100 | 0 | 100 | 191 | 23.2 | C |
| 22 | Dry Qz. | Partially hydr. | 40/100 | 0 | 60 | 188 | 17.9 | C |
| 23 | Dry Qz. | Partially hydr. | 40/100 | 0.7 | 100 | 162 | 16.7 | C |
| 24 | Dry Qz. | Partially hydr. | 40/100 | 0.7 | 60 | 155 | 11.5 | C |
| 25 | Dry Qz. | Hydrated | 35/125 | 0 | 100 | 215 | 27.6 | C |
| 26 | Dry Qz. | Hydrated | 35/125 | 0 | 60 | 155 | 15.0 | C |
| 27 | Dry Qz. | Hydrated | 35/125 | 0.7 | 100 | 231 | 17.6 | C |
| 28 | Dry Qz. | Hydrated | 35/125 | 0.7 | 60 | 215 | 11.4 | C |
| 29 | Dry Qz. | Hydrated | 40/100 | 0 | 100 | 178 | 15.2 | C |
| 30 | Dry Qz. | Hydrated | 40/100 | 0 | 60 | 162 | 7.1 | C |
| 31 | Dry Qz. | Hydrated | 40/100 | 0.7 | 100 | 139 | 8.9 | C |
| 32 | Dry Qz. | Hydrated | 40/100 | 0.7 | 60 | 125 | 5.4 | C |
| 33 | Plag. | Hydrated | 50/75 | 0.7 | 100 | 83 | 1.7 | C |

**Table 4.1 Parameter values and breakoff dynamics across the parametric study.** Where values deviate from those used in the reference model, this is highlighted in grey. CC/CL thickness is a ratio of crustal to whole lithospheric thickness. Breakoff time is measure relative to initial collision. Breakoff location is either within the oceanic lithosphere (O) or continental lithosphere (C). Abbreviations: FL = flow law, CC = continental crust. CL = continental lithosphere, RH = radiogenic heating, OP = overriding plate, BO = breakoff, Plag. = plagioclase, hydr. = hydrated, Qz. = quartzite.

We first describe the development of the dynamical process of collision and breakoff and discuss any dehydration and melting for a reference model (Model 1, Section 4.3.1), which

will be shown to produce only small amounts of melt, and then for a model with a shallower breakoff depth that produces a significantly larger amount of melt (Model 13, Section 4.3.2). Next, we summarise the variation in breakoff dynamics and melting observed across the full parameter range of models within this study (Sections 4.3.3 and 4.3.4).

### 4.3.1 Reference model: breakoff dynamics and melting

Reference Model 1 (Table 4.1, Fig. 4.2) has parameter values that represent a typical continental collision zone. After an initial period of oceanic subduction (Figs. 4.2A, 4.2I, and 4.2Q) and roll-back, the continental lithosphere enters the subduction zone (Figs. 4.2B, 4.2J, and 4.2R). The convergence velocity decreases due to the positive buoyancy of the continental crust (Figs. 4.2C, 4.2K, and 4.2S), until the former passive margin stagnates at a depth of 150 km (Figs. 4.2D, 4.2L, and 4.2T). The temperature of the stagnated slab increases, which weakens both the buoyant subducted continental crust and oceanic lithosphere and results in necking within the oceanic lithosphere in this model (Figs. 4.2E, 4.2M, and 4.2U). The subducted continental crust begins to flow upwards, whilst necking proceeds through viscous deformation and results in final breakoff 44 Myr after initial collision at a depth of 240 km (Figs. 4.2F, 4.2N, and 4.2V). In total, the process from initial necking to slab breakoff lasts for 14 Myr. Buoyant crustal flow continues and leads to slight upwelling of asthenospheric mantle underneath the continental crust (Figs. 4.2G, 4.2O, and 4.2W).

Throughout oceanic subduction, breakdown of hydrous minerals within the sediments, oceanic crust and lithospheric mantle result in mantle wedge melting and hydration of the overriding lithosphere (Fig. 4.2I), as expected for oceanic subduction. As the continental lithosphere enters the subduction zone, melting of the mantle wedge corner declines and then stops completely 10 Myr after initial collision (Figs. 4.2J, 4.2K and 4.3A). The oceanic crust and lithosphere continue to dehydrate throughout the early stages of collision, due to the sustained increasing slab temperature (Fig. 4.2J). However, the reduction in convergence velocity causes a steepening of the subducted slab, which results in the flux of water moving upwards into the subducted mantle lithosphere and continental crust (Fig. 4.2K). Another consequence of this steepening is the appearance of saturated melting in the oceanic crust at depths > 200 km due to fluid advection (Bouilhol et al. 2015), as the subducted slab begins to neck and crustal temperatures exceed 1000 °C, but does not reach sufficient volumes to be extracted (i.e. > 8wt%, Figs. 4.2J, 4.2K, 4.2L and 4.3A). As the continental crust subsequently begins to be exhumed, small amounts of the deepest part of the subducted continental crust and sediments melt due to decompression melting (Figs. 4.2N, 4.2O, 4.2P

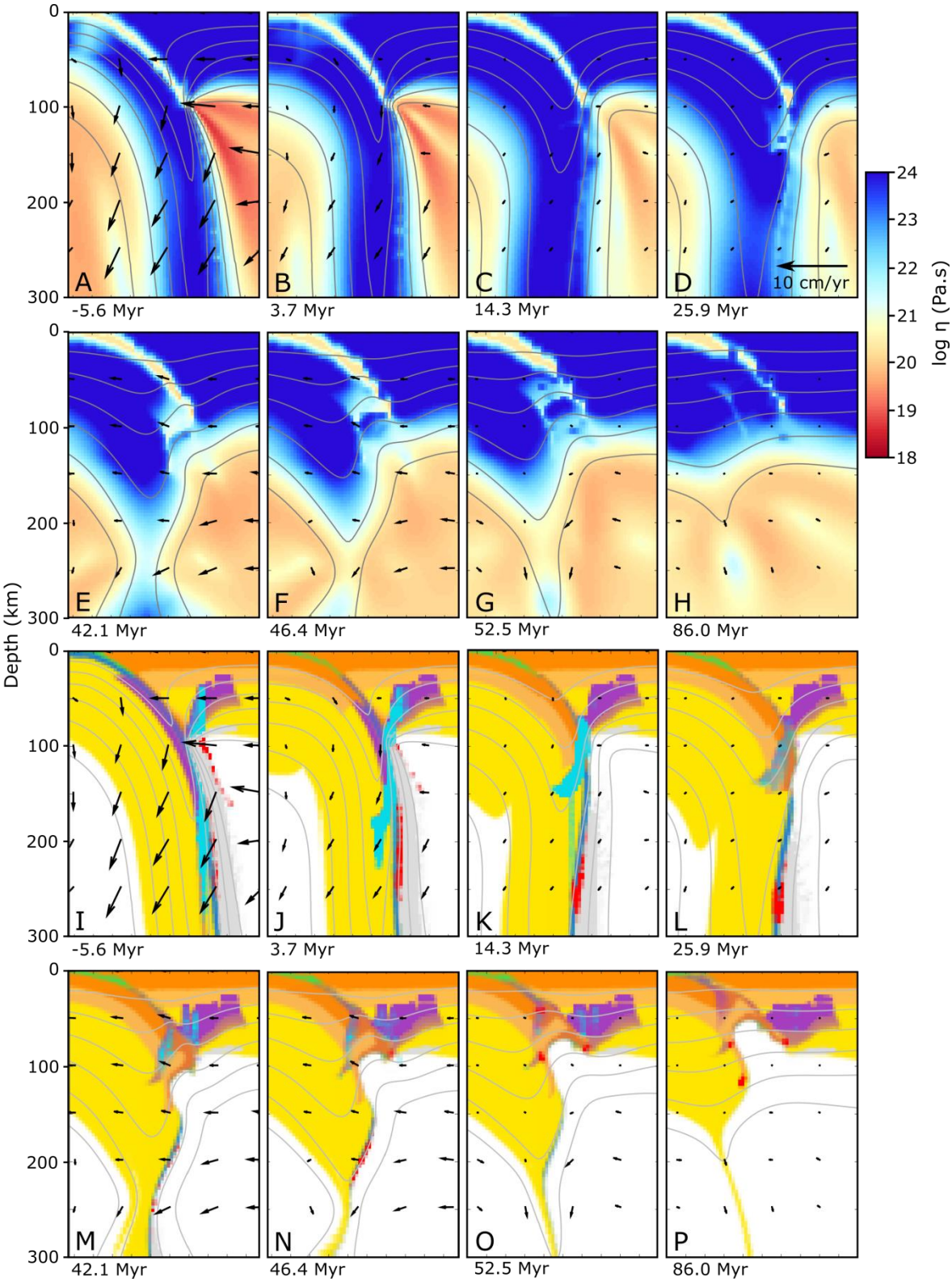
Depth (km)
0
100
200
300
A
B
C
D
-5.6 Myr
3.7 Myr
14.3 Myr
25.9 Myr
10 cm/yr
E
F
G
H
42.1 Myr
46.4 Myr
52.5 Myr
86.0 Myr
I
J
K
L
-5.6 Myr
3.7 Myr
14.3 Myr
25.9 Myr
M
N
O
P
42.1 Myr
46.4 Myr
52.5 Myr
86.0 Myr
log η (Pa.s)
24
23
22
21
20
19
18

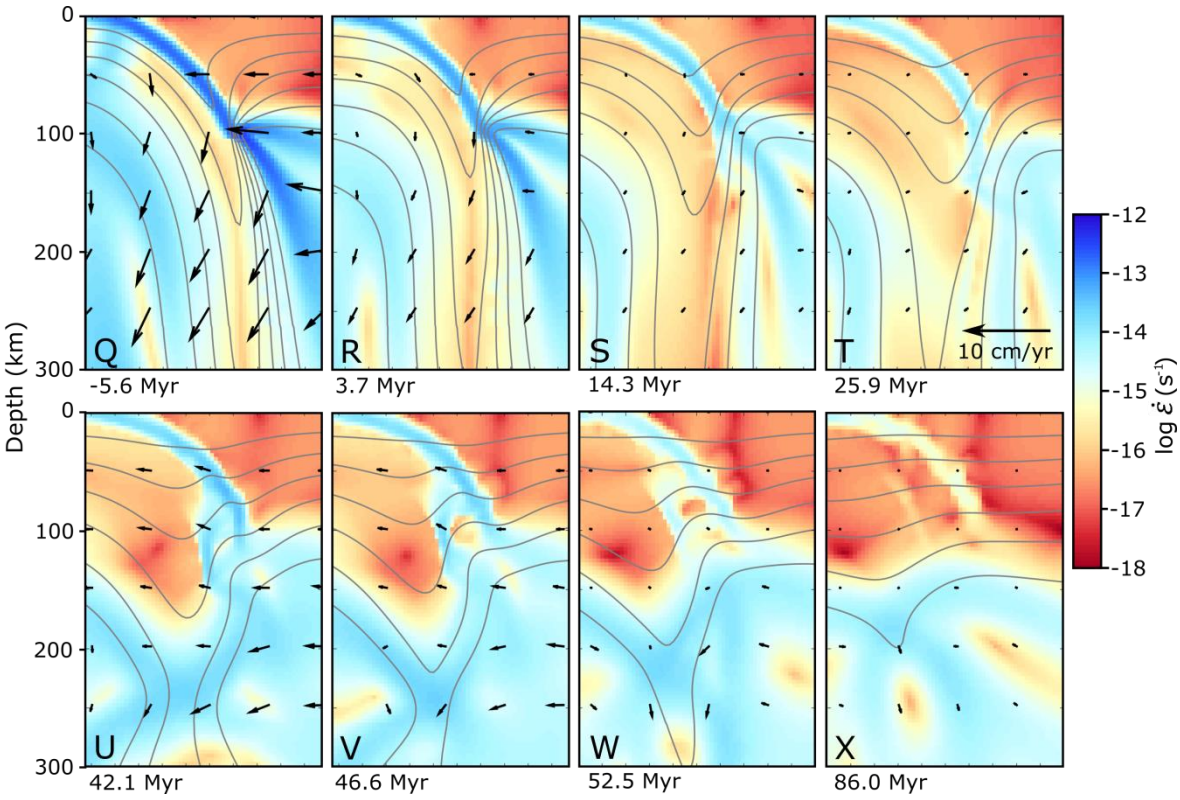


**Figure 4.2: Dynamics and melting of Model 1 (reference model).** Dynamics of Model 1 show oceanic subduction (Figs. 4.2A, 4.2I, and 4.2Q), continental subduction (Figs. 4.2B, 4.2J, and 4.2R), slab stagnation (Figs. 4.2D, 4.2L, and 4.2T), final breakoff (Figs. 4.2F, 4.2N, and 4.2V) and crustal exhumation (Figs. 4.2G, 4.2O, and 4.2W). Figs. 4.2A - 4.2H show the viscosity, 4.2I - 4.2P the position of different compositional materials based upon the locations of tracer particles within the model, and Q-X the strain rate. For the materials, hydration and melt colour legend see Fig. 4.1. Temperature contours are in grey and have an interval of 200 °C. The black arrows show the velocity of material from the point where the arrow begins. The scale for these velocity vectors is given in Figs. 4.1D and 4.1T and is representative of all panels. Timings are given relative to the time of initial collision. The horizontal length for each panel is 200 km.

and 4.3A). The continental crust can also become significantly hydrated throughout the collisional process (~2 wt%), resulting in small amounts of upper crustal melting at shallow depths of 50-100 km (Figs. 4.2O and 4.3A). This progresses for 15 Myr before the crust ceases exhuming and crustal temperatures decrease.

### 4.3.2 Shallow breakoff model: breakoff dynamics and melting

Model 13 (Table 4.1, Fig. 4.4) is characterised by a weaker crustal rheology, thicker continental crust and thinner continental lithosphere with respect to the reference model, and is chosen as a clear example of the other end of the spectrum of the explored parameter

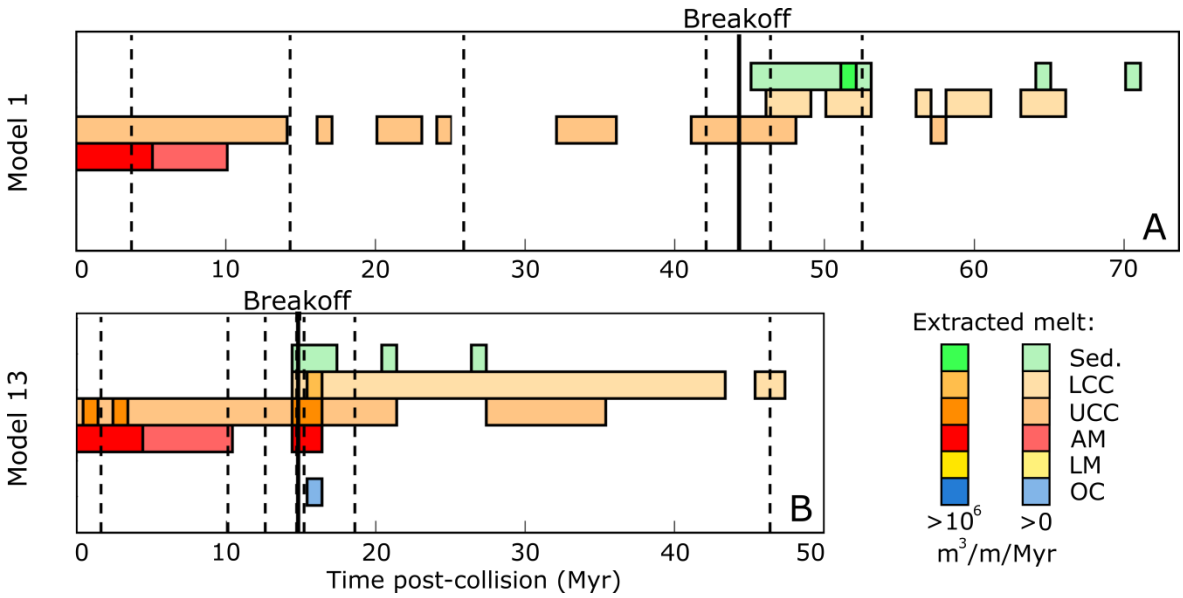


**Figure 4.3: Melting of Model 1 (reference model) and Model 13 (shallow breakoff model).** The extracted melt through time is shown below for each model. The vertical dashed lines show the times given in Figs. 4.2 and 4.4, while the vertical solid line defines the point of break-off. Pale colours show where any melt is extracted within 1 Myr, while bright colours represent melt that exceeds a limit of $1x10^6$ $m^3/m/Myr$. The volumes of melt are based on the thermodynamic database and are defined in $m^3/m/Myr$ (or in subsequent figures for total melt, $m^3/m$), but are only provided to compare the amount of melting observed through time between different models. For reference, if extrusive melt would spread evenly over a distance of 100 km, a volume of $1x10^8$ $m^3/m$ would correspond to a melt thickness of 1 km.

space, as it shows significant differences in breakoff depth, timing and location, and provides a clear example of the breakoff-related melting that we observe across the parametric study. The continental crust is subducted to similar depths after collision as compared to Model 1 (Fig. 4.4K). At the passive margin, necking and weakening of the crust and mantle lithosphere occurs, which progresses through both simple shearing and viscous necking (Fig. 4.4D, 4.4E, 4.4L, 4.4M, 4.4T, and 4.4U). Slab breakoff in this model occurs within the continental lithosphere at a significantly shallower depth of 170 km and with a shorter breakoff time of 15 Myr after initial collision (Fig. 4.4E, 4.4M, and 4.4U).

A continuum of melting is observed, affecting different lithologies at different depth, whilst slab breakoff proceeds after collision. Melting occurs along the edge of the stagnated continental crust during necking of the slab (Fig. 4.4M), which also leads to small amounts of sediment melting (Fig. 4.3B). This melting results from heating of continental crustal material within the tips of the detached slab as it descends into the mantle (Fig. 4.4N), and continues for a short-lived period after breakoff. This heating also results in the breakdown

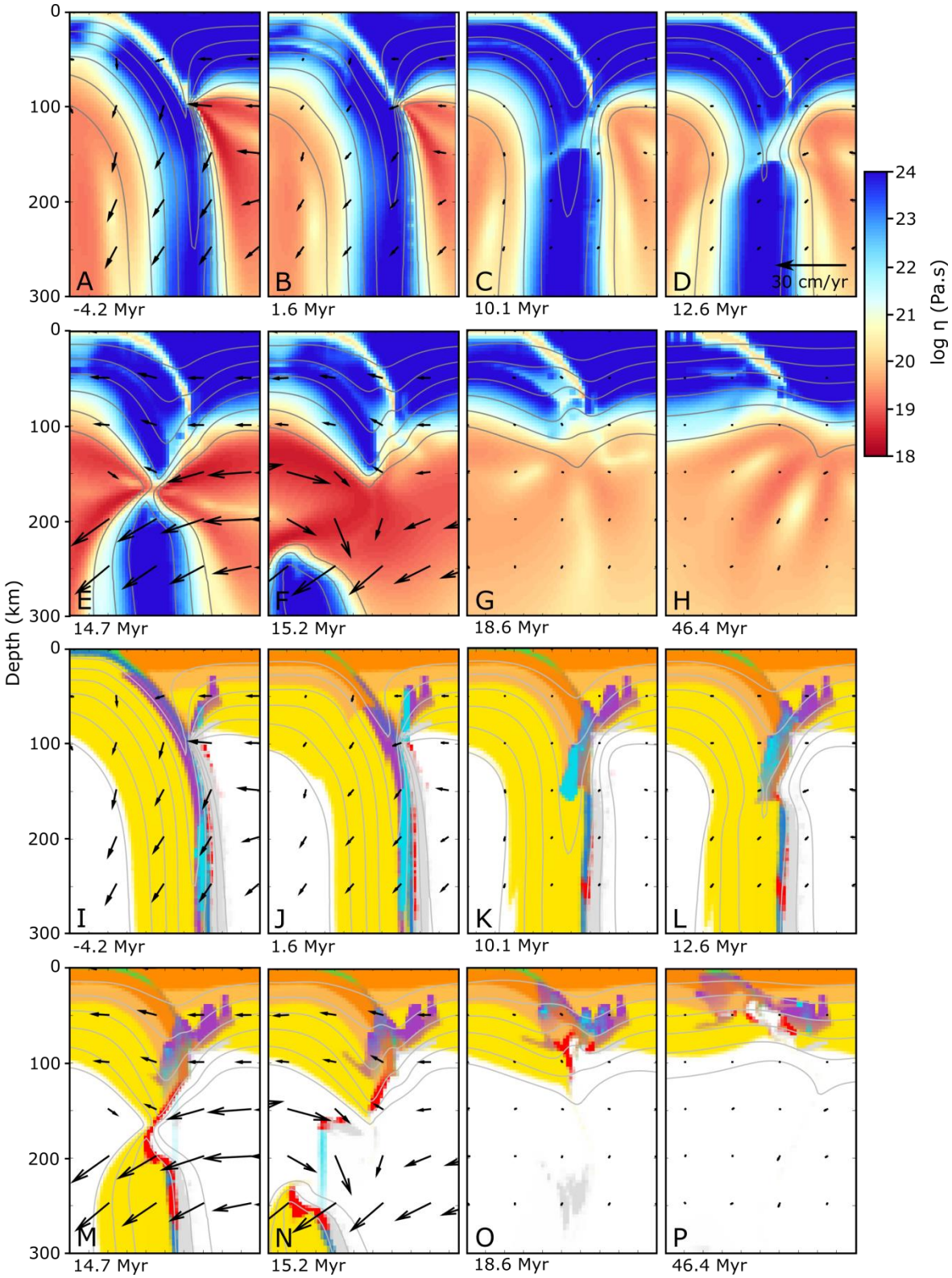
Depth (km)
0
100
200
300
A
B
C
D
30 cm/yr
-4.2 Myr
1.6 Myr
10.1 Myr
12.6 Myr
E
F
G
H
14.7 Myr
15.2 Myr
18.6 Myr
46.4 Myr
I
J
K
L
-4.2 Myr
1.6 Myr
10.1 Myr
12.6 Myr
M
N
O
P
14.7 Myr
15.2 Myr
18.6 Myr
46.4 Myr
log η (Pa.s)
24
23
22
21
20
19
18

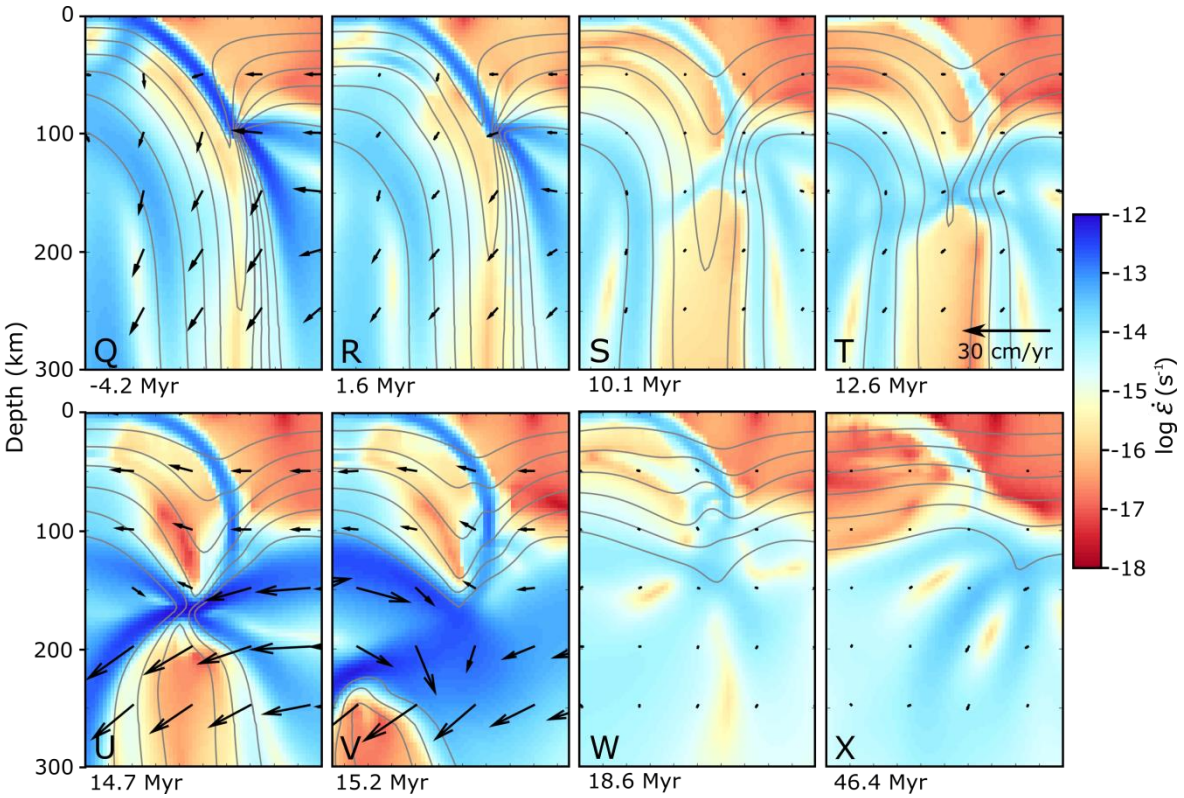


**Figure 4.4: Dynamics and melting of Model 13 (shallow breakoff model).** Dynamics of Model 13 show oceanic subduction (Figs. 4.4A, 4.4I, and 4.4Q), continental subduction (Figs. 4.4B, 4.4J, and 4.4R), slab stagnation (Figs. 4.4C, 4.4K, and 4.4S), final breakoff (Figs. 4.4E, 4.4M, and 4.4U), descent of the detached slab (Figs. 4.4F, 4.4N, and 4.4V) and eduction of the continental plate (Figs. 4.4G, 4.4O, and 4.4W). Figs. 4.4A - 4.4H show the viscosity, 4.4I - 4.4P the position of different compositional materials based upon the locations of tracer particles within the model, and 4.4Q - 4.4X the strain rate. Materials, temperature contours, velocity vectors, and panel width are as in Fig. 4.2.

of stable hydrous phases within crustal material in this area leading to deep (~150 km) asthenospheric melting (Fig. 4.4N). Asthenospheric melting begins 4 Myr after the cessation of subduction related magmatism, at the time of breakoff (Fig. 4.3B). The locus of this melting progresses into the foreland region over time, due to the movement of the detached slab towards the subducting plate as it descends deeper into the mantle (Fig. 4.4N). Asthenospheric melting can last only a few Myrs, since it is caused by the flux of water released from the detached part of the slab which rapidly sinks into the mantle. A more prolonged period of continental crustal melting begins during crustal exhumation, at around the same time as breakoff, and is sustained for over 30 Myr, increasing as the exhumation advances and decreasing as the plates become stable and cool (Figs. 4.4O and 4.3B).

### 4.3.3 Breakoff dynamics across the parametric study

We decided to focus on the conditions that lead to relatively shallow and rapid slab breakoff, which has been shown above to favour slab breakoff associated melting. As a consequence, most models in our chosen parameter range exhibit shallower and more rapid breakoff than the reference Model 1 (Fig. 4.5, Table 4.1). Breakoff localises where tensile stresses, between the dense oceanic lithosphere and buoyant continental lithosphere, exceed the local strength of the slab. This condition depends upon a number of factors. Firstly, whilst within

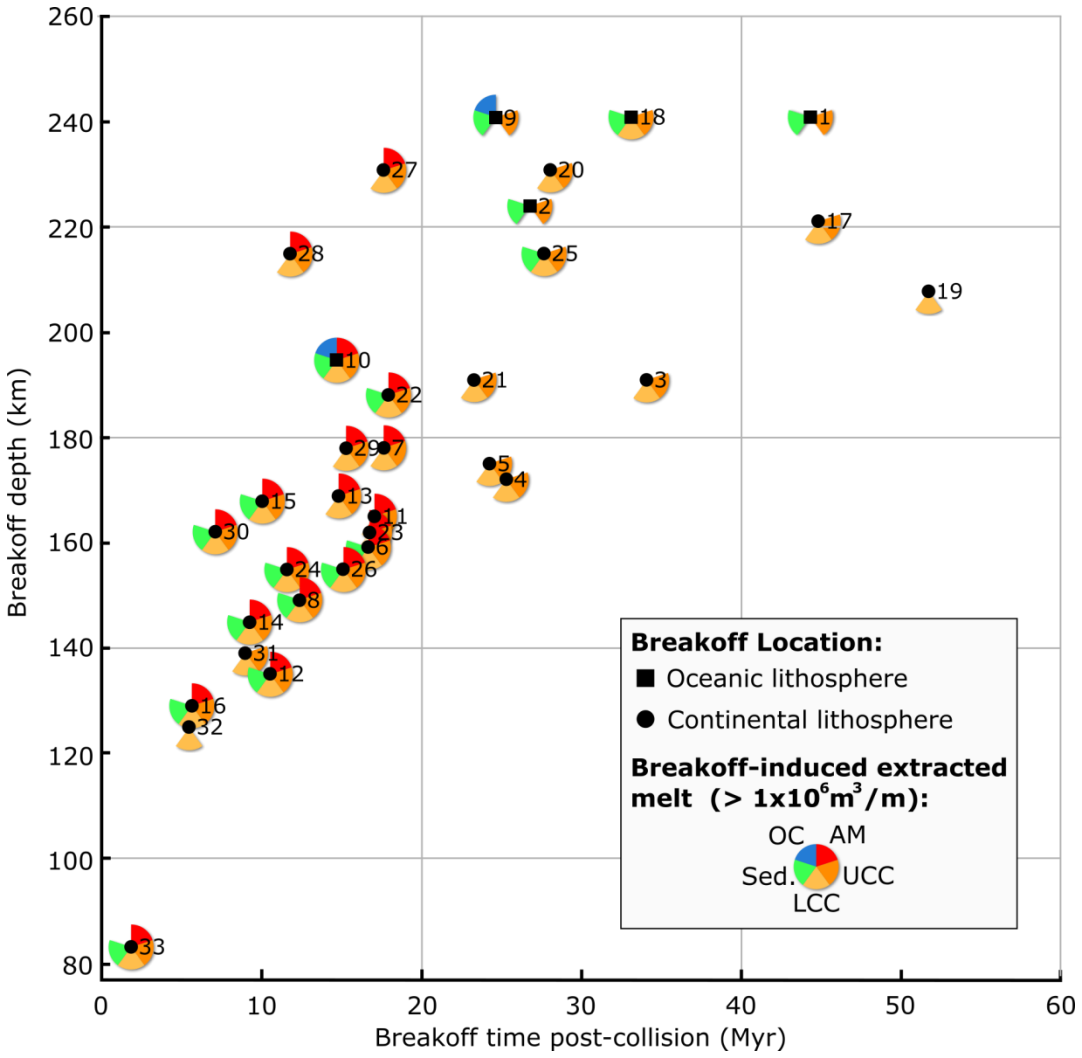


**Figure 4.5: Breakoff depth versus break-off time across the parametric study.** (See Table 4.1 for details of each model). Models which show melt extraction over $1x10^6$ $m^3/m$ as a direct result of break-off are highlighted for the asthenospheric mantle, upper and lower continental crust, sediments and oceanic crust. Squares refer to models with break-off in the oceanic part of the slab and circles indicate break-off in the continental part of the slab. Models 1-32 are those within the 5D parametric study, whilst Model 33 is an anomalous case, designed to induce very shallow breakoff.

the oceanic lithosphere, these tensile stresses increase towards the surface, as the slab at that point supports more of the dense, subducted slab underneath. Secondly, the strength of the slab is in part controlled by the width of the slab and the strength of the mantle lithosphere and continental crust. Thirdly, the thickness of the cold slab core also determines the location of breakoff, which increases by thermal diffusion whilst the slab is stagnated. This is reduced by a thinner overriding plate and a shorter time between collision and breakoff, allowing the slab to start warming up at a shallower depth. Fourthly, the thickness of the continental crust plays a complex role. A thicker continental crust reduces the integrated strength of the lithosphere, in part because crustal material is intrinsically weaker than mantle material, but also because the strength of the continental crust can be further reduced by radiogenic heating. However, counterintuitively a weaker crustal rheology (and in some cases an increase in radiogenic heating) generally leads to an increase in breakoff depth. This results from a greater crust-mantle decoupling and earlier exhumation of the crust, locally reducing the buoyancy of the continental part of the slab, and therefore also reducing the tensile stresses in the slab underneath. Full delamination of the mantle lithosphere from the continental crust can ensue in these cases (Fig. 4.6), leading to slab roll-back before a final breakoff event that occurs when the slab has weakened sufficiently through heat diffusion.

Despite the wide range of breakoff depths that are observed (Fig. 4.5), breakoff does not occur at depths shallower than the base of the overriding lithospheric mantle for any of the conditions applied within the parametric study (Models 1-32). To explore the consequences of even shallower breakoff and its possible magmatic effects, we add another model that lies outside the systematic parameter space, which induces breakoff at a depth of 83 km by using 50 km thick continental crust within a very thin, 70 km, continental lithosphere, with a crustal radiogenic heating of 0.7 $\mu Wm^{-3}$ (Model 33 - Figs. 4.5 and 4.7). However, other conditions, such as the subduction of a very young subducting oceanic plate, or using models where a low-temperature plasticity deformation mechanism such as Peierl's mechanism is at work (Kameyama et al., 1999), may also lead to shallow breakoff (see Duretz et al., 2011).

### 4.3.4 Melting across the parametric study

Post-collisional melting in these models occurs due to a variety of dynamical processes, including slab breakoff (which exposes lithosphere of the detached slab to hot mantle temperatures, leading to dehydration and saturated melting), decompression melting resulting from exhumation, and melting linked to delamination or extension. Below we consider the pattern of melting for each material that is directly related to slab breakoff and that reaches sufficient amounts to be extracted.

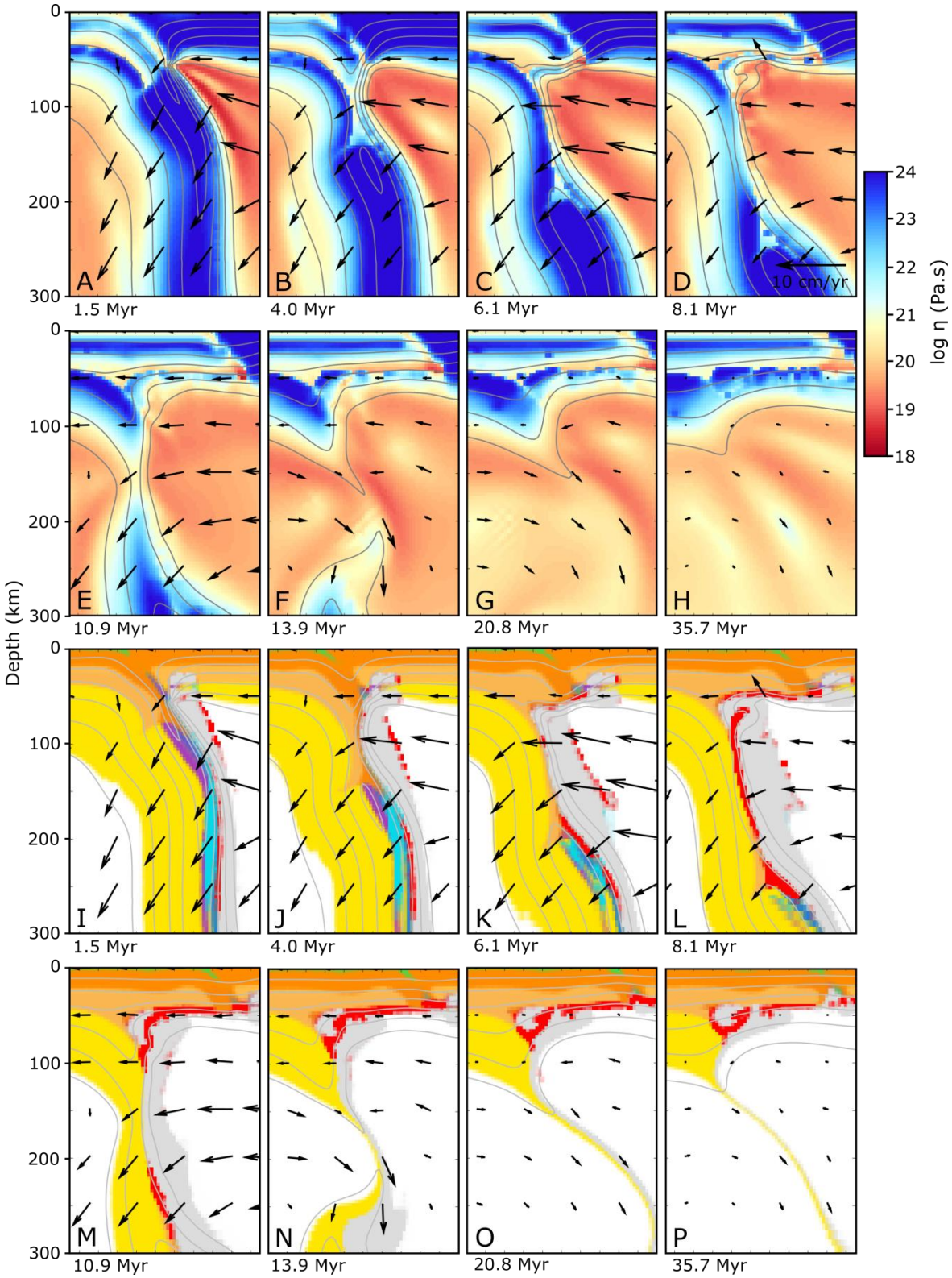
Depth (km)
0
100
200
300
A
B
C
D
10 cm/yr
1.5 Myr
4.0 Myr
6.1 Myr
8.1 Myr
E
F
G
H
10.9 Myr
13.9 Myr
20.8 Myr
35.7 Myr
I
J
K
L
1.5 Myr
4.0 Myr
6.1 Myr
8.1 Myr
M
N
O
P
10.9 Myr
13.9 Myr
20.8 Myr
35.7 Myr
log η (Pa.s)
24
23
22
21
20
19
18

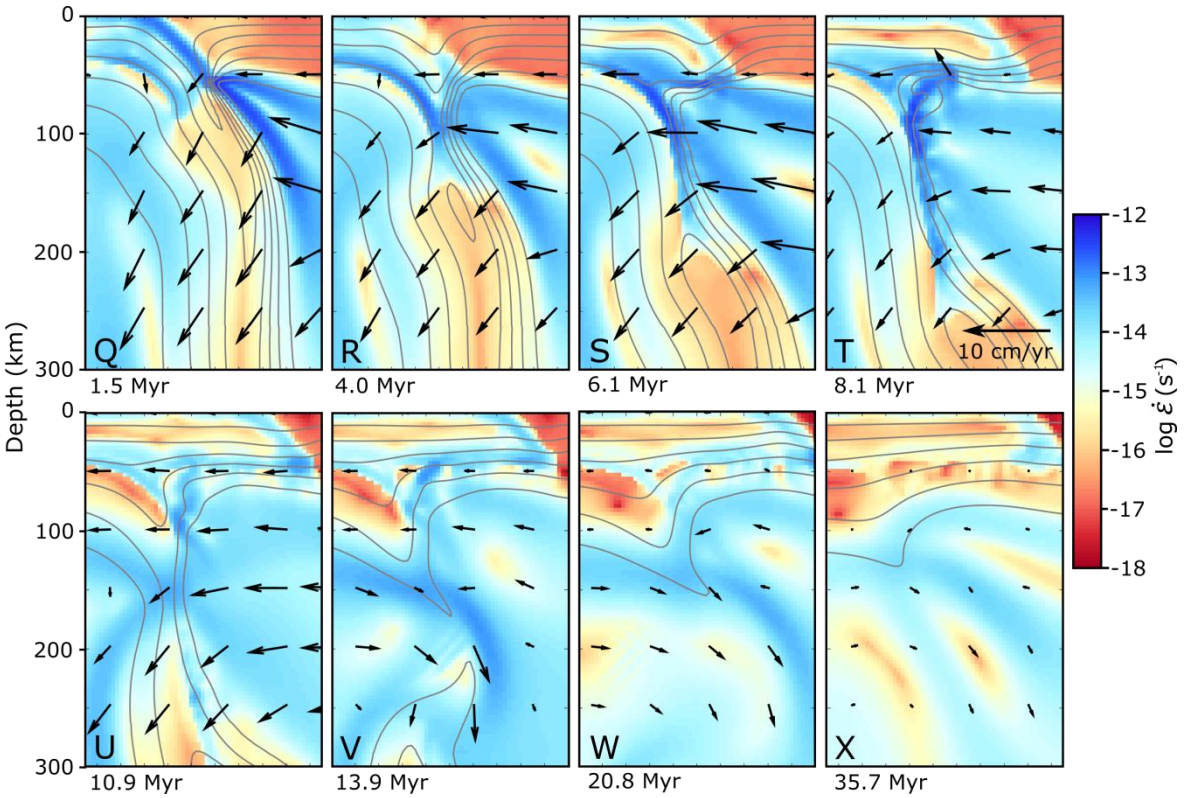


**Figure 4.6: Dynamics and melting of Model 24 (delamination model).** Model 24 (which uses a weaker (dry quartzite) continental crustal flow law): crust-mantle delamination, resulting in both asthenospheric mantle melting and melting of the delaminating lower continental crust. Dynamics of Model 24 show continental subduction (Figs. 4.6A, 4.6I, and 4.6Q), necking of the continental crust (Figs. 4.6B, 4.6J, and 4.6R), delamination (Figs. 4.6C, 4.6K, and 4.6S) and significant continental crustal melting (Figs. 4.6D, 4.6L, and 4.6T), slab necking (Figs. 4.6E, 4.6M, and 4.6U), slab breakoff (Figs. 4.6F, 4.6N, and 4.6V), and post-breakoff melting of the continental crust (Figs. 4.6G, 4.6H, 4.6O, 4.6P, 4.6W, and 4.6X). Panels are as in Fig. 4.2.

Continental crust melting due to slab breakoff is present across most of the parametric study. It does not show a clear correlation with the breakoff depth nor the location of breakoff, whether within the oceanic or continental lithosphere (Fig. 4.5). It is instead dependent upon the maximum depth of the subducted continental crust with respect to the thickness of the overriding plate. For breakoff within the continental lithosphere, melting can occur around the location of necking and breakoff when the slab increases in temperature at this location (Fig. 4.4M). The continental crust can still melt in some instances where breakoff occurs within the oceanic lithosphere, due to heating of the crust within the upper detached slab, after breakoff (Fig. 4.8). This takes place when the overriding lithosphere is relatively thin, and hence the crust is in close proximity to hotter asthenospheric mantle. Melting of the sediments is also dependent upon the thickness of the overriding plate. This melting is

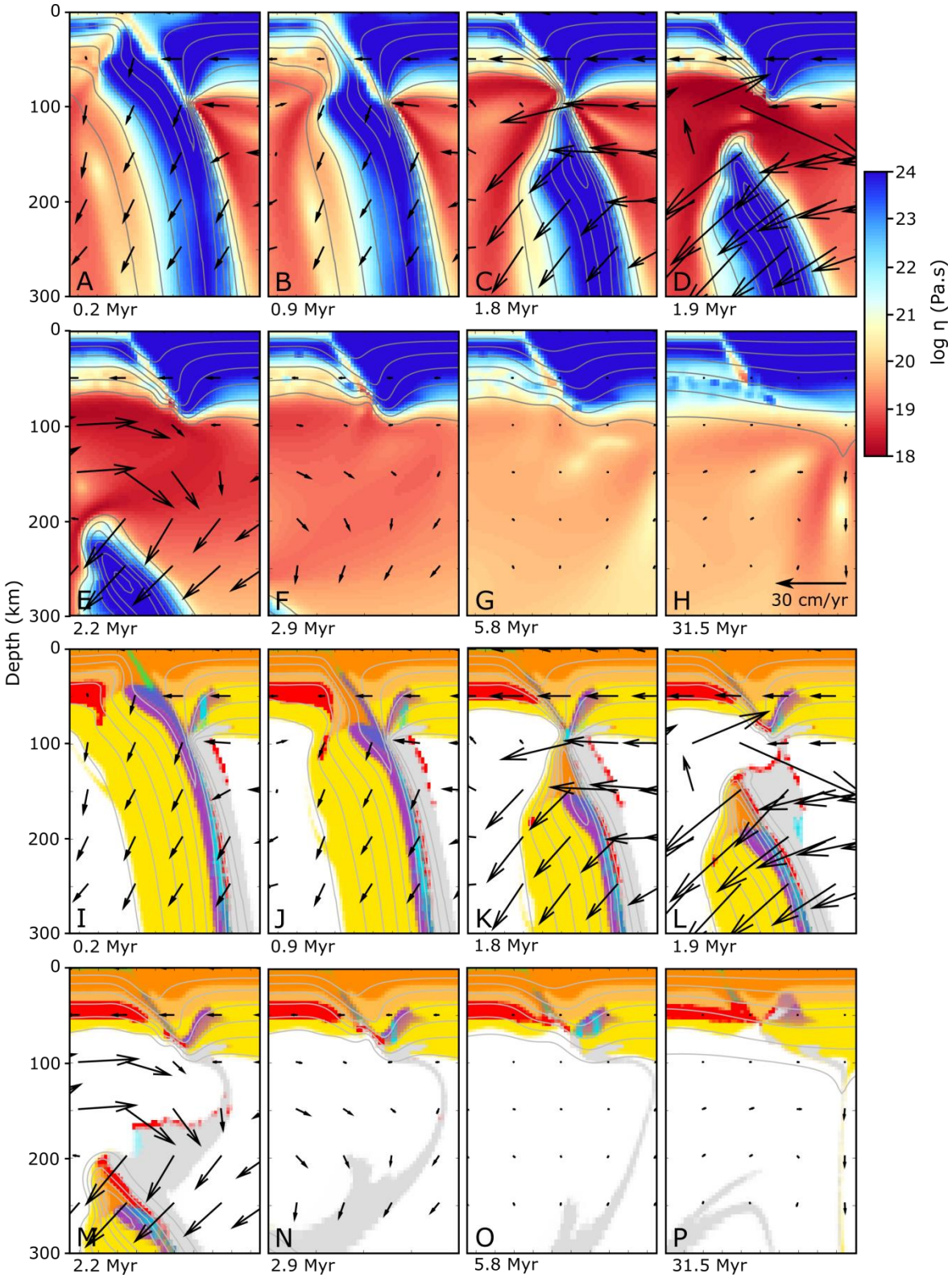
Depth (km)
0
100
200
300
A
B
C
D
0.2 Myr
0.9 Myr
1.8 Myr
1.9 Myr
E
F
G
H
2.2 Myr
2.9 Myr
5.8 Myr
31.5 Myr
30 cm/yr
I
J
K
L
0.2 Myr
0.9 Myr
1.8 Myr
1.9 Myr
M
N
O
P
2.2 Myr
2.9 Myr
5.8 Myr
31.5 Myr
log η (Pa.s)
24
23
22
21
20
19
18

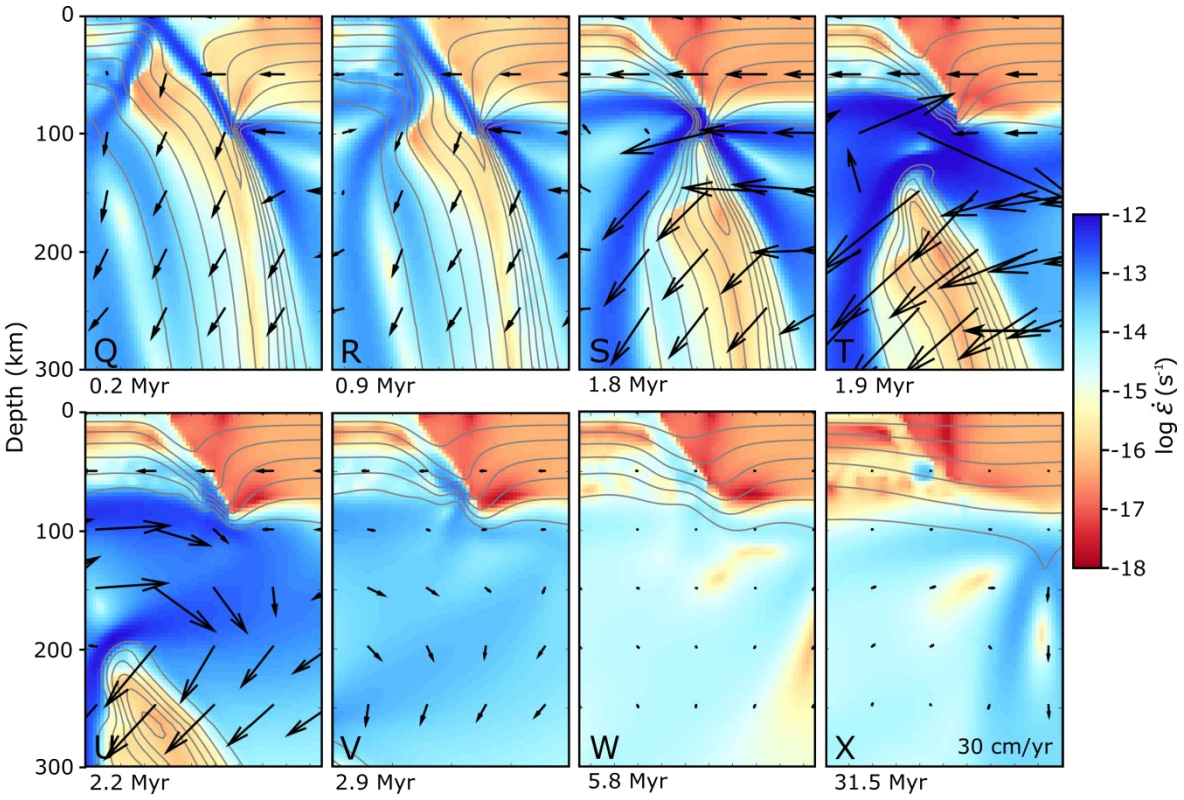


**Figure 4.7: Dynamics and melting of Model 33.** Model 33: breakoff occurs at ~80 km, showing no melting of the lithospheric mantle adjacent to the suture, nor any significant thermal perturbation in the lithosphere at the location of breakoff. Large areas of melting (although less than the extraction threshold) are observed towards the base of the crust within the subducting continental lithosphere. This is a result of the higher crustal geotherm created by the imposed model conditions, and is not linked to the collision or breakoff process. Dynamics of Model 33 show continental subduction (Figs. 4.7A, 4.7I, and 4.7Q), necking of the continental lithosphere (Figs. 4.7B, 4.7J, and 4.7R), slab breakoff (Figs. 4.7C, 4.7K, and 4.7S) and melting of the asthenospheric mantle and crustal tip (Figs. 4.7D 4.7E, 4.7L, 4.7M, 4.7T, and 4.7U), thermal relaxation (Figs. 4.7F - 4.7H, 4.7N - 4.7P, 4.7V - 4.7X). Panels are as in Fig. 4.2.

widespread throughout our models, as some sediments are always carried down atop the subducting slab, independent of the breakoff dynamics.

Asthenospheric melting is observed in only a few cases (e.g. Models 12 - 16, Fig. 4.9). This melting is linked to the breakoff depth and timing (Fig. 4.5). Hydration of the inflowing mantle is essential for asthenospheric melting to take place. A shorter, faster detachment increases the likelihood that sufficient water will be retained within the detached oceanic lithosphere after breakoff. The tip of detached continental crust is also able to store water that could potentially be released through dehydration. However, when melting occurs in the

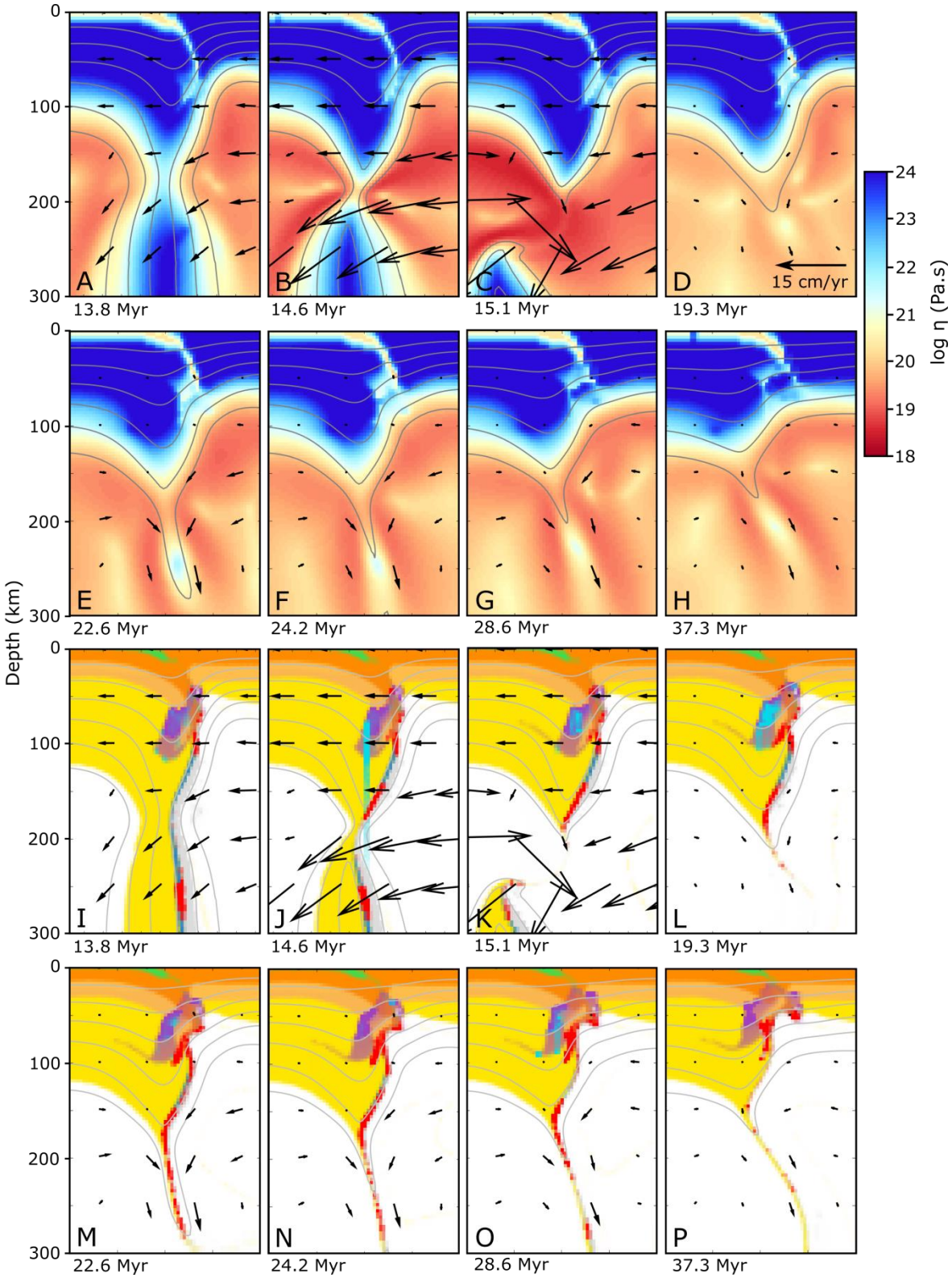
Depth (km)
0
100
200
300
A
B
C
D
15 cm/yr
13.8 Myr
14.6 Myr
15.1 Myr
19.3 Myr
E
F
G
H
22.6 Myr
24.2 Myr
28.6 Myr
37.3 Myr
I
J
K
L
13.8 Myr
14.6 Myr
15.1 Myr
19.3 Myr
M
N
O
P
22.6 Myr
24.2 Myr
28.6 Myr
37.3 Myr
log η (Pa.s)
24
23
22
21
20
19
18

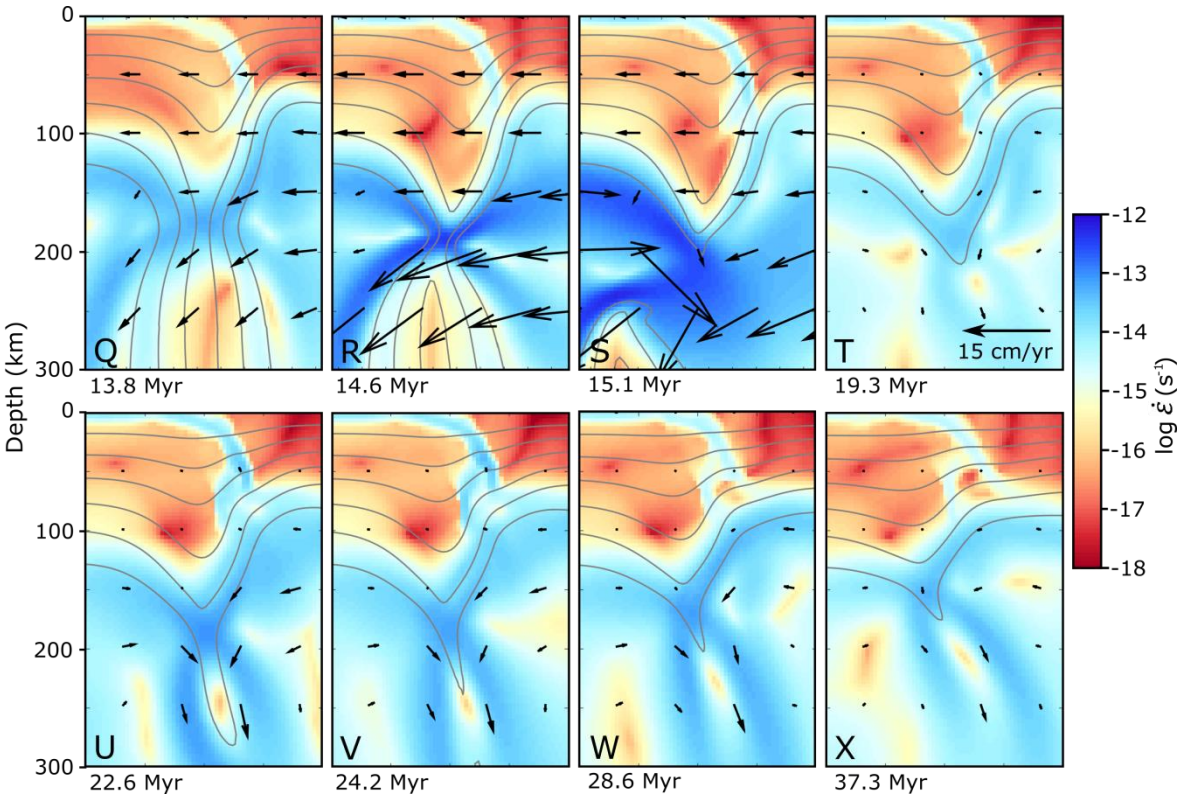


**Figure 4.8: Dynamics and melting of Model 10 (oceanic crustal melting model).** Model 10: melting of the oceanic crust which can take place if breakoff occurs within the oceanic lithosphere, due to the later dripping away of denser, eclogitised oceanic crust. Dynamics of Model 10 show slab necking (Figs. 4.8A, 4.8I, and 4.8Q), slab breakoff (Figs. 4.8B, 4.8J, and 4.8R), descent of the detached slab (Figs. 4.8C, 4.8K, and 4.8S), dripping and melting of the oceanic crust (Figs. 4.8D - 4.8H, 4.8L - 4.8P, and 4.8T - 4.8X). Panels are as in Fig. 4.2.

continental crustal material, all the water is consumed, preventing the presence of free water in the inflowing asthenospheric mantle and the induction of melting.

Oceanic crustal melting is not a common feature across our parametric study. This only occurs in two cases (Models 9 & 10), for which breakoff occurs within the oceanic lithosphere (Fig. 4.5). After breakoff, the upper, stagnated portion of the plate continues to heat up, weakening the oceanic crust that is still present. As this eclogitised crust is denser than the surrounding mantle, it drips off and melts as it descends, occurring 10 Myr after breakoff (Fig. 4.8).

We do not observe any post-collisional melting in the overriding mantle lithosphere, except for Model 33, which shows very small amounts of melt extraction (<$5 \times 10^5$ $m^3$/m). This occurs at the very base of the overriding plate, to the right of the suture (Fig. 4.7L), where it is hydrated by a flux of water from the underlying slab. Melting at this location occurs

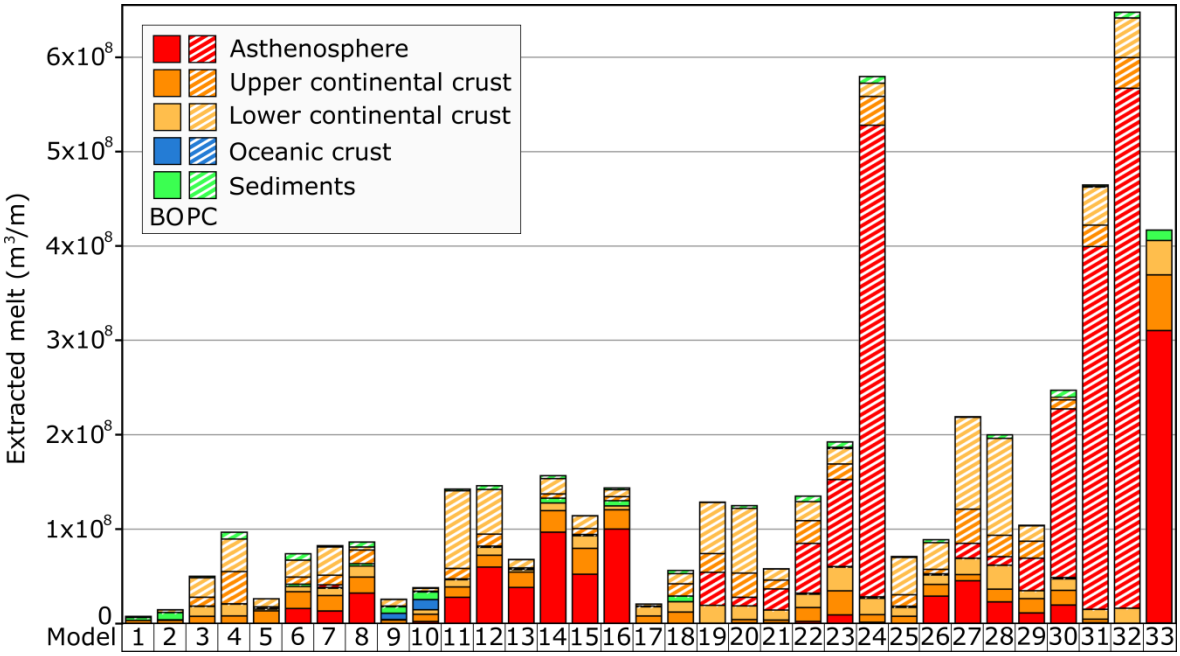


**Figure 4.9: A comparison of the amount of melt extracted for all models.** Bright colours represent breakoff-related melting (BO), whilst colours with white hatching represent the remaining total post-collisional magmatism (PC), from processes such as crustal exhumation, extension, and delamination (see Figs. 4.10 and 4.6 for examples of these). Significant crust-mantle delamination occurs in Models 19-24 and 27-32, which can induce large volumes of continental crustal and asthenospheric melting.

before and after continental collision, and also during the process of slab necking and breakoff.

Melting is also generated through other mechanisms that are not directly a result of slab breakoff. Small amounts of decompression melting of the continental crust can occur during exhumation towards the surface, which is not necessarily initiated by the slab breakoff (Figs. 4.2O and 4.4O). Larger amounts of melting can be generated at the base of the continental crust as a result of heating from upwelling asthenospheric mantle during post-collisional extension (e.g. Model 11 - Figs. 4.9 and 4.10). Finally, significant melting of both the continental crust and the inflowing asthenospheric mantle can take place during mantle lithospheric delamination, for some models which implement a weaker crustal rheology (e.g. Model 24 - Figs. 4.6 and 4.9 (also for Models 19-23 and 27-32)).

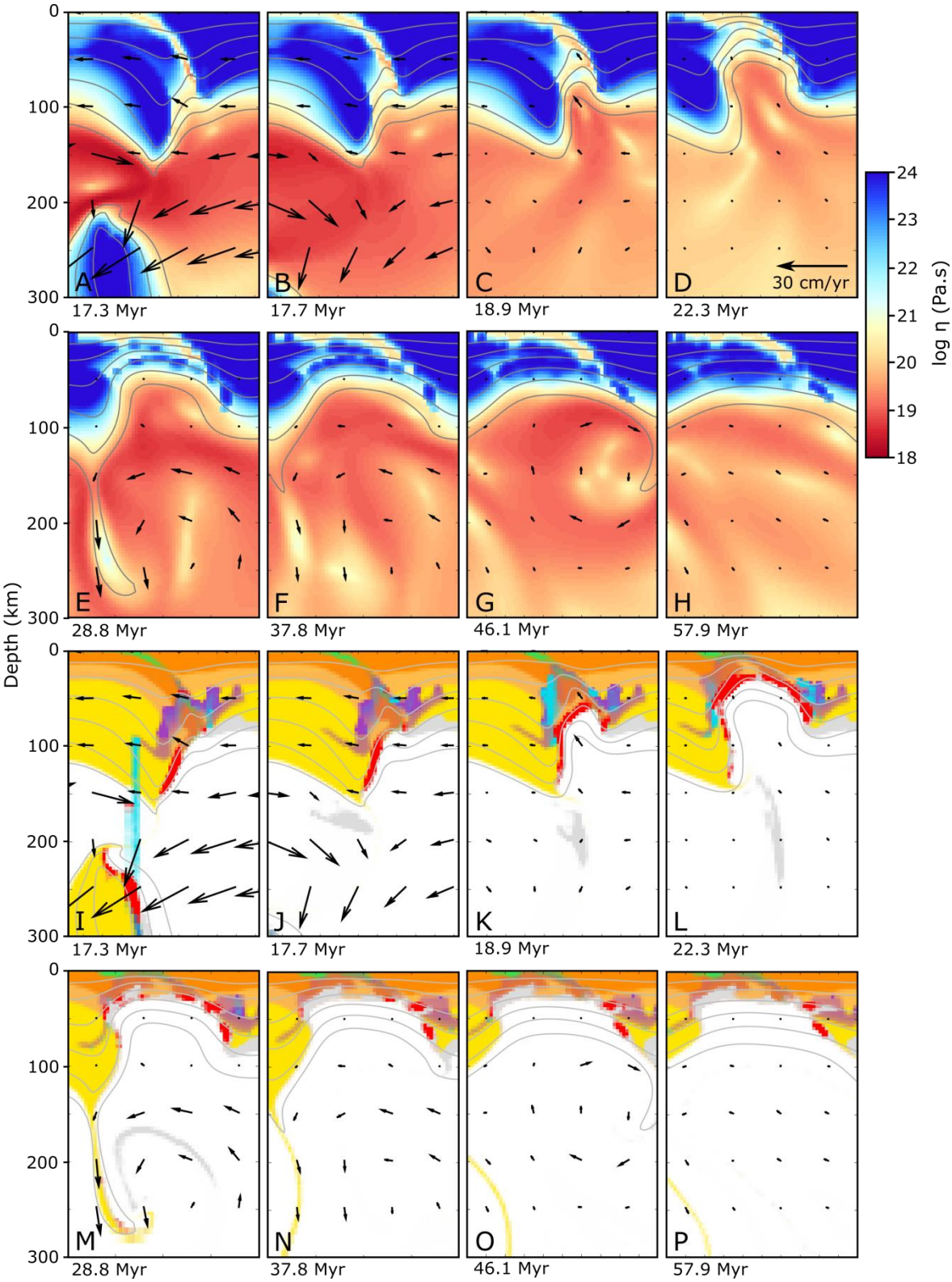
Depth (km)
0
100
200
300
A
B
C
D
30 cm/yr
17.3 Myr
17.7 Myr
18.9 Myr
22.3 Myr
E
F
G
H
28.8 Myr
37.8 Myr
46.1 Myr
57.9 Myr
I
J
K
L
17.3 Myr
17.7 Myr
18.9 Myr
22.3 Myr
M
N
O
P
28.8 Myr
37.8 Myr
46.1 Myr
57.9 Myr
log η (Pa.s)
24
23
22
21
20
19
18

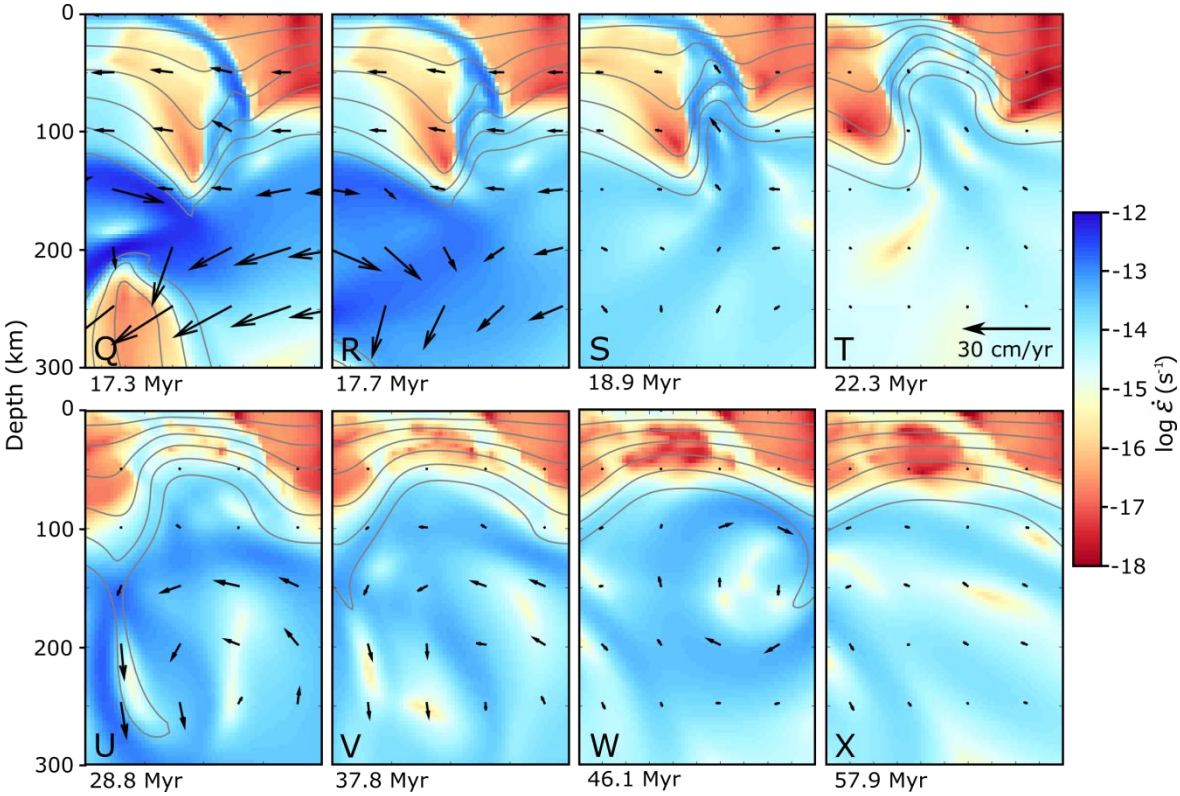


**Figure 4.10: Dynamics and melting of Model 11 (post-collisional extension model).** Model 11: upwelling of hot asthenospheric mantle and melting of the continental crust. Dynamics of Model 11 show descent of the detached slab (Figs. 4.10A, 4.10B, 4.10I, 4.10J, 4.10Q, and 4.10R), asthenospheric upwelling and extension (Figs. 4.10C - 4.10E, 4.10K - 4.10M, and 4.10S - 4.10U), and thermal relaxation (Figs. 4.10F - 4.10H, 4.10N - 4.10P, and 4.10V - 4.10X). Panels are as in Fig. 4.2.

## 4.4 Discussion

In convergence zones, changes in magmatic compositions are often interpreted in terms of changes in the dynamics of the system, such as a change in dip angle (Gutscher et al., 2000), or onset of continental collision (e.g. Bouilhol et al. 2013), and after collision, abrupt shifts in composition are commonly hypothesised to represent slab breakoff (e.g. Zhu et al., 2011). Observed post-collisional melts are usually small in volume and distributed fairly sparsely compared to subduction-related melting. Our study enables us to better constrain the source and conditions required for such melting. Our results show that post-collisional magmatism due to slab breakoff is feasible, but perhaps not as easy to achieve as previously suggested by kinematic models. Below we discuss the conditions required to melt the different components of the system.

### 4.4.1 Lithospheric mantle melting

The models of Davies & von Blanckenburg (1995) show that the upwelling of asthenosphere upon breakoff can cause a thermal perturbation and melting of the overriding metasomatised mantle lithosphere (Fig. 4.11A). Subsequently many post-collisional magmatic observations, with geochemical signatures typical of metasomatised mantle lithosphere, have been interpreted as the result of the process of slab breakoff induced melting (e.g. von Blanckenburg & Davies 1995; Kohn & Parkinson 2002; Ahmadzadeh et al. 2010). However, we do not observe any lithospheric mantle melting, adjacent to the slab window upon slab breakoff in our study. Below we consider a number of possible reasons why breakoff, under the conditions imposed here, might be unable to induce a sufficient thermal perturbation to generate melting.

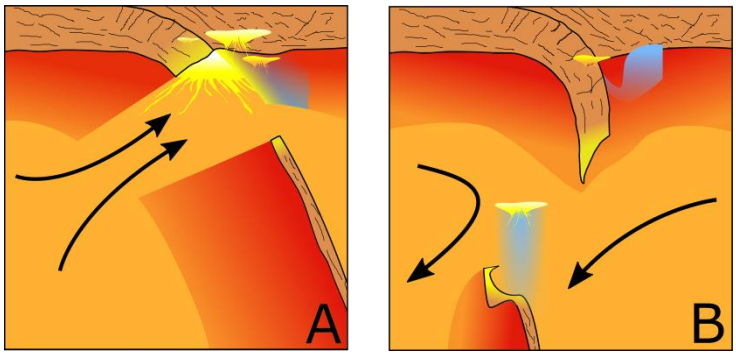


**Figure 4.11: Schematic representations of breakoff-related melting.** A - possible melting induced by very shallow breakoff (similar to that suggested by Davies and von Blanckenburg (1995)) and B - melting induced by deeper breakoff, as observed in this study.

One key requisite of the aforementioned model is that, for melting to occur at the subduction interface (or resulting suture), breakoff needs to be at depths shallower than the base of the overriding lithosphere (Fig. 4.11A). Our results, and those of previous numerical studies, suggest breakoff at these depths is not common, and perhaps only occurs under unusual conditions (Fig. 4.5) (e.g. Duretz et al., 2011; van Hunen and Allen, 2011). Hence, hot asthenospheric material may not normally be brought into direct contact with the colder overriding lithosphere (Fig. 4.11B). This implies that lithospheric melting near the suture, directly as a result of breakoff, may not be a common phenomenon, and the depth of breakoff should be considered before using lithospheric melts as an indicator of direct exposure of overriding lithosphere to hot asthenosphere due to the formation of a slab window upon breakoff. However, even for breakoff at depths shallower than the base of the overriding lithosphere, no significant melting of the lithosphere adjacent to the suture is observed (Fig. 4.7). The model of lithospheric mantle melting relies on hydration (metasomatism) of the

overlying lithosphere from previous oceanic subduction, which will lower the solidus, and will be more prone to melting in the event of a thermal perturbation. Although our models predict a wet solidus that is very close to those determined experimentally (e.g. Condamine and Médard, 2014) for metasomatic mantle, the thermal perturbation does not extend sufficiently into the overriding plate in order to significantly melt this metasomatised area (Figs. 4.7L and 4.7O). In their models, Davies and von Blanckenburg (1995) found that a period of 25 Myr is required to heat a point only 15 km away from suture, following breakoff at a depth of 80 km, and prolonged heating would be required for this thermal perturbation to penetrate further into the overriding lithosphere. Our model calculations agree with these findings: the rapid descent of the slab and subsequent cooling of the plate in our model prevents the hydrated portion of the lithosphere from exceeding 800 °C. Unless the slab descends more slowly into the mantle, and hence the asthenospheric flow is sustained for a longer period of time, it seems unlikely that the metasomatised mantle lithosphere would be able to be heated sufficiently to melt. Furthermore, throughout our study, the most common mode of breakoff is through viscous necking of the slab, in accordance with the results of Gerya et al. (2004) and Duretz et al. (2012). For the shallow breakoff model, this style of necking results in a thin film (< 10 km) of crustal material and sediments remaining below the overriding lithosphere, which further shields the lithospheric mantle from a more significant thermal perturbation. So, instead of overriding lithospheric melting, we observe an increase in melting of this thinned layer of subducted continental crust upon breakoff, as it reaches temperatures of 600-1000 °C (Figs. 4.7L, 4.7M, and 4.7N).

Hence, slab breakoff may not commonly be shallow enough to expose the overriding lithosphere to hotter mantle asthenosphere, or may not be able to heat up the overriding lithosphere to partial melting conditions. Therefore, other mechanisms may be at work to melt the mantle lithosphere in post-collisional areas. We don’t rule out the general mechanism of slab breakoff induced melting of the overriding lithosphere, but we suggest that in several localities of post-collisional magmatism, slab breakoff and subsequent slab window heating may not be the most likely cause for melting of the mantle lithosphere. This is consistent with some observations from post-collisional areas, for example the Iranian plateau, where magmatism is prolonged, widespread and occurs hundreds of kilometres from the suture (e.g. Kaislaniemi et al., 2014).

### 4.4.2 Asthenospheric mantle melting

We do not observe any dry decompressional melting of asthenosphere in our study, in agreement with the conclusion of Davies and von Blanckenburg (1995) that this is unlikely

to take place, as very shallow breakoff depths of less than 50 km are required. However, our results show that melting of asthenospheric mantle can take place where the mantle is percolated by the devolatilisation of metamorphic water from the slab tip. Indeed, slab breakoff provides a mechanism to heat marginally hydrated areas of the subducted slab, releasing water that otherwise is likely to remain stable (Fig. 4.11B). In some cases the tip of the detached slabs melts, and may contribute significantly to this metasomatic agent. This slab fluid/melt triggers melting of the asthenospheric mantle above the subducting slab tip. This melting is short-lived, synchronous with slab breakoff, and would not exceed a few Myrs. Although the resulting magmas might be chemically distinct, with a strong slab affinity, such as a clear enrichment in potassium (as continental material is involved), it might be difficult to clearly identify those magmas in the geological record due to their short lived appearance. Nevertheless, potassic magmatism observed in the Mediterranean would fit both the spatial, temporal and compositional occurrence observed in our models (e.g. De Astis et al., 2006).

### 4.4.3 Crustal melting

Slab breakoff-induced melting of the continental crust and sediments may be a more common occurrence in post-collisional areas than breakoff-induced mantle melting. The increase in temperature of this subducted material during slab necking and breakoff is sufficient to generate significant amounts of melt. This melting is not only constrained to the more extreme cases of fast and shallow breakoff (such as for asthenospheric melting), but is widespread across our study, being instead primarily dependent upon the maximum depth of continental crustal subduction and overriding plate thickness. We would expect crustal melts to be extruded in localised, linear belts of magmatism near the suture, which may be a more reliable indicator of breakoff than observations of lithospheric mantle melts.

Some studies have suggested the observations of mafic melts may be due to a heating of the detached oceanic lithosphere upon slab breakoff (Jahangiri, 2007; Omrani et al., 2008). We find that melting of the mafic, oceanic crust is a rare feature, occurring under very specific conditions. Instead, the melting of the lower continental crust during breakoff may be a more likely cause, which may produce a similar geochemical signature.

### 4.4.4 Other post-collisional melting across the parametric study

Our models show several melting mechanisms not directly related to slab breakoff. Separation of the crust and mantle lithosphere in the subducting slab occurs for the majority

of models where a weaker (dry quartzite) continental crustal rheology is used (Fig. 4.6), due to the reduced coupling between the crust and mantle lithosphere, in agreement with other numerical studies (Duretz and Gerya, 2013; Magni et al., 2013; Schott and Schmeling, 1998). This generates significant melting at the base of the delaminated crust (e.g. Göğüş and Pysklywec, 2008; Ueda et al., 2012), and can also generate some asthenospheric melting, through the dehydration of crust within the delaminating slab (e.g. Models 19-24 and 27-32, Fig. 4.9). Exhumation of the continental crust and in some cases subsequent extension can also lead to crustal melting through both decompression melting and heating around areas of hot inflowing asthenosphere (Figs. 4.2N, 4.4O and 4.10L). All these melting processes are not strictly slab breakoff generated, although they may occur during or be accentuated by breakoff. In some collisional areas today (Arabia-Eurasia, India-Eurasia), convergence is still ongoing long after the initial collision (Molnar and Tapponnier, 1975), which suggests that additional compressional forces might be at work (e.g. Becker and Faccenna, 2011), and the extensional processes observed in the presented models and discussed above might not commonly take place. However, delamination and exhumation have been suggested to occur and account for melting in some areas (e.g. Keskin, 2003; Kohn and Parkinson, 2002). Additionally, melting may also have been generated through post-collisional extensional processes within older continental collisional settings, such as the Western Gneiss Region, Norway (Gordon et al., 2013; Labrousse et al., 2004).

## 4.5 Conclusions

The occurrence of or changes in post-collisional magmatism are often attributed to slab breakoff. In this study, we used numerical modelling to quantify melting processes during post-collisional slab breakoff. Our results suggest that the classical style of slab breakoff related magmatism, i.e. lithospheric melts from the exposure in a slab window created by slab breakoff (Fig. 4.11A), may not commonly occur, since breakoff depths are typically deeper than the overriding plate thickness, and may not be able to induce a significant thermal perturbation in the overriding lithosphere. However, melting of the continental crust and sediments provides an alternative, viable mechanism for generating magmatism through breakoff (Fig. 4.11B). Observations of crustal melts in collisional areas may commonly be a result of breakoff, and may be a more reliable indicator of the occurrence of slab necking and breakoff than mantle derived melts, provided these are not long-lived and located within narrow belts parallel to the suture. The inflowing asthenosphere can also melt through hydration from the detached, descending slab, although this is only likely when breakoff occurs at relatively shallow depths and shortly after initial collision (< 20 Myr).

Slab breakoff is unable to induce the observed prolonged periods of post-collisional magmatism, or those observed 100s of kms away from the suture zone. Therefore, it is unlikely that the breakoff process by itself can account for all observations of magmatism in post-collisional areas, and additional, alternative mechanisms are required to account for the diverse nature of magmatic observations and to explain some of the post-collisional magmatism that has previously been attributed to breakoff.

# Chapter 5

# Discussion and conclusions

## 5.1 Summary of results

This thesis has addressed whether the process of slab breakoff following the collision of two continental plates is a viable means of inducing post-collisional magmatism. Following the kinematic models of Davies and von Blanckenburg (1995), which show heating of the overriding lithospheric mantle and decompression melting of the asthenosphere may occur after very shallow breakoff (see Chapter 1.2.2), many studies across post-collisional areas have invoked these mechanisms to account for magmatic observations. However, subsequent numerical studies suggest that breakoff at the depth required for this style of melting may not commonly occur in collisional environments. Therefore we assess whether shallow breakoff may be capable of inducing post-collisional melting, and whether other mechanisms may be at work, particularly following deeper slab breakoff, to generate some of the post-collisional magmatism that is observed today.

*Chapter 3* - explores a range of parameters which may have a significant control on the breakoff depth, and hence may influence the generation of post-collisional magmatism. The effect of these parameters on the timing of breakoff and induced mantle flow patterns is also studied. A range of breakoff dynamics is observed across the systematic parametric study, although the very shallow and deep breakoff depths found in previous numerical studies are not observed. By imposing a weak continental lithosphere, through a thicker continental crust, a thinner continental mantle lithosphere, an increase in radiogenic heat production, or a weaker crustal rheology, breakoff can localise within the subducted continental lithosphere rather than the oceanic, leading to significant decreases in breakoff depth. The thickness of the cold slab core can also significantly affect the depth of breakoff, by affecting the temperature profile of and around the slab and hence the weakest point within the slab. Despite these variations, breakoff always occurs at depths significantly deeper than the base of the overriding lithosphere. No prolonged mantle flow is also observed in close proximity

to the lithosphere, which could increase the lithospheric temperature above the solidus. Therefore melting of the overriding mantle lithosphere, based on the dynamics observed in these models, seems unlikely. Application of the parameterised solidus to these results suggests hydration of mantle material may be a more viable way of reducing the solidus to ambient conditions during collision. The increase in temperature within the subducted slab during collision could potentially induce dehydration melting, or release fluids to generate hydrous melting in other locations.

*Chapter 4* - further investigates those parameters which are most likely to decrease the breakoff depth and hence possibly increase the generation of post-collisional melting. This study makes use of a thermodynamic database to accurately determine the occurrence of (de)hydration reactions and melting within a number of materials. Under most circumstances, slab breakoff is too deep to generate any lithospheric melting. If representative of typical collision zones, interpretations of magmatic observations which invoke the breakoff-induced melting mechanisms suggested by Davies and von Blanckenburg (1995), which only apply to very shallow breakoff, should be considered only after careful deliberation of the dynamics of the collisional system involved. However, even where slab breakoff localises shallower than the overriding lithosphere, the mantle flow is not sustained for long enough to sufficiently heat the hydrated overriding plate to cause significant magmatism. Instead, for relatively shallow breakoff, which occurs fairly soon after collision, some melting of the inflowing asthenosphere is observed, as this becomes hydrated through the release of water from the tip of the heating detached slab. More significantly, melting of the subducted continental crust is a more common feature throughout the study, even where breakoff occurs fairly deep in the mantle. This is due to the heating of the crustal tip within the detached part of the slab and/or heating of the continental crust within the upper, stagnated part of the slab during necking and breakoff. Therefore, melts with a crustal signature representative of the subducted slab may be a more reliable indicator of the occurrence of breakoff, than the presence of melts originating from the overriding lithospheric mantle. These results also show many other processes may be at work to generate continental crustal melts, including post-collisional extension, crustal decompression melting during exhumation, and delamination of the crust and lithospheric mantle. Even within this study, it is sometimes hard to distinguish which processes are responsible for this melting. Therefore, although breakoff may be capable of inducing some post-collisional melting, we suggest that this is unable to account for the whole range of compositions, timings and distributions of magmatism that are observed, and that the interplay between many different processes might need to be considered to gain a full understanding of the thermodynamics of collisional systems.

## 5.2 Suggestions for future study

### 5.2.1 Thermodynamic database and melting calculations

The conclusions from Chapter 4 are based upon the data from the thermodynamic database, Perple_X. Although this has allowed a good perspective on the possibility of melting for different materials, there are also a number of limitations to the approach that has been used. As discussed in Chapter 2.5.2, the use of predefined lookup tables, based upon the thermodynamic database, inhibits the ability to track any changes in composition that occurs as a result of melting. To address this, any material that exceeds a melt extraction threshold is prevented from subsequently re-melting. However, to compare these results more accurately with magmatic observations, and to gain a fuller picture of the processes occurring in collision zones, a fully coupled database should be implemented, by referring to the Perple_X database directly when and where needed in the calculation. This can be done for any composition, and so would allow the tracking of changing compositions and the calculation of melting dependent upon these compositions. This has been implemented into the current version of Citcom; however, the significant time cost of the calculations involved in this currently prevents it from being a feasible method to use for large scale geodynamical models.

In addition to a changing composition upon melting, the process of melt segregation and migration should also be considered. These processes could have an effect on both the dynamics of the system and the resulting composition and distribution of the melts. The used method neglects the process of two-phase flow, any compaction, and the effect of melt on viscosity and buoyancy, which may influence the dynamics of collision and breakoff. However, the different timescales of melt flow and mantle dynamics and the large computational time required pose complications. This has started to be addressed for the code ASPECT through implementing an adaptive mesh refinement and iterative schemes capable of handling high viscosity contrasts for the code (Dannberg and Heister, 2015). However, this method also currently ignores the expected compositional variations. The implementation of six different materials in Chapter 4 has allowed a first-order insight into the expected overall composition of any melt, but is a simplification of a complex process. Variations in melt composition can arise from changes in the source rock composition, the melting depth, reactions with the country rock, the rate of magma ascent, mixing between the residual and crustal partial melts, and even the physical process of melt migration (Annen et al., 2006; Jackson et al., 2005, 2003; Solano et al., 2012). All these processes make the

inclusion of melt migration in large-scale geodynamical models particularly complicated, but would allow a better understanding of whether melts produced at depth, such as around the location of breakoff in these models, would be observable at or near the surface, and also would provide more realistic information on the expected compositions of these melts, allowing a better comparison with observations from post-collisional areas.

The uncertainty in the values used as melt extraction thresholds also prevents a realistic estimate of the amount of extracted melting that would be expected at or near the surface. Volumes of melt have been calculated in Chapter 4 based upon these thresholds, but given the uncertainty in the thresholds, should only be used in a relative sense. However, if the total amount of melt could be accurately determined and hence compared to observations from post-collisional areas, this may prove useful when considering the possible processes responsible for post-collisional melting.

Finally, one perhaps significant limitation of the thermodynamic database is the depth to which this can be extrapolated. Bouilhol et al. (2015) have modified the melt solid solution for the asthenospheric mantle (used in Chapter 4) from that of White et al. (2001) so as to better represent high pressure conditions. This is especially critical for the models presented in Chapter 4, as breakoff, and any subsequent melting, can occur within the middle of the upper mantle. The lookup table for all materials in this study has only been calculated up to a maximum pressure of 9 GPa (equivalent to a depth of ~275 km for the mantle) (see Chapter 2.5.1 and Table 2.5), due to uncertainty in the stable mineral assemblages at higher pressures. Hence, melts beyond this pressure are not present in the models, not because material reaches conditions that are sub-solidus, but because it exceeds the pressure range for which the lookup tables have been calculated. For example, the volume and duration of both the crustal melting within the tip of the detached slab and the release of water from this material (and the subsequent melting of the asthenospheric mantle) following breakoff may be underestimated. This is because the detached slab descends deeper into the upper mantle whilst melting is still ongoing (Fig. 4.4N). The formation of supercritical fluids at high pressures may further put into question the reliability of the calculated stable phase assemblages even at pressures within the range of the lookup tables. However, for the process of breakoff, and indeed in other geodynamical processes, the migration of water and melting at these depths is of key importance for understanding thermo-dynamical processes.

### 5.2.2 3D models of mantle flow and melting during slab breakoff

The flow within the Earth's mantle is an inherently three dimensional process, only being accurately represented in two dimensions where structural variations parallel to the trench are minimal. van Hunen and Allen (2011) show that 2D modelling of collision and breakoff produces very similar dynamical results to those in 3D, when collision occurs uniformly along the length of a subduction trench. However, two factors may mean 3D modelling is important when investigating the process of slab breakoff. Firstly, collisional environments can be very complex, involving adjacent oceanic basins and continental plates, which may affect the dynamics of collision and breakoff. The above study shows that any asymmetry in collision will affect the location of initial breakoff within the 3D slab and the process of slab tearing. Subsequently, numerical models have investigated different 3D collisional scenarios, including: the breakoff dynamics resulting from the collision of a continental corner (Li et al., 2013), including the effect that a transform boundary between the oceanic and continental plates may have (Duretz et al., 2014); and the effect of the collision of multiple continental blocks on the pattern of back-arc spreading in the Mediterranean region (Magni et al., 2014b).

Secondly, the induced 3D mantle flow patterns resulting from these more complex geometries, or simply resulting from the process of slab tearing itself, may have significant consequences for magmatism, and has been little investigated by numerical studies. Menant et al. (2016) demonstrate the importance of 3D subduction and collision dynamics and resulting mantle flow on the magmatic evolution, which controls the resulting emplacement of magmas. An expansion of this study to include the effects of 3D mantle flow on the magma genesis would be beneficial, and along-strike variations in collision dynamics could also be considered. This may be particularly applicable when comparing results to regions such as the Central Apennines, Calabrian Arc, the Aegean region, and the Gibraltar Arc, where there are significant along strike variations in the slab and collisional dynamics. A 3D model may lead to an increase in the amount of melt generation in certain collisional environments through a number of different mechanisms. Firstly, an increase in melting of the asthenosphere could occur through dry decompressional melting, when mantle upwells from behind the detached slab towards areas of thin oceanic lithosphere, rather than towards continental lithosphere as observed in the studies in this thesis. This could occur in areas where continental collision takes place adjacent to sections of ongoing oceanic subduction. Magni et al. (2014b) show where multiple continental blocks enter a collision zone, the formation of, and extension within an intervening backarc basin may develop. After breakoff within the continental slabs, mantle material flows through the slab windows towards this

newly formed backarc basin. Secondly, faster and more prolonged mantle flow patterns could be generated, resulting from either the formation of vertical tears in the subducting slab or from faster and more abrupt breakoff events, due to greater slab pull forces acting as a result of continuing subduction further along the subduction trench. This may lead to a faster upwelling of mantle material and an increase in asthenospheric melting, which could be further enhanced by an increase in the release of fluids from other sections of the subducted slab. A possible increase and prolongation of mantle flow through the slab window could also result in additional heating of both the overriding mantle lithosphere, and subducted continental crust, which may raise the temperature of these above the solidus. Experiments could be carried out using coupled thermo-petrological models where continental blocks are positioned adjacent to areas of ongoing subduction, to investigate the effect that 3D subduction dynamics and mantle flow patterns may have on the generation of breakoff-induced melting.

### 5.2.3 A study of magmatic processes during delamination

When calculating the amount of magmatism following collision (Chapter 4), this study shows that the process of delamination is capable of producing a significantly greater amount of melting than any other processes that are observed (e.g. Models 24 & 30-32 - Fig. 4.9). The aim in this study was to focus specifically on the effects of slab breakoff; however, these results show that whole crustal-lithosphere delamination may be a viable mechanism for generating significant amounts of melting (Chapter 4). The inflow of hot asthenospheric material melt both the base of the overlying crust that has been removed from the descending mantle lithosphere, and any crust that has remained attached to this lithosphere (Fig. 4.6). Previous numerical studies have found similar results, including both the dynamics of this system and the melting of the crust (Duretz and Gerya, 2013; Ueda et al., 2012). The melting of inflowing asthenospheric mantle in front of the delaminating slab is also observed. This occurs during the delamination between the subducting continental crust and lithospheric mantle, due to the dewatering of crustal and sedimentary material which remain attached to the descending mantle lithosphere. This hydrates the inflowing mantle and depresses the solidus in this region (Fig. 4.6).

Many areas globally show the presence of thick lithospheric roots around the site of collision (e.g. Priestley et al., 2012), suggesting that delamination processes are not currently occurring. However, a form of delamination has been proposed for the magmatic activity occurring within Eastern Anatolia where the mantle lithosphere is very thin. Keskin (2003) suggests the process of slab steepening beneath a weak accretionary wedge could have

occurred in this region, before a later breakoff event. Bartol and Govers (2014) also find that the present-day topography and surface heat flow is consistent with a delamination event below both the Central and Eastern Anatolian plateaux. This delamination could have led to mantle upwelling and significant melting, as a result of the decompression process and hotter asthenosphere coming into contact with accretionary material at shallow depths. This is very similar dynamically to many of the models in this study which implement a dry quartzite crustal rheology for both the upper and lower crust. Although such crustal rheology is perhaps weaker than the average lower crust, this may be more in line with the weaker accretionary wedge material in Eastern Anatolia (Keskin, 2003). Further investigation into the conditions required to generate crustal and mantle melting would be useful for considering where this may be observed. Additionally, modelling the specific scenario presented for Eastern Anatolia may be useful in understanding the link between the dynamics and magmatism in this area.

### 5.2.4 The change in collision dynamics and magmatism resulting from far-field forces

Upon collision, the main driving force that results from the negative buoyancy of the subducting oceanic lithosphere is counteracted by the positive buoyancy of the continental lithosphere. Following slab breakoff the downward force from the stagnated slab is removed. Hence, it is to be expected that convergence would stop and eduction of the slab (i.e. the coherent return of the continental lithosphere to the surface) may even occur after breakoff. However, some collision zones show that the plates continue to converge after initial collision, suggesting an additional driving force may be present. This is the case for the India-Asia collision, where plate reconstructions show convergence over the past 50 Myr (Copley et al., 2010; Molnar and Tapponnier, 1975). Many differing explanations have been proposed to account for this, including: deformation within the Tibetan plateau which can accommodate some convergence including crustal thickening and continental underthrusting (Molnar and Tapponnier, 1975); continued subduction of the continental lithosphere after removal of the more buoyant continental crust (Capitanio et al., 2010; Patriat and Achache, 1984); continued slab pull forces from subduction to the east and west of the main collision (Li et al., 2008a); and mantle drag from deeper mantle convection (Becker and Faccenna, 2011), and lateral extrusion (Patriat and Achache, 1984). Explanations also include those which are not directly related to the collisional process, including: removal of thickened lithosphere (Molnar and Stock, 2009); an increased viscous resistance from the mantle lithosphere (Clark, 2012); and the effect of mantle plumes (Cande and Stegman, 2011; Van Hinsbergen et al., 2011). Similarly, for the earlier collision between north and south China,

Dong et al. (2013) suggested that subduction of eclogitised mafic crust during collision could continue to drive convergence.

Within the parametric studies (Chapters 3 and 4), convergence completely stops after collision, and extensional processes are even observed within a post-collisional setting after breakoff. This has also been modelled in other studies which do not impose any outside driving forces (e.g. Duretz et al., 2012). Some of the suggested means of continued convergence could be observable in the models presented here, but some would require a change in model setup. Numerical models which do not observe eduction, but instead result in slab uplift and underplating after breakoff, are a result of imposed inflow velocities along the boundaries (e.g. Li et al., 2013). This could be considered a first order approximation of the effect that a plume may have, or the presence of mantle flow patterns which are not related to the collision and breakoff process.

Preliminary models were designed where an outflow velocity is imposed along the right hand side boundary (Fig. 5.1); the initial outflow velocity is not turned off, but is reduced in magnitude to prevent the slab being sucked through the right hand side boundary too rapidly. An inflow velocity along the left hand side boundary was also tested (such as that which could be generated by mid-ocean ridge push forces or mantle plumes), but this imposes a velocity directly on the subducting slab, often resulting in lateral migration of the subduction zone out of the model domain.

These initial results show that imposing a mantle flow does not significantly alter the breakoff depth, but does reduce the breakoff time by almost half, probably due to the imposed additional stress field that lowers the (stress-dependent) viscosity of the modelled materials. The continental crust is also subducted significantly deeper, resulting in final breakoff within the continental lithosphere (Fig. 5.1C). Hence the imposed flow both provides an additional force on the buoyant continental crust and aids the necking of the slab through dislocation creep. The slab subsequently underplates the overriding lithosphere, leading to slight relamination of the continental crust as it heats up within the thickened lithosphere (Fig. 5.1D). The amount of melt extracted from the continental crust is over twice that with no imposed mantle flow; a result of the deep subduction of the continental crust. Subsequently, the crust remains partially molten within the thickened lithosphere, but does not reach significant degrees of melting to be extracted. To explore more thoroughly the effect that mantle flow patterns may have on melting during collision, the solidus of the crust needs to be constrained more reliably at greater depths.

Further studies could investigate the change in breakoff dynamics and melting for varying mantle flow velocities, and look at the flow required to prevent the eduction of the slab. A variety of different parameters could be varied to give a range in the type of collisional environment. Alternatively, data from mantle circulation computations (such as those based on seismic tomography (e.g. Faccenna et al., 2013; Faccenna and Becker, 2010)) could be used to define the boundary conditions of the flow field and look specifically at the collisions occurring between India and Eurasia, Arabian and Eurasia, or within the Mediterranean region.

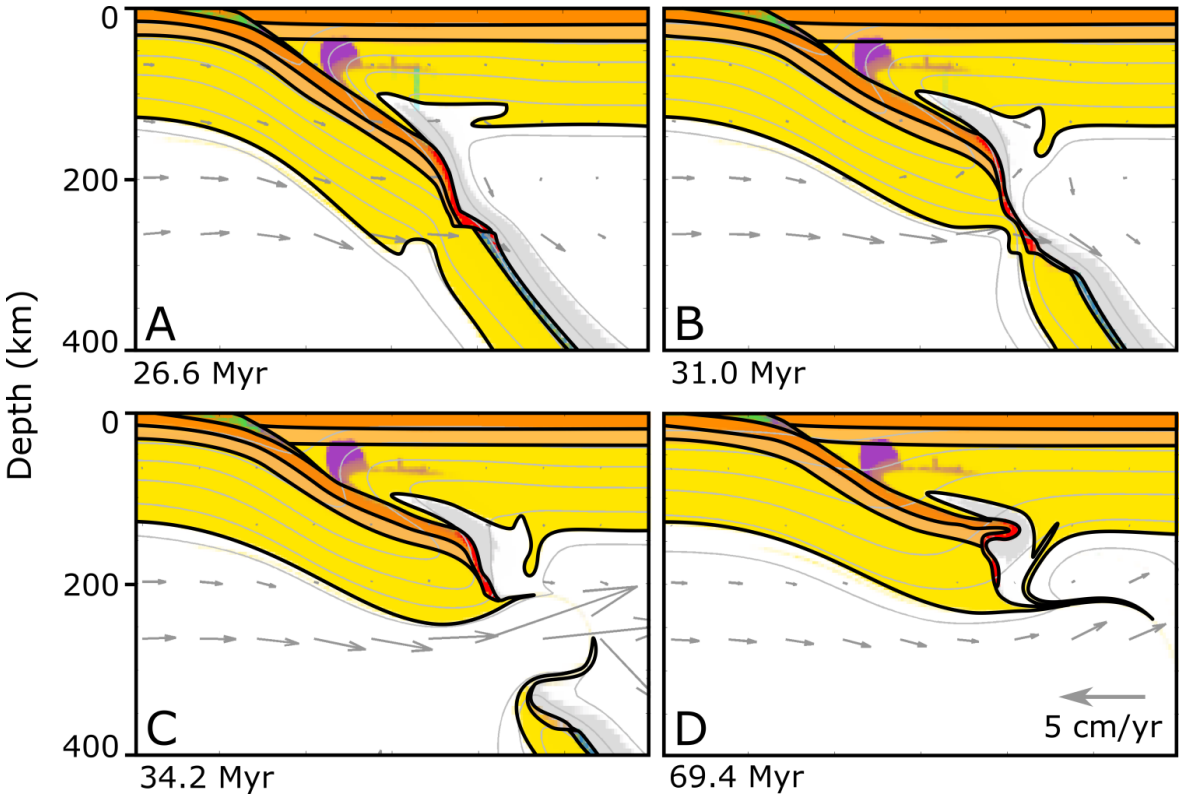


**Figure 5.1: Slab breakoff dynamics with a background mantle flow.** An outflow velocity is imposed out of the right hand side boundary. Breakoff occurs at a similar depth compared to the case with no outflow (see Fig. 3.1C), but within the continental lithosphere, and results in underplating of the slab below the overriding plate.

### 5.2.5 The effect of mantle plumes on magmatism during collision and breakoff

In addition to the driving force that mantle plumes may have during continental collision, plumes may also have a thermal and magmatic effect during slab breakoff. Due to their hotter temperature, plumes may cause thermal weakening of a slab which could aid in the breakoff process. Plumes may also heat material above the slab and perhaps induce melting of the overriding lithosphere, along with more crustal melting within the detached slab.

Macera et al. (2008) suggest a slab-plume interaction to explain the HIMU (high $^{238}U/^{204}Pb$) component within the south-eastern Alps volcanics, perhaps indicative of a deep mantle signature. A similar mechanism has also been suggested within the Arabia-Anatolia-Aegean system, with the Afar upwelling perhaps promoting slab breakoff (Faccenna et al., 2013). Analogue modelling of slab-plume interactions have been undertaken where a plume was positioned behind a retreating slab, which show that based upon buoyancy considerations, the plume conduit can be considerably deflected by the slab motion and can also act to decrease the rate of subduction (Mériaux et al., 2015). However, this work does not include the thermal effects of a plume, which are perhaps more important when investigating the role that plumes may have during slab breakoff.

A similar scenario could be modelled using numerical simulations, to determine the possible impact of a plume during continental collision. These could include both magmatic and dynamical effects, perhaps inducing faster and shallower breakoff which may have further consequences for melting. The conditions required for such effects could also be constrained. Wang et al. (2015) found that for plumes to generate significant thermomechanical erosion below continental cratons, a significant degree of metasomatic modification is also required, and it may be that this or other factors are required to induce or accelerate the breakoff process. A number of properties of a plume could be varied, such as the size, buoyancy and excess temperature. The location of the plume could also be adjusted to determine the relative impact based on the distance from the site of collision. Duggen et al. (2009) suggest that plume material is capable of flowing large distances (>1500 km) whilst entrained below the lithosphere and can hence have a magmatic effect over a large distance from the plume head.

### 5.2.6 Post-collisional magmatism within an early Earth

The dynamics of both collision and breakoff are likely to have been significantly different within the early Earth. Hotter mantle temperatures, perhaps 300 K higher than at present-day, along with a possible change in both the oceanic and continental plate strength and buoyancy, subduction velocity and amount of radiogenic heating from present day conditions may have contributed to this (Sizova et al., 2014; van Hunen and Moyen, 2012). The emergence of ultra-high pressure metamorphism (UHPM) around 540-530 Ma indicates the subduction of continental crust to depths great enough to produce these high pressure minerals and perhaps represents a change in collisional style to that similar to today (Maruyama and Liou, 1998). Based upon the numerical modelling of collision and breakoff under present day collision, van Hunen and Allen (2011) suggest that a lower slab strength

during the Archaean could be responsible for earlier and shallower breakoff, hence precluding the formation of UHPM. This was investigated more thoroughly by Sizova et al. (2014), who model the effect that an increase in mantle temperature, radiogenic heat production, and thickness and chemical buoyancy of the continental lithosphere has on collisional dynamics. For an increase in mantle temperature of 80-100 K, broadly corresponding to the Neoproterozoic, a change in collision mode is observed, which results in significantly shallower breakoff.

The development of post-collisional breakoff and its magmatic effect from early Earth conditions to present day could be further explored using the models that have been developed here. Preliminary tests were conducted, systematically increasing the ambient mantle temperature for the reference model (see Chapter 4) from 1350 °C to 1430 °C, with an interval of 20 °C (Fig. 5.2). Both the breakoff depth and breakoff time decrease with increasing mantle temperature (Figs. 5.2A and 5.2B); the timing showing a linear dependence upon the temperature most likely due to the weakening mantle lithosphere and increase in dislocation creep during necking. A slight decrease in the maximum subduction depth of the continental crust is also observed for an increase in temperature between 1350 and 1410 °C (from 155-142 km), and a further more significant decrease to 122 km when the temperature is increased to 1430 °C (Fig. 5.2C). It is unknown whether the effect of temperatures higher than those tested here would be to continue these trends and whether they would result in significantly different collisional and breakoff dynamics. The effect that this may have on post-collisional magmatism is also currently unexplored. During tests with ambient mantle temperatures of 1450 °C and above, oceanic subduction failed to develop due to early slab breakoff during this period. This may be an artefact of the model setup, and the weak zone parameters may need to be adjusted to prevent this. The effect of melt weakening is also not considered, which Sizova et al. (2010) find to be a key parameter in controlling the development of subduction within the early Earth, and hence implementation of this within the model setup may be necessary.

Here only the effect of temperature has been explored, but a number of factors which may have been different in the early Earth could be varied as well, creating a multi-dimensional parametric study as in Chapter 4, as the relative importance of these is unknown. Possible parameters which could be varied include the ambient mantle temperature, radiogenic heat production, crustal rheology, water content, and continental lithospheric buoyancy and thickness, as in Sizova et al. (2014), Furthermore, the oceanic plate age, oceanic crustal thickness, subduction velocity, the effect of melt and hydration weakening, and amount of initial hydration could be varied. The early Earth may have been hotter but may also have

been drier, which would have had a significant effect on both the rheology and the melt generation. The phase transition at the base of the upper mantle would also have been affected by a variation in temperature, and hence a different bottom boundary condition or the inclusion of a lower mantle may be required.

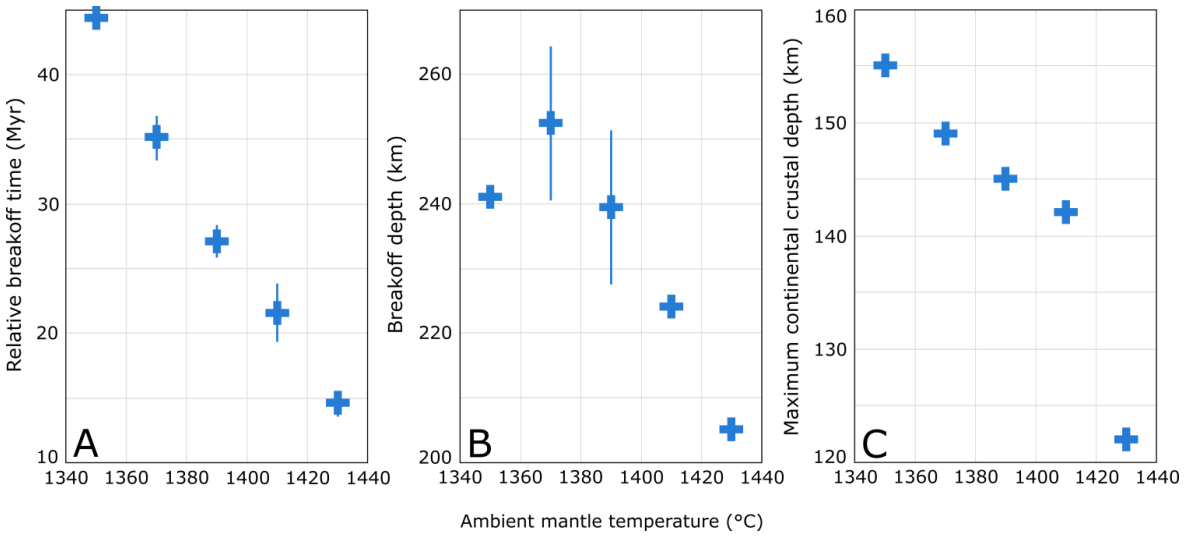


**Figure 5.2: The effect on breakoff dynamics with increasing ambient mantle temperature.** Temperature increase from 1350 °C to 1430 °C. For these preliminary models, data values were stored less frequently during the model calculation. Hence, the exact values for breakoff depth and timing have been calculated less accurately. The range in this uncertainty is represented by the blue, vertical lines in A and B.

## 5.3 Thesis summary

The results presented in this thesis show that the relationship between magmatism and slab breakoff, within the context of a continental collision, is perhaps a more complex process than previously considered. Other geodynamical processes may often be at work alongside breakoff, and it may be difficult to distinguish the relative effects of these. Magmatism within post-collisional areas is most likely the result of many geodynamic processes, and although breakoff may be capable of inducing some of this melting, it appears unlikely to account for the wide variety of magmatic observations

.

# Bibliography


Ahmadzadeh, G., Jahangiri, A., Lentz, D., Mojtahedi, M., 2010. Petrogenesis of Plio-Quaternary post-collisional ultrapotassic volcanism in NW of Marand, NW Iran. J. Asian Earth Sci. 39, 37–50.

Allen, M.B., Kheirkhah, M., Neill, I., Emami, M.H., McLeod, C.L., 2013. Generation of arc and within-plate chemical signatures in collision zone magmatism: Quaternary lavas from Kurdistan Province, Iran. J. Petrol. 54, 887–911.

Altunkaynak, Ş., Genç, Ş.C., 2008. Petrogenesis and time-progressive evolution of the Cenozoic continental volcanism in the Biga Peninsula, NW Anatolia (Turkey). Lithos 102, 316–340.

Andrews, E.R., Billen, M.I., 2009. Rheologic controls on the dynamics of slab detachment. Tectonophysics 464, 60–69.

Annen, C., Blundy, J.D., Sparks, R.S.J., 2006. The genesis of intermediate and silicic magmas in deep crustal hot zones. J. Petrol. 47, 505–539. doi:10.1093/petrology/egi084

Bartol, J., Govers, R., 2014. A single cause for uplift of the Central and Eastern Anatolian plateau? Tectonophysics 637, 116–136. doi:10.1016/j.tecto.2014.10.002

Baumann, C., Gerya, T. V., Connolly, J. a. D., 2010. Numerical modelling of spontaneous slab breakoff dynamics during continental collision. Geol. Soc. London, Spec. Publ. 332, 99–114. doi:10.1144/SP332.7

Becker, T.W., Faccenna, C., 2011. Mantle conveyor beneath the Tethyan collisional belt. Earth Planet. Sci. Lett. 310, 453–461. doi:10.1016/j.epsl.2011.08.021

Bijwaard, H., Spakman, W., Engdahl, E.R., 1998. Closing the gap between regional and global travel time tomography. J. Geophys. Res. 103, 30055. doi:10.1029/98JB02467

Bird, P., 1979. Continental delamination and the Colorado Plateau. J. Geophys. Res. 84, 7561–7571.

Bird, P., 1978. Initiation of intracontinental subduction in the Himalaya. J. Geophys. Res. 83, 4975–4987.

Bottrill, A.D., Van Hunen, J., Allen, M.B., 2012. Insight into collision zone dynamics from topography: Numerical modelling results and observations. Solid Earth 3, 387–399. doi:10.5194/se-3-387-2012

Bouilhol, P., Magni, V., van Hunen, J., Kaislaniemi, L., 2015. A numerical approach to melting in warm subduction zones. Earth Planet. Sci. Lett. 411, 37–44.

Brown, M., 2007. Crustal melting and melt extraction, ascent and emplacement in orogens: mechanisms and consequences. J. Geol. Soc. London. 164, 709–730. doi:10.1144/0016-76492006-171

Buiter, S.J.H., Govers, R., Wortel, M.J.R., 2002. Two-dimensional simulations of surface deformation caused by slab detachment. Tectonophysics 354, 195–210. doi:10.1016/S0040-1951(02)00336-0

Bureau, H., Keppler, H., 1999. Complete miscibility between silicate melts and hydrous fluids in the upper mantle: Experimental evidence and geochemical implications. Earth Planet. Sci. Lett. 165, 187–196. doi:10.1016/S0012-821X(98)00266-0

Bürgmann, R., Dresen, G., 2008. Rheology of the Lower Crust and Upper Mantle: Evidence from Rock Mechanics, Geodesy, and Field Observations. Annu. Rev. Earth Planet. Sci.

36, 531–567. doi:10.1146/annurev.earth.36.031207.124326

Burkett, E.R., Billen, M.I., 2010. Three-dimensionality of slab detachment due to ridge-trench collision: Laterally simultaneous boudinage versus tear propagation. Geochemistry, Geophys. Geosystems 11, 1–21. doi:10.1029/2010GC003286

Byerlee, J., 1978. Friction of rocks. Pure Appl. Geophys. PAGEOPH 116, 615–626. doi:10.1007/BF00876528

Cande, S.C., Stegman, D.R., 2011. Indian and African plate motions driven by the push force of the Réunion plume head. Nature 475, 47–52. doi:10.1038/nature10174

Capitanio, F. a., Morra, G., Goes, S., Weinberg, R.F., Moresi, L., 2010. India–Asia convergence driven by the subduction of the Greater Indian continent. Nat. Geosci. 3, 136–139. doi:10.1038/ngeo725

Castillo, P.R., 2012. Adakite petrogenesis. Lithos 134–135, 304–316. doi:10.1016/j.lithos.2011.09.013

Chatelain, J., Molnar, P., Prévot, R., Isacks, B., 1992. Detachment of part of the downgoing slab and uplift of the New Hebrides (Vanuatu) Islands. Geophys. Res. Lett. 19, 1507–1510.

Chen, R.X., Zheng, Y.F., Gong, B., 2011. Mineral hydrogen isotopes and water contents in ultrahigh-pressure metabasite and metagranite: Constraints on fluid flow during continental subduction-zone metamorphism. Chem. Geol. 281, 103–124. doi:10.1016/j.chemgeo.2010.12.002

Chen, Y., Zhu, D.C., Zhao, Z.D., Meng, F.Y., Wang, Q., Santosh, M., Wang, L.Q., Dong, G.C., Mo, X.X., 2014. Slab breakoff triggered ca. 113Ma magmatism around Xainza area of the Lhasa Terrane, Tibet. Gondwana Res. 26, 449–463. doi:10.1016/j.gr.2013.06.005

Chertova, M. V., Geenen, T., Van Den Berg, A., Spakman, W., 2012. Using open sidewalls for modelling self-consistent lithosphere subduction dynamics. Solid Earth 3, 313–326. doi:10.5194/se-3-313-2012

Chiu, H.Y., Chung, S.L., Zarrinkoub, M.H., Mohammadi, S.S., Khatib, M.M., Iizuka, Y., 2013. Zircon U-Pb age constraints from Iran on the magmatic evolution related to Neotethyan subduction and Zagros orogeny. Lithos 162–163, 70–87. doi:10.1016/j.lithos.2013.01.006

Chopin, C., 1984. Coesite and pure pyrope in high-grade blueschists of the Western Alps: a first record and some consequences. Contrib. to Mineral. Petrol. 86, 107–118. doi:10.1007/BF00381838

Chung, S.L., Chu, M.F., Ji, J., O'Reilly, S.Y., Pearson, N.J., Liu, D., Lee, T.Y., Lo, C.H., 2009. The nature and timing of crustal thickening in Southern Tibet: Geochemical and zircon Hf isotopic constraints from postcollisional adakites. Tectonophysics 477, 36–48. doi:10.1016/j.tecto.2009.08.008

Chung, S.L., Chu, M.F., Zhang, Y., Xie, Y., Lo, C.H., Lee, T.Y., Lan, C.Y., Li, X., Zhang, Q., Wang, Y., 2005. Tibetan tectonic evolution inferred from spatial and temporal variations in post-collisional magmatism. Earth-Science Rev. 68, 173–196.

Clark, M.K., 2012. Continental collision slowing due to viscous mantle lithosphere rather than topography. Nature 483, 74–77. doi:10.1038/nature10848

Condamine, P., Médard, E., 2014. Experimental melting of phlogopite-bearing mantle at 1 GPa: Implications for potassic magmatism. Earth Planet. Sci. Lett. 397, 80–92. doi:10.1016/j.epsl.2014.04.027

Connolly, J.A.D., 2009. The geodynamic equation of state: What and how. Geochemistry,

Geophys. Geosystems 10. doi:10.1029/2009GC002540

Connolly, J.A.D., 2005. Computation of phase equilibria by linear programming: A tool for geodynamic modeling and its application to subduction zone decarbonation. Earth Planet. Sci. Lett. 236, 524–541. doi:10.1016/j.epsl.2005.04.033

Copley, A., Avouac, J.P., Royer, J.Y., 2010. India-Asia collision and the Cenozoic slowdown of the Indian plate: Implications for the forces driving plate motions. J. Geophys. Res. Solid Earth 115, 1–14. doi:10.1029/2009JB006634

Coulon, C., Megartsi, M., Fourcade, S., Maury, R.C., Bellon, H.B., Louni-Hacini, A., Cotten, J., Coutelle, A., Hermitte, D., 2002. Post-collisional transition from calc-alkaline to alkaline volcanism during the Neogene in Oranie (Algeria): magmatic expression of a slab breakoff. Lithos 62, 87–110.

Currie, C.A., Hyndman, R.D., 2006. The thermal structure of subduction zone back arcs. J. Geophys. Res. Solid Earth 111, 1–22. doi:10.1029/2005JB004024

Dannberg, J., Heister, T., 2015. 3D Compressible Melt Transport with Adaptive Mesh Refinement. EGU Gen. Assem. Conf. Abstr. 17, 6826.

Davies, J.H., von Blanckenburg, F., 1995. Slab breakoff: A model of lithosphere detachment and its test in the magmatism and deformation of collisional orogens. Earth Planet. Sci. Lett. 129, 85–102.

De Astis, G., Kempton, P.D., Peccerillo, A., Wu, T.W., 2006. Trace element and isotopic variations from Mt. Vulture to Campanian volcanoes: constraints for slab detachment and mantle inflow beneath southern Italy. Contrib. to Mineral. Petrol. 151, 331–351.

Di Giuseppe, E., Van Hunen, J., Funiciello, F., Faccenna, C., Giardini, D., 2008. Slab stiffness control of trench motion: Insights from numerical models. Geochemistry, Geophys. Geosystems 9, 1–19. doi:10.1029/2007GC001776

Dilek, Y., Altunkaynak, Ş., 2007. Cenozoic Crustal Evolution and Mantle Dynamics of Post-Collisional Magmatism in Western Anatolia. Int. Geol. Rev. 49, 431–453.

Dilek, Y., Imamverdiyev, N., Altunkaynak, Ş., 2010. Geochemistry and tectonics of Cenozoic volcanism in the Lesser Caucasus (Azerbaijan) and the peri-Arabian region: collision-induced mantle dynamics and its magmatic fingerprint. Int. Geol. Rev. 52, 536–578.

Dong, S., Gao, R., Yin, A., Guo, T., Zhang, Y., Hu, J., Li, J., Shi, W., Li, Q., 2013. What drove continued continent-continent convergence after ocean closure? Insights from high-resolution seismic-reflection profiling across the Daba Shan in central China. Geology 41, 671–674. doi:10.1130/G34161.1

Duggen, S., Hoernle, K.A., Hauff, F., Klügel, A., Bouabdellah, M., Thirlwall, M.F., 2009. Flow of Canary mantle plume material through a subcontinental lithospheric corridor beneath Africa to the Mediterranean. Geology 37, 283–286. doi:10.1130/G25426A.1

Duretz, T., Gerya, T. V., 2013. Slab detachment during continental collision: Influence of crustal rheology and interaction with lithospheric delamination. Tectonophysics 602, 124–140. doi:10.1016/j.tecto.2012.12.024

Duretz, T., Gerya, T. V., Kaus, B.J.P., Andersen, T.B., 2012a. Thermomechanical modeling of slab eduction. J. Geophys. Res. Solid Earth 117, 2011–2012. doi:10.1029/2012JB009137

Duretz, T., Gerya, T. V., May, D.A., 2011. Numerical modelling of spontaneous slab breakoff and subsequent topographic response. Tectonophysics 502, 244–256.

Duretz, T., Gerya, T. V., Spakman, W., 2014. Slab detachment in laterally varying subduction zones: 3-D numerical modeling. Geophys. Res. Lett. 41, 1951–1956.

doi:10.1002/2014GL059472

Duretz, T., Schmalholz, S.M., Gerya, T. V., 2012b. Dynamics of slab detachment. Geochemistry, Geophys. Geosystems 13.

England, P.C., Thompson, A., 1986. Some thermal and tectonic models for crustal melting in continental collision zones. Geol. Soc. London, Spec. Publ. 19, 83–94.

Ernst, W.G., 1999. Hornblende, the continent maker - Evolution of H2O during circum-Pacific subduction versus continental collision. Geology 27, 675–678. doi:10.1130/0091-7613(1999)027<0675

Ernst, W.G., Mosenfelder, J.L., Leech, M.L., Liu, J., 1998. H2O recycling during continental collision: phase equilibrium and kinetic considerations.

Faccenda, M., Burlini, L., Gerya, T. V., Mainprice, D., 2008. Fault-induced seismic anisotropy by hydration in subducting oceanic plates. Nature 455, 1097–1100. doi:10.1038/nature07376

Faccenda, M., Minelli, G., Gerya, T. V., 2009. Coupled and decoupled regimes of continental collision: Numerical modeling. Earth Planet. Sci. Lett. 278, 337–349.

Faccenna, C., Becker, T.W., 2010. Shaping mobile belts by small-scale convection. Nature 465, 602–605.

Faccenna, C., Becker, T.W., Jolivet, L., Keskin, M., 2013. Mantle convection in the Middle East: Reconciling Afar upwelling, Arabia indentation and Aegean trench rollback. Earth Planet. Sci. Lett. 375, 254–269. doi:10.1016/j.epsl.2013.05.043

Faccenna, C., Becker, T.W., Lallemand, S., Lagabrielle, Y., Funiciello, F., Piromallo, C., 2010. Subduction-triggered magmatic pulses: A new class of plumes? Earth Planet. Sci. Lett. 299, 54–68. doi:10.1016/j.epsl.2010.08.012

Faccenna, C., Civetta, L., D'Antonio, M., Funiciello, F., Margheriti, L., Piromallo, C., 2005. Constraints on mantle circulation around the deforming Calabrian slab. Geophys. Res. Lett. 32, 1–4. doi:10.1029/2004GL021874

Faccenna, C., Molin, P., Orecchio, B., Olivetti, V., Bellier, O., Funiciello, F., Minelli, L., Piromallo, C., Billi, A., 2011. Topography of the Calabria subduction zone (southern Italy): Clues for the origin of Mt. Etna. Tectonics 30, 1–20. doi:10.1029/2010TC002694

Faul, U.H., 1997. Permeability of partially molten upper mantle rocks from experiments and percolation theory. J. Geophys. Res. 102, 10299. doi:10.1029/96JB03460

Fowler, C.M.R., 2005. The solid Earth, 2nd ed. Cambridge University Press, Cambridge.

Fukao, Y., Obayashi, M., 2013. Subducted slabs stagnant above, penetrating through, and trapped below the 660 km discontinuity. J. Geophys. Res. Solid Earth 118, 5920–5938. doi:10.1002/2013JB010466

Fukao, Y., Obayashi, M., Inoue, H., Nenbai, M., 1992. Subducting slabs stagnant in the mantle transition zone. J. Geophys. Res. 97, 4809. doi:10.1029/91JB02749

Fukao, Y., Obayashi, M., Nakakuki, T., 2009. Stagnant Slab: A Review. Annu. Rev. Earth Planet. Sci. 37, 19–46. doi:10.1146/annurev.earth.36.031207.124224

Funiciello, F., Faccenna, C., Heuret, A., Lallemand, S., Di Giuseppe, E., Becker, T.W., 2008. Trench migration, net rotation and slab-mantle coupling. Earth Planet. Sci. Lett. 271, 233–240. doi:10.1016/j.epsl.2008.04.006

Garel, F., Goes, S., Davies, D.R., Davies, J.H., Kramer, S.C., Wilson, C.R., 2014. Interaction of subducted slabs with the mantle transition-zone: A regime diagram from 2-D thermo-mechanical models with a mobile trench and an overriding plate. Geochemistry, Geophys. Geosystems 15, 1739–1765.

Gerya, T., 2010. Introduction to Numerical Geodynamic Modelling. Cambridge University Press, Cambridge.

Gerya, T. V., Yuen, D.A., 2003. Rayleigh - Taylor instabilities from hydration and melting propel “cold plumes” at subduction zones. Earth Planet. Sci. Lett. 212, 47–62. doi:10.1016/S0012-821X(03)00265-6

Gerya, T. V., Yuen, D.A., Maresch, W. V., 2004. Thermomechanical modelling of slab detachment. Earth Planet. Sci. Lett. 226, 101–116.

Ghasemi, A., Talbot, C.J., 2006. A new tectonic scenario for the Sanandaj-Sirjan Zone (Iran). J. Asian Earth Sci. 26, 683–693.

Ghazian, R.K., Buiter, S.J.H., 2013. A numerical investigation of continental collision styles. Geophys. J. Int. 193, 1133–1152. doi:10.1093/gji/ggt068

Göğüş, O.H., Psyklywec, R.N., 2008. Mantle lithosphere delamination driving plateau uplift and synconvergent extension in eastern Anatolia. Geology 36, 723–726. doi:10.1130/G24982A.1

Göğüş, O.H., Pysklywec, R.N., 2008. Near-surface diagnostics of dripping or delaminating lithosphere. J. Geophys. Res. Solid Earth 113, 1–11. doi:10.1029/2007JB005123

Gordon, S.M., Whitney, D.L., Teyssier, C., Fossen, H., 2013. U-Pb dates and trace-element geochemistry of zircon from migmatite, Western Gneiss Region, Norway: Significance for history of partial melting in continental subduction. Lithos 170–171, 35–53. doi:10.1016/j.lithos.2013.02.003

Govers, R., Wortel, M.J.R., 2005. Lithosphere tearing at STEP faults: Response to edges of subduction zones. Earth Planet. Sci. Lett. 236, 505–523. doi:10.1016/j.epsl.2005.03.022

Guo, Z., Wilson, M., Zhang, M., Cheng, Z., Zhang, L., 2013. Post-collisional, K-rich mafic magmatism in south Tibet: Constraints on Indian slab-to-wedge transport processes and plateau uplift. Contrib. to Mineral. Petrol. 165, 1311–1340. doi:10.1007/s00410-013-0860-y

Gutscher, M.A., Maury, F., Eissen, J.P., Bourdon, E., 2000. Can slab melting be caused by flat subduction? Geology 28, 535–538. doi:10.1130/0091-7613(2000)28<535:CSMBCB>2.0.CO;2

Hacker, B.R., 1996. Eclogite Formation and the Rheology, Buoyancy, Seismicity, and H20 Content of Oceanic Crust, in: Bebout, G., Scholl, D.W., Kirby, S.H., Platt, J.P. (Eds.), Subduction: Top to Bottom, Geophyicsal Monograph 96. American Geophysical Union, Washington D.C., pp. 337–346.

Hacker, B.R., Gerya, T. V., Gilotti, J.A., 2013. Formation and exhumation of ultrahigh-pressure terranes. Elements 9, 289–293. doi:10.2113/gselements.9.4.289

Harris, N., Massey, J., 1994. Decompression and anatexis of Himalayan metapelites. Tectonics 13, 1537–1546.

Harrison, T.M., Grove, M., Lovera, O.M., Catlos, E.J., 1998. Greater Himalayan Crystallines. J. Geophys. Res. 103, 27017–27032.

Hart, S.R., Zindler, A., 1986. In search of a bulk-Earth composition. Chem. Geol. 57, 247–267. doi:10.1016/0009-2541(86)90053-7

Hermann, J., Zheng, Y.F., Rubatto, D., 2013. Deep fluids in subducted continental crust. Elements 9, 281–287. doi:10.2113/gselements.9.4.281

Hirth, G., Kohlstedt, D., 2003. Rheology of the upper mantle and the mantle wedge: A view from the experimentalists. Geophys. Monogr. Ser. 138, 83–105. doi:10.1029/138GM06

Hirth, G., Kohlstedt, D.L., 1996. Melt Extraction and the Evolution of the Lithosphere 144,

93–108.

Holland, T.J.B., Powell, R., 1998. An internally consistent thermodynamic data set for phases of petrological interest. J. Metamorph. Geol. 16, 309–343. doi:10.1111/j.1525-1314.1998.00140.x

Holt, A.F., Becker, T.W., Buffett, B.A., 2015. Trench migration and overriding plate stress in dynamic subduction models. Geophys. J. Int. 201, 172–192. doi:10.1093/gji/ggv011

Hou, Z.Q., Zheng, Y.C., Zeng, L. Sen, Gao, L.E., Huang, K.X., Li, W., Li, Q.Y., Fu, Q., Liang, W., Sun, Q.Z., 2012. Eocene-Oligocene granitoids in southern Tibet: Constraints on crustal anatexis and tectonic evolution of the Himalayan orogen. Earth Planet. Sci. Lett. 349–350, 38–52. doi:10.1016/j.epsl.2012.06.030

Isacks, B., Molnar, P., 1969. Mantle earthquake mechanisms and the sinking of the lithopshere.

Ismail-Zadeh, A., Tackley, P., 2010. Computational Methods for Geodynamics. Cambridge University Press, Cambridge.

Ito, K., Kennedy, G.C., 1971. An experimental study of the basalt-garnet granulite-eclogite transition. Struct. Phys. Prop. Earth's Crust 303–314.

Jackson, M.D., Cheadle, M.J., Atherton, M.P., 2003. Quantitative modeling of granitic melt generation and segregation in the continental crust. J. Geophys. Res. 108, 2332. doi:10.1029/2001JB001050

Jackson, M.D., Gallagher, K., Petford, N., Cheadle, M.J., 2005. Towards a coupled physical and chemical model for tonalite-trondhjemite-granodiorite magma formation. Lithos 79, 43–60. doi:10.1016/j.lithos.2004.05.004

Jadamec, M.A., Billen, M.I., 2012. The role of rheology and slab shape on rapid mantle flow: Three-dimensional numerical models of the Alaska slab edge. J. Geophys. Res. Solid Earth 117, 1–20. doi:10.1029/2011JB008563

Jahangiri, A., 2007. Post-collisional Miocene adakitic volcanism in NW Iran: Geochemical and geodynamic implications. J. Asian Earth Sci. 30, 433–447.

James, D.E., Fouch, M.J., Carlson, R.W., Roth, J.B., 2011. Slab fragmentation, edge flow and the origin of the Yellowstone hotspot track. Earth Planet. Sci. Lett. 311, 124–135. doi:10.1016/j.epsl.2011.09.007

Ji, W.-Q., Wu, F.-Y., Chung, S.-L., Wang, X.-C., Liu, C.-Z., Li, Q.-L., Liu, Z.-C., Liu, X.-C., Wang, J.-G., 2016. Eocene Neo-Tethyan slab breakoff constrained by 45 Ma oceanic island basalt–type magmatism in southern Tibet. Geology 44, G37612.1.

Ji, W.Q., Wu, F.Y., Chung, S.L., Li, J.X., Liu, C.Z., 2009. Zircon U-Pb geochronology and Hf isotopic constraints on petrogenesis of the Gangdese batholith, southern Tibet. Chem. Geol. 262, 229–245. doi:10.1016/j.chemgeo.2009.01.020

Kaislaniemi, L., 2015. Dynamic modelling of post-collisional magmatism. PhD Thesis. Durham University.

Kaislaniemi, L., van Hunen, J., 2014. Dynamics of lithospheric thinning and mantle melting by edge-driven convection: Application to Moroccan Atlas mountains. Geochemistry, Geophys. Geosystems 15, 3175–3189. doi:10.1002/2013GC005162

Kaislaniemi, L., van Hunen, J., Allen, M.B., Neill, I., 2014a. Sublithospheric small-scale convection - A mechanism for collision zone magmatism. Geology 42, 291–294.

Kaislaniemi, L., van Hunen, J., Allen, M.B., Neill, I., 2014b. Sublithospheric small-scale convection-A mechanism for collision zone magmatism. Geology 42, 291–294.

Kameyama, M., Yuen, D.A., Karato, S.I., 1999. Thermal-mechanical effects of low-

temperature plasticity (the Peierls mechanism) on the deformation of a viscoelastic shear zone. Earth Planet. Sci. Lett. 168, 159–172. doi:10.1016/S0012-821X(99)00040-0

Karato, S., Wu, P., 1993. Rheology the Upper Mantle : Synthesis 260.

Katz, R.F., Spiegelman, M., Langmuir, C.H., 2003. A new parameterization of hydrous mantle melting. Geochemistry, Geophys. Geosystems 4, 1–19. doi:10.1029/2002GC000433

Kaufmann, G., Lambeck, K., 2002. Glacial isostatic adjustment and the radial viscosity profile from inverse modeling. J. Geophys. Res. 107, 2280. doi:10.1029/2001JB000941

Keskin, M., 2003. Magma generation by slab steepening and breakoff beneath a subduction-accretion complex: An alternative model for collision-related volcanism in Eastern Anatolia, Turkey. Geophys. Res. Lett. 30.

Keskin, M., Genç, Ş.C., Tüysüz, O., 2008. Petrology and geochemistry of post-collisional Middle Eocene volcanic units in North-Central Turkey: Evidence for magma generation by slab breakoff following the closure of the Northern Neotethys Ocean. Lithos 104, 267–305.

Kheirkhah, M., Allen, M.B., Emami, M., 2009. Quaternary syn-collision magmatism from the Iran/Turkey borderlands. J. Volcanol. Geotherm. Res. 182, 1–12. doi:10.1016/j.jvolgeores.2009.01.026

Kheirkhah, M., Neill, I., Allen, M.B., 2015. Petrogenesis of OIB-like basaltic volcanic rocks in a continental collision zone: Late Cenozoic magmatism of Eastern Iran. J. Asian Earth Sci. 106, 19–33. doi:10.1016/j.jseaes.2015.02.027

Kheirkhah, M., Neill, I., Allen, M.B., Ajdari, K., 2013. Small-volume melts of lithospheric mantle during continental collision: Late Cenozoic lavas of Mahabad, NW Iran. J. Asian Earth Sci. 74, 37–49.

Kohn, M.J., Parkinson, C.D., 2002. Petrologic case for Eocene slab breakoff during the Indo-Asian collision. Geology 30, 591–594.

Labrousse, L., Andersen, T.B., Asgard, P., Hebert, R., Maluski, H., Schärer, U., 2004. Pressure-temperature-time deformation history of the exhumation of ultra-high pressure rocks in the Western Gneiss Region, Norway. Geol. Soc. Am. Spec. Pap. 380, 155–183. doi:10.1130/0-8137-2380-9.155

Labrousse, L., Duretz, T., Gerya, T., 2015. H<inf>2</inf>O-fluid-saturated melting of subducted continental crust facilitates exhumation of ultrahigh-pressure rocks in continental subduction zones. Earth Planet. Sci. Lett. 428, 151–161. doi:10.1016/j.epsl.2015.06.016

Lallemand, S., Heuret, A., Boutelier, D., 2005. On the relationships between slab dip, back-arc stress, upper plate absolute motion, and crustal nature in subduction zones. Geochemistry, Geophys. Geosystems 6. doi:10.1029/2005GC000917

Lambeck, K., 1998. Sea-level change, flacial rebound and mantle viscosity for northen Europe. Geophys 134, 102–144.

Lee, H.Y., Chung, S.L., Ji, J., Qian, Q., Gallet, S., Lo, C.H., Lee, T.Y., Zhang, Q., 2012. Geochemical and Sr-Nd isotopic constraints on the genesis of the Cenozoic Linzizong volcanic successions, southern Tibet. J. Asian Earth Sci. 53, 96–114.

Lee, H.Y., Chung, S.L., Lo, C.H., Ji, J., Lee, T.Y., Qian, Q., Zhang, Q., 2009. Eocene Neotethyan slab breakoff in southern Tibet inferred from the Linzizong volcanic record. Tectonophysics 477, 20–35. doi:10.1016/j.tecto.2009.02.031

Li, C., Hilst, R.D. Van Der, Meltzer, A.S., Engdahl, E.R., 2008a. Subduction of the Indian lithosphere beneath the Tibetan Plateau and Burma 274, 157–168.

doi:10.1016/j.epsl.2008.07.016

Li, C., Van Der Hilst, R.D., Engdahl, E.R., Burdick, S., 2008b. A new global model for P wave speed variations in Earth's mantle. Geochemistry, Geophys. Geosystems 9. doi:10.1029/2007GC001806

Li, L., Liao, X., Fu, R., 2002. Slab breakoff depth : A slowdown subduction model. Geophys. Res. Lett. 29, 10–12. doi:10.1029/2001GL013420

Li, W.C., Chen, R.X., Zheng, Y.F., Hu, Z., 2014. Dehydration and anatexis of UHP metagranite during continental collision in the Sulu orogen. J. Metamorph. Geol. 32, 915–936.

Li, Z.-H., Xu, Z., Gerya, T., Burg, J.P., 2013. Collision of continental corner from 3-D numerical modeling. Earth Planet. Sci. Lett. 380, 98–111.

Ma, L., Wang, B. Di, Jiang, Z.Q., Wang, Q., Li, Z.X., Wyman, D.A., Zhao, S.R., Yang, J.H., Gou, G.N., Guo, H.F., 2014. Petrogenesis of the Early Eocene adakitic rocks in the Napuri area, southern Lhasa: Partial melting of thickened lower crust during slab break-off and implications for crustal thickening in southern Tibet. Lithos 196–197, 321–338. doi:10.1016/j.lithos.2014.02.011

Macera, P., Gasperini, D., Ranalli, G., Mahatsente, R., 2008. Slab detachment and mantle plume upwelling in subduction zones: An example from the Italian South-Eastern Alps. J. Geodyn. 45, 32–48. doi:10.1016/j.jog.2007.03.004

Macpherson, C.G., Dreher, S.T., Thirlwall, M.F., 2006. Adakites without slab melting: High pressure differentiation of island arc magma, Mindanao, the Philippines. Earth Planet. Sci. Lett. 243, 581–593. doi:10.1016/j.epsl.2005.12.034

Magni, V., Bouilhol, P., van Hunen, J., 2014a. Deep water recycling through time. Geochemistry, Geophys. Geosystems 15, 4203–4216.

Magni, V., Faccenna, C., van Hunen, J., Funiciello, F., 2014b. How collision triggers backarc extension: Insight into mediterranean style of extension from 3-d numerical models. Geology 42, 511–514. doi:10.1130/G35446.1

Magni, V., Faccenna, C., Van Hunen, J., Funiciello, F., 2013. Delamination vs. break-off: The fate of continental collision. Geophys. Res. Lett. 40, 285–289. doi:10.1002/grl.50090

Magni, V., Van Hunen, J., Funiciello, F., Faccenna, C., 2012. Numerical models of slab migration in continental collision zones. Solid Earth 3, 293–306. doi:10.5194/se-3-293-2012

Mahéo, G., Guillot, S., Blichert-Toft, J., Rolland, Y., Pêcher, A., 2002. A slab breakoff model for the neogene thermal evolution of South Karakorum and South Tibet. Earth Planet. Sci. Lett. 195, 45–58. doi:10.1016/S0012-821X(01)00578-7

Maruyama, S., Liou, J.G., 1998. Initiation of ultrahigh-pressure metamorphism and its significance on the Proterozoic-Phanerozoic boundary. Isl. Arc 7, 6–35.

Maunder, B., van Hunen, J., Magni, V., Bouilhol, P., 2016. Relamination of mafic subducting crust throughout Earth's history. Earth Planet. Sci. Lett. 449, 206–216. doi:10.1016/j.epsl.2016.05.042

Maury, R.C., Fourcade, S., Coulon, C., El Azzouzi, M., Bellon, H., Coutelle, A., Ouabadi, A., Semroud, B., Megartsi, M., Cotten, J., Belanteur, O., Louni-Hacini, A., Piqué, A., Capdevila, R., Hernandez, J., Réhault, J.-P., 2000. Post-collisional Neogene magmatism of the Mediterranean Maghreb margin: A consequence of slab breakoff. Comptes Rendus l'Academie Sci. - Ser. IIa Sci. la Terre des Planetes 331, 159–173.

Menant, A., Sternai, P., Jolivet, L., Guillou-Frottier, L., Gerya, T., 2016. 3D numerical

modeling of mantle flow, crustal dynamics and magma genesis associated with slab roll-back and tearing: The eastern Mediterranean case. Earth Planet. Sci. Lett. 442, 93–107.

Mériaux, C.A., Duarte, J.C., Schellart, W.P., Mériaux, A.S., 2015. A two-way interaction between the Hainan plume and the Manila subduction zone. Geophys. Res. Lett. 42, 5796–5802. doi:10.1002/2015GL064313

Mitrovica, J.X., Forte, A.M., 2004. A new inference of mantle viscosity based upon joint inversion of convection and glacial isostatic adjustment data. Earth Planet. Sci. Lett. 225, 177–189. doi:10.1016/j.epsl.2004.06.005

Mo, X., Hou, Z., Niu, Y., Dong, G., Qu, X., Zhao, Z., Yang, Z., 2007. Mantle contributions to crustal thickening during continental collision: Evidence from Cenozoic igneous rocks in southern Tibet. Lithos 96, 225–242. doi:10.1016/j.lithos.2006.10.005

Mo, X., Niu, Y., Dong, G., Zhao, Z., Hou, Z., Zhou, S., Ke, S., 2008. Contribution of syncollisional felsic magmatism to continental crust growth: A case study of the Paleogene Linzizong volcanic Succession in southern Tibet. Chem. Geol. 250, 49–67. doi:10.1016/j.chemgeo.2008.02.003

Molnar, P., Stock, J.M., 2009. Slowing of India's convergence with Eurasia since 20 Ma and its implications for Tibetan mantle dynamics. Tectonics 28, 1–11. doi:10.1029/2008TC002271

Molnar, P., Tapponnier, P., 1975. Cenozoic tectonics of Asia: Effects of a continental collision. Science (80-. ). 189, 419–426.

Moresi, L., Gurnis, M., 1996. Constraints on the lateral strength of slabs from three-dimensional dynamic flow models. Earth Planet. Sci. Lett. 38, 15–28.

Moresi, L., Zhong, S., Gurnis, M., 1996. The accuracy of finite element solutions of Stokes's flow with strongly varying viscosity. Phys. Earth Planet. Inter. 97, 83–94.

Moresi, L.N., Solomatov, V.S., 1995. Numerical investigation of 2D convection with extremely large viscosity variations.

Nakakuki, T., Mura, E., 2013. Dynamics of slab rollback and induced back-arc basin formation. Earth Planet. Sci. Lett. 361, 287–297. doi:10.1016/j.epsl.2012.10.031

Neill, I., Meliksetian, K., Allen, M.B., Navarsardyan, G., Karapetyan, S., 2013. Pliocene-Quaternary volcanic rocks of NW Armenia: Magmatism and lithospheric dynamics within an active orogenic plateau. Lithos 180–181, 200–215.

Nemcok, M., Pospisil, L., Lexa, J., Donelick, R.A., 1998. Tertiary subduction and slab break-off model of the Carpathian-Pannonian region. Tectonophysics 295, 307–340. doi:10.1016/S0040-1951(98)00092-4

Omrani, J., Agard, P., Whitechurch, H., Benoit, M., Prouteau, G., Jolivet, L., 2008. Arc-magmatism and subduction history beneath the Zagros Mountains, Iran: A new report of adakites and geodynamic consequences. Lithos 106, 380–398.

Pang, K.N., Chung, S.L., Zarrinkoub, M.H., Mohammadi, S.S., Yang, H.M., Chu, C.H., Lee, H.Y., Lo, C.H., 2012. Age, geochemical characteristics and petrogenesis of Late Cenozoic intraplate alkali basalts in the Lut-Sistan region, eastern Iran. Chem. Geol. 306–307, 40–53. doi:10.1016/j.chemgeo.2012.02.020

Patriat, P., Achache, J., 1984. India–Eurasia collision chronology has implications for crustal shortening and driving mechanism of plates. Nature 311, 615–621. doi:10.1038/311615a0

Paulson, A., Zhong, S., Wahr, J., 2007. Inference of mantle viscosity from GRACE and relative sea level data. Geophys. J. Int. 171, 497–508. doi:10.1111/j.1365-

246X.2007.03556.x

Peacock, S.M., 1996. Thermal and Petrologic Structure of Subduction Zones. Geophys. Monogr. Ser. 119–133. doi:10.1029/GM096p0119

Peacock, S.M., 1990. Fluid processes in subduction zones. Science (80-. ). 248, 329–337.

Pearce, J.A., Bender, J.F., De Long, S.E., Kidd, W.S.F., Low, P.J., Guner, Y., Saroglu, Y., Yilmaz, Y., Moorbath, S., Mitchell, J.G., 1990. Genesis of collision volcanism in Eastern Anatolia, Turkey. J. Volcanol. Geotherm. Res. 44, 182–229.

Piromallo, C., Becker, T.W., Funiciello, F., Faccenna, C., 2006. Three-dimensional instantaneous mantle flow induced by subduction. Geophys. Res. Lett. 33, 5–8. doi:10.1029/2005GL025390

Plank, T., Langmuir, C.H., 1998. The chemical composition of subducting sediment and its consequences for the crust and mantle. Chem. Geol. 145, 325–394. doi:10.1016/S0009-2541(97)00150-2

Priestley, K., McKenzie, D., 2006. The thermal structure of the lithosphere from shear wave velocities. Earth Planet. Sci. Lett. 244, 285–301.

Priestley, K., McKenzie, D., Barron, J., Tatar, M., Debayle, E., 2012. The Zagros core: Deformation of the continental lithospheric mantle. Geochemistry, Geophys. Geosystems 13, 1–21.

Quinquis, M.E.T., Buiter, S.J.H., 2014. Testing the effects of basic numerical implementations of water migration on models of subduction dynamics. Solid Earth 5, 537–555. doi:10.5194/se-5-537-2014

Ranalli, G., 1995. Rheology of the Earth. Springer Science & Business Media.

Ranero, C.R., Villaseñor, A., Morgan, J.P., Weinrebe, W., 2005. Relationship between bend-faulting at trenches and intermediate-depth seismicity. Geochemistry, Geophys. Geosystems 6. doi:10.1029/2005GC000997

Rosenbaum, G., Gasparon, M., Lucente, F.P., Peccerillo, A., Miller, M.S., 2008. Kinematics of slab tear faults during subduction segmentation and implications for Italian magmatism. Tectonics 27, 1–16. doi:10.1029/2007TC002143

Rudnick, R.L., Gao, S., 2003. 3.01 - Composition of the Continental Crust. Treatise on Geochemistry 1, 1–64. doi:http://dx.doi.org/10.1016/B0-08-043751-6/03016-4

Rüpke, L.H., Morgan, J.P., Hort, M., Connolly, J.A.D., 2004. Serpentine and the subduction zone water cycle. Earth Planet. Sci. Lett. 223, 17–34.

Schmidt, M.W., Poli, S., 1998. Experimentally based water budgets for dehydrating slabs and consequences for arc magma generation. Earth Planet. Sci. Lett. 163, 361–379. doi:10.1016/S0012-821X(98)00142-3

Schott, B., Schmeling, H., 1998. Delamination and detachment of a lithospheric root. Tectonophysics 296, 225–247. doi:10.1016/S0040-1951(98)00154-1

Sizova, E., Gerya, T., Brown, M., 2014. Contrasting styles of Phanerozoic and Precambrian continental collision. Gondwana Res. 25, 522–545. doi:10.1016/j.gr.2012.12.011

Sizova, E., Gerya, T., Brown, M., Perchuk, L.L., 2010. Subduction styles in the Precambrian: Insight from numerical experiments. Lithos 116, 209–229. doi:10.1016/j.lithos.2009.05.028

Smith, D.C., 1984. Coesite in clinopyroxene in the Caledonides and its implications for geodynamics. Nature 310, 641–644. doi:10.1038/310641a0

Sobolev, A. V., Chaussidon, M., 1996. H2O concentrations in primary melts from supra-subduction zones and mid-ocean ridges: Implications for H2O storage and recycling in

the mantle. Earth Planet. Sci. Lett. 137, 45–55. doi:10.1016/0012-821X(95)00203-O

Solano, J.M.S., Jackson, M.D., Sparks, R.S.J., Blundy, J.D., Annen, C., 2012. Melt segregation in deep crustal hot zones: A mechanism for chemical differentiation, crustal assimilation and the formation of evolved magmas. J. Petrol. 53, 1999–2026. doi:10.1093/petrology/egs041

Stein, C.A., Stein, S., 1992. A model for the global variation in oceanic depth and heat flow with lithospheric age. Nature 356, 133–135. doi:10.1038/359123a0

Sternai, P., Jolivet, L., Menant, A., Gerya, T., 2014. Driving the upper plate surface deformation by slab rollback and mantle flow. Earth Planet. Sci. Lett. 405, 110–118. doi:10.1016/j.epsl.2014.08.023

Tatsumi, Y., 1986. Formation of the volcanic front in subduction zones. Geophys. Res. Lett. 13, 717–720.

Tatsumi, Y., Hamilton, D.L., Nesbitt, R.W., 1986. Chemical characteristics of fluid phase released from a subducted lithosphere and origin of arc magmas: Evidence from high-pressure experiments and natural rocks. J. Volcanol. Geotherm. Res. 29, 293–309. doi:10.1016/0377-0273(86)90049-1

Thompson, A.B., 1992. Water in the Earth's upper mantle. Nature 358, 295–302. doi:10.1038/355242a0

Thorkelson, D.J., 1996. Subduction of diverding plates and the principles of slab window formation. Tectonophysics 255, 47–63.

Turcotte, D.L., Schubert, G., 2002. Geodynamics. Cambridge.

Ueda, K., Gerya, T. V., Burg, J.P., 2012. Delamination in collisional orogens: Thermomechanical modeling. J. Geophys. Res. Solid Earth 117, 1–25. doi:10.1029/2012JB009144

van de Zedde, D.M.A., Wortel, M.J.R., 2001. Shallow slab detachment as a transient source of heat at midlithospheric depths. Tectonics 20, 868–882.

van der Hilst, R., Engdhal, R., Spakman, W., Nolet, G., 1991. Tomographic imaging of subducted lithosphere below northwest Pacific island arcs. Nature 353, 37–43. doi:10.1038/351111a0

Van Hinsbergen, D.J.J., Steinberger, B., Doubrovine, P. V., Gassmöller, R., 2011. Acceleration and deceleration of India-Asia convergence since the Cretaceous: Roles of mantle plumes and continental collision. J. Geophys. Res. Solid Earth 116, 1–20. doi:10.1029/2010JB008051

van Hunen, J., Allen, M.B., 2011. Continental collision and slab break-off: A comparison of 3-D numerical models with observations. Earth Planet. Sci. Lett. 302, 27–37. doi:10.1016/j.epsl.2010.11.035

van Hunen, J., Moyen, J.-F., 2012. Archean Subduction: Fact or Fiction? Annu. Rev. Earth Planet. Sci. 40, 195–219. doi:10.1146/annurev-earth-042711-105255

Van Hunen, J., Van Den Berg, A.P., Vlaar, N.J., 2002. On the role of subducting oceanic plateaus in the development of shallow flat subduction. Tectonophysics 352, 317–333. doi:10.1016/S0040-1951(02)00263-9

van Hunen, J., Zhong, S., Shapiro, N.M., Ritzwoller, M.H., 2005. New evidence for dislocation creep from 3-D geodynamic modeling of the Pacific upper mantle structure. Earth Planet. Sci. Lett. 238, 146–155. doi:10.1016/j.epsl.2005.07.006

Vogt, K., Gerya, T. V., Castro, A., 2012. Crustal growth at active continental margins: Numerical modeling. Phys. Earth Planet. Inter. 192–193, 1–20. doi:10.1016/j.pepi.2011.12.003

von Blanckenburg, F., Davies, J.H., 1995. Slab breakoff: A model for syncollisional magmatism and tectonics in the Alps. Tectonics 14, 120–131.

Walker, R.T., Gans, P., Allen, M.B., Jackson, J., Khatib, M., Marsh, N., Zarrinkoub, M., 2009. Late Cenozoic volcanism and rates of active faulting in eastern Iran. Geophys. J. Int. 177, 783–805. doi:10.1111/j.1365-246X.2008.04024.x

Wang, H., Agrusta, R., Van Hunen, J., 2015. Advantages of a conservative velocity interpolation (CVI) scheme for particle-in-cellmethods with application in geodynamic modeling. Geochemistry Geophys. Geosystems 16, 2015–2023. doi:10.1002/2015GC005918.Received

Wang, H., van Hunen, J., Pearson, D.G., 2015. The thinning of subcontinental lithosphere: The roles of plume impact andmetasomatic weakening. Geochemistry Geophys. Geosystems 16, 1156–1171. doi:10.1002/2014GC005684.Key

Warren, C.J., Beaumont, C., Jamieson, R.A., 2008. Formation and exhumation of ultra-high-pressure rocks during continental collision: Role of detachment in the subduction channel. Geochemistry, Geophys. Geosystems 9, 1–33. doi:10.1029/2007GC001839

Warren, C.J., Beaumont, C., Jamieson, R.A., 2008. Modelling tectonic styles and ultra-high pressure (UHP) rock exhumation during the transition from oceanic subduction to continental collision. Earth Planet. Sci. Lett. 267, 129–145. doi:10.1016/j.epsl.2007.11.025

Wen, D.R., Liu, D., Chung, S.L., Chu, M.F., Ji, J., Zhang, Q., Song, B., Lee, T.Y., Yeh, M.W., Lo, C.H., 2008. Zircon SHRIMP U-Pb ages of the Gangdese Batholith and implications for Neotethyan subduction in southern Tibet. Chem. Geol. 252, 191–201.

White, R.W., Powell, R., Holland, T.J.B., 2001. Calculation of partial melting equilibria in the system Na2O- CaO-K2O-FeO-MgO-Al2O3-SiO2-H2O (NCKFMASH). J. Metamorph. Geol. 19, 139–153. doi:10.1046/j.0263-4929.2000.00303.x

Whitney, D.L., Teyssier, C., Rey, P.F., 2009. The consequences of crustal melting in continental subduction. Lithosphere 1, 323–327. doi:10.1130/L62.1

Wilson, C.R., Spiegelman, M., van Keken, P.E., Hacker, B.R., 2014. Fluid flow in subduction zones: The role of solid rheology and compaction pressure. Earth Planet. Sci. Lett. 401, 261–274. doi:10.1016/j.epsl.2014.05.052

Wong A Ton, S.Y.M., Wortel, M.J.R., 1997. Slab detachment in continental collision zones: An analysis of controlling parameters. Geophys. Res. Lett. 24, 2095–2098. doi:10.1029/97GL01939

Workman, R.K., Hart, S.R., 2005. Major and trace element composition of the depleted MORB mantle (DMM). Earth Planet. Sci. Lett. 231, 53–72. doi:10.1016/j.epsl.2004.12.005

Wortel, M.J., Spakman, W., 2000. Subduction and slab detachment in the Mediterranean-Carpathian region. Science (80-. ). 290, 1910–1917.

Xia, Q.X., Zheng, Y.F., Zhou, L.G., 2008. Dehydration and melting during continental collision: Constraints from element and isotope geochemistry of low-T/UHP granitic gneiss in the Dabie orogen. Chem. Geol. 247, 36–65. doi:10.1016/j.chemgeo.2007.09.013

Xu, Y.G., Lan, J.B., Yang, Q.J., Huang, X.L., Qiu, H.N., 2008. Eocene break-off of the Neo-Tethyan slab as inferred from intraplate-type mafic dykes in the Gaoligong orogenic belt, eastern Tibet. Chem. Geol. 255, 439–453. doi:10.1016/j.chemgeo.2008.07.016

Yardley, B.W.D., 2009. Review The role of water in the evolution of the continental crust. J. Geol. Soc. London. 166, 585–600. doi:10.1144/0016-76492008-101.Review

Yoshioka, S., Wortel, M.J.R., 1995. Three-dimensional numerical modeling of detachment of subducted lithosphere. J. Geophys. Res. 100, 20,220-223,244.

Yoshioka, S., Yuen, D.A., Larsen, T.B., 1994. Slab weakening: Mechanical and thermal-mechanical consequences for slab detachment.

Zandt, G., Humphreys, E., 2008. Toroidal mantle flow through the western U.S. slab window. Geology 36, 295–298. doi:10.1130/G24611A.1

Zhao, Z.-F., Dai, L.-Q., Zheng, Y.-F., 2013. Postcollisional mafic igneous rocks record crust-mantle interaction during continental deep subduction. Sci. Rep. 3.

Zheng, Y.-F., 2009. Fluid regime in continental subduction zones: petrological insights from ultrahigh-pressure metamorphic rocks. J. Geol. Soc. London. 166, 763–782.

Zheng, Y.-F., Hermann, J., 2014. Geochemistry of continental subduction-zone fluids. Earth, Planets Sp. 66, 1–16.

Zheng, Y.F., 2012. Metamorphic chemical geodynamics in continental subduction zones. Chem. Geol. 328, 5–48. doi:10.1016/j.chemgeo.2012.02.005

Zheng, Y.F., Gao, T.S., Wu, Y.B., Gong, B., Liu, X.M., 2007. Fluid flow during exhumation of deeply subducted continental crust: Zircon U-Pb age and O-isotope studies of a quartz vein within ultrahigh-pressure eclogite. J. Metamorph. Geol. 25, 267–283. doi:10.1111/j.1525-1314.2007.00696.x

Zheng, Y.F., Xia, Q.X., Chen, R.X., Gao, X.Y., 2011. Partial melting, fluid supercriticality and element mobility in ultrahigh-pressure metamorphic rocks during continental collision. Earth-Science Rev. 107, 342–374. doi:10.1016/j.earscirev.2011.04.004

Zhong, S., Zuber, M.T., Moresi, L., Gurnis, M., 2000. Role of temperature-dependent viscosity and surface plates in spherical shell models of mantle convection. J. Geophys. Res. 105, 11063–11082.

Zhu, D.C., Zhao, Z.D., Niu, Y., Mo, X.X., Chung, S.L., Hou, Z.Q., Wang, L.Q., Wu, F.Y., 2011. The Lhasa Terrane: Record of a microcontinent and its histories of drift and growth. Earth Planet. Sci. Lett. 301, 241–255.

# Appendix A

# Model setup

## A.1 Derivation of the radiogenic geotherm within the crust and mantle lithosphere

To assess the effect that radiogenic heating within the continental crust may have on the collision and breakoff dynamics, a radiogenic heat component is included within the crustal material and the initial geotherm is also altered, to mimic the process of long-term radiogenic heat production. This geotherm can be derived for within both the crust and remaining mantle lithosphere, by constraining the surface temperature and that at the base of the lithosphere ($T_0$ and Tm), along with the average crustal radiogenic heat production, $H_c$. Beginning with Eq. (2.4), and assuming a stationary, steady-state system for crustal material with a uniform radiogenic heat production:

$$k\frac{\partial^2 T_c}{\partial z^2} + H_c = 0 \tag{A.1}$$

where k is the thermal conductivity, z is the depth, and $T_c$ is the temperature within the continental crust, giving:

$$T_c = T_0 + Az - \frac{H_c z^2}{2k} \tag{A.2}$$

where A is a constant to be solved. Below the crust, the temperature increases linearly to the base of the lithosphere and there is no radiogenic heat production:

$$k\frac{\partial^2 T_{lm}}{\partial z^2} = 0 \tag{A.3}$$

$$T_{lm} = T_m + B(z - z_l) \tag{A.4}$$

where $T_{lm}$ is the temperature within the lithospheric mantle, B is a constant to be solved, and $z_l$ is the depth to the base of the lithosphere. By defining at the base of the crust ($z_c$) that:

$$T_c = T_{lm} \tag{A.5}$$

$$\frac{\partial T_c}{\partial z} = \frac{\partial T_{lm}}{\partial z} \tag{A.6}$$

A and B are solved for, to give:

$$T_c = T_0 + \left(\frac{T_m - T_0}{z_l} + \frac{H_c z_c}{k} - \frac{H_c {z_c}^2}{2kz_l}\right) z - \frac{H_c z^2}{2k} \tag{A.7}$$

$$T_{lm} = T_m + \left(\frac{T_m - T_0}{z_l} - \frac{H_c {z_c}^2}{2kz_l}\right)(z - z_l) \tag{A.8}$$

These are non-dimensionalised using Eqs. (2.7) - (2.10), and the non-dimensionalisation for H:

$$H = H' \frac{k\Delta T}{h^2} \tag{A.9}$$

where ΔT is the reference temperature difference, to give:

$$T_c = T_0 + \left(\frac{T_m - T_0}{z_l} + H_c z_c - \frac{H_c {z_c}^2}{2z_l}\right) z - \frac{H_c z^2}{2} \tag{A.10}$$

$$T_{lm} = T_m + \left(\frac{T_m - T_0}{z_l} - \frac{H_c {z_c}^2}{2z_l}\right)(z - z_l) \tag{A.11}$$

where the primes are again removed for clarity.

# Appendix B

# Technical details of the various numerical melting implementations

Below the more technical details of some of the hydration and melting implementations addressed in Chapter 2.5 are described. These include: the derivation, from the parameterised solidus, of the equations used to determine the increase in temperature of bulk water content to induce melting (Section B.1); the implementation of the method to approximate the mantle wedge hydration, including an example of a model calculation which applies this (Section B.2); the method used to migrate free water and re-hydrate particles (Section B.3); implementation of the thermodynamic (de)hydration reactions with a parameterised solidus (section B.4); a comparison of the solidus for undepleted mantle material from the parameterisation and the thermodynamic database, including the effect on the model results (Section B.5); and methods to approximate the melt depletion when implementing the lookup tables (Section B.6). The methods outlined in Sections B.1 and B.2 can be implemented when the parameterised solidus is used to determine the generation of melt, and Chapter 3 makes use of the equations derived in Section B.1. Those methods outlined in Sections B.3 and B.6 can be implemented when the thermodynamic database is used to determine the occurrence of (de)hydration reactions and melt generation, and are included in the study in Chapter 4.

## B.1 Post-processing application of parameterised solidus

The implementation of the parameterised solidus of Katz et al. (2003) is outlined below, which is applied after the model calculation, along with the derivation of the equations for the increase in temperature and bulk water content that would be required to generate melting. This is included in Chapter 3, as a first order approximation of the amount of mantle melting that slab breakoff may induce, or the change in conditions that would be required to induce this melting. Table B.1 summarises all the parameters that are used in this section.

The amount of melting, F, is determined based upon the temperature of material with respect to the solidus and liquidus (see Katz et al. (2003) for full details):

$$F = \left( \frac{T - (T_{sol} - \Delta T))}{T_{liq}^{lherz} - T_{sol}} \right)^{\beta_1} \tag{B.1}$$

where $T_{sol}$ is the solidus temperature, $T_{liq}^{lherz}$ the lherzolite liquidus temperature, both as a function of pressure and temperature, $\beta_1$ is a constant, and $\Delta T$ is a term subtracted from the solidus and liquidus to account for the decrease in temperature due to any water that may be present:

$$\Delta T = K X_{H2O}{}^{\gamma} \tag{B.2}$$

K and $\gamma$ are constants, and $X_{H2O}$ is the concentration of water in the melt which is modelled using a bulk distribution coefficient ($D_{H2O}$) to determine the partitioning between the solid and the melt:

$$X_{H2O} = \frac{X_{H2O}^{bulk}}{D_{H2O} + F(1 - D_{H2O})} \tag{B.3}$$

where $X_{H2O}^{bulk}$ is the bulk water in the solid phase. As the amount of water that is partitioned into the melt, $X_{H2O}$, depends upon the melt fraction, which is itself dependent upon the amount of water in the melt, no closed form analytical solution exists. Eqs. (B.1) - (B.3) are combined and re-arranged to remove the melt fraction, giving:

$$\frac{X_{H2O}^{bulk}}{D_{H2O} + (1 - D_{H2O}) \left( \frac{T - (T_{sol} - K X_{H2O}{}^{\gamma})}{T_{liq}^{lherz} - T_{sol}} \right)^{\beta_1}} - X_{H2O} = 0 \tag{B.4}$$

This is subsequently solved for $X_{H2O}$ using a root finder, fzero, within the Matlab programming language. Minimum and maximum limits for $X_{H2O}$ are required when calling the root finder, which are determined as below:

*Minimum limit:* The minimum value corresponds to the minimum amount of water required to achieve any melting. For melting to take place:

$$T - (T_{sol} - KX_{H2O}{}^{\gamma}) > 0 \tag{B.5}$$

If the temperature exceeds the solidus then the minimum value of $X_{H2O}$ $\left(X_{H2O_{min}}\right)$ is defined as 0 wt%. Otherwise, for any melting to take place the minimum value is defined as equal to:

$$X_{H2O\,min} = \left(\frac{T_{sol} - T}{K}\right)^{\frac{1}{\gamma}} \tag{B.6}$$

If this minimum value exceeds 100 wt% or the amount of water stored in a water-saturated melt,$X_{H2O}^{sat}$, the melt fraction is set to 0. This is calculated as:

$$X_{H2O}^{sat} = \chi_1 P^{\lambda} + \chi_2 P \tag{B.7}$$

where P is the pressure and $\chi_1$ and $\chi_2$ are constants.

*Maximum limit:* The maximum limit for $X_{H2O}$ $\left(X_{H2O_{max}}\right)$ is set to 100 wt%.

The root finder is then applied if melting is theoretically possible, to determine the value of $X_{H2O,}$ and the melt fraction is subsequently calculated using this value.

The parameterisation also includes separate equations for melt fraction to account for the loss of cpx from the system. It is anticipated that the results will not exceed the amount of melt at which this occurs (~ > 20 wt%), and so it is not included in the model. However, the amount of melt at which this extraction takes place is calculated and it is checked that the determined melt fraction does not exceed this. If no melt is formed, the above parameterisation is also used to determine the increase in temperature and/or the amount of bulk water that would be required to generate any melting. From Eq. (B.4) the amount of water required is:

$$X_{H2O}^{bulk} = X_{H2O\,min}\left(D_{H2O} + (1 - D_{H2O})\left(\frac{T - \left(T_{sol} - KX_{H2O\,min}{}^{\gamma}\right)}{T_{liq}^{lherz} - T_{sol}}\right)^{\beta_1}\right) \tag{B.8}$$

where $X_{H2O\,min}$ is calculated as in Eq. (B.6). From Eqs. (B.3) and (B.5) the increase in temperature ($T_{inc}$) is calculated by:

$$T_{inc} = T_{sol} - K\left(\frac{X_{H2O}^{bulk}}{D_{H2O} + F(1 - D_{H2O})}\right)^{\gamma} \quad \text{(B.9)}$$

assuming that F approaches 0, giving:

$$T_{inc} = T_{sol} - K\left(\frac{X_{H2O}^{bulk}}{D_{H2O}}\right)^{\gamma} \quad \text{(B.9)}$$

| Symbol | Parameter | Units | Default value |
|---|---|---|---|
| F | weight fraction of melting | - | - |
| T | temperature | °C | - |
| $T_{sol}$ | solidus temperature | °C | - |
| $T_{liq}^{lherz}$ | lherzolite liquidus temperature | °C | - |
| ΔT | change in solidus or liquidus temperature due to presence of water | °C | - |
| $\beta_1$ | a constant for calculating F | - | 1.50 |
| K | a constant for calculating ΔT | °C wt%$^{-\gamma}$ | 43 |
| γ | a constant for calculating ΔT | - | 0.75 |
| $X_{H2O}$ | concentration of water in the melt | wt% | - |
| $D_{H2O}$ | bulk distribution coefficient | - | 0.01 |
| $X_{H2O}^{bulk}$ | bulk water in the solid phase | wt% | - |
| $X_{H2O\,min}$ | minimum water content for the solidus to be exceeded | wt% | - |
| $X_{H2O}^{sat}$ | water content in a water-saturated melt | wt% | - |
| P | pressure | GPa | - |
| $\chi_1$ | a constant for calculating $X_{H2O}^{sat}$ | wt% GPa$^{-\lambda}$ | 12.00 |

| | | | |
|---|---|---|---|
| $\chi_2$ | a constant for calculating $X_{H2O}^{sat}$ | wt% $GPa^{-1}$ | 1.00 |
| $T_{inc}$ | increase in temperature required to exceed the solidus | °C | - |

**Table B.1: Parameter symbols and units used in the equations to determine the melt fraction according to the parameterised solidus.** See Katz et al. (2003) for further details.

## B.2 Hydration of a mantle wedge

A possible way to model the hydration of the mantle wedge during subduction is outlined below, which does not require the use of a thermodynamic database to determine the (de)hydration of material. A limit for the maximum hydration depth is defined, above which it is possible for material to become hydrated. Below this limit it is assumed that the slab has become fully dehydrated or any remaining water is able to be carried in stable phases deeper into the mantle. The column of elements which lies directly above crustal or sedimentary material within the subducting slab is defined as having a fixed water content. Only mantle material is hydrated, as the parameterised solidus is only applicable for this material. This can be useful in situations where material does not remain static, such as a subduction zone, and hence an initial hydration state cannot simply be defined which is applicable throughout the model calculation. This method is not used in Chapters 3 and 4, but an example of the hydration and melting profile that is generated during breakoff when applying this method is shown in Fig. B.1, which was calculated during the development of the melting implementation.

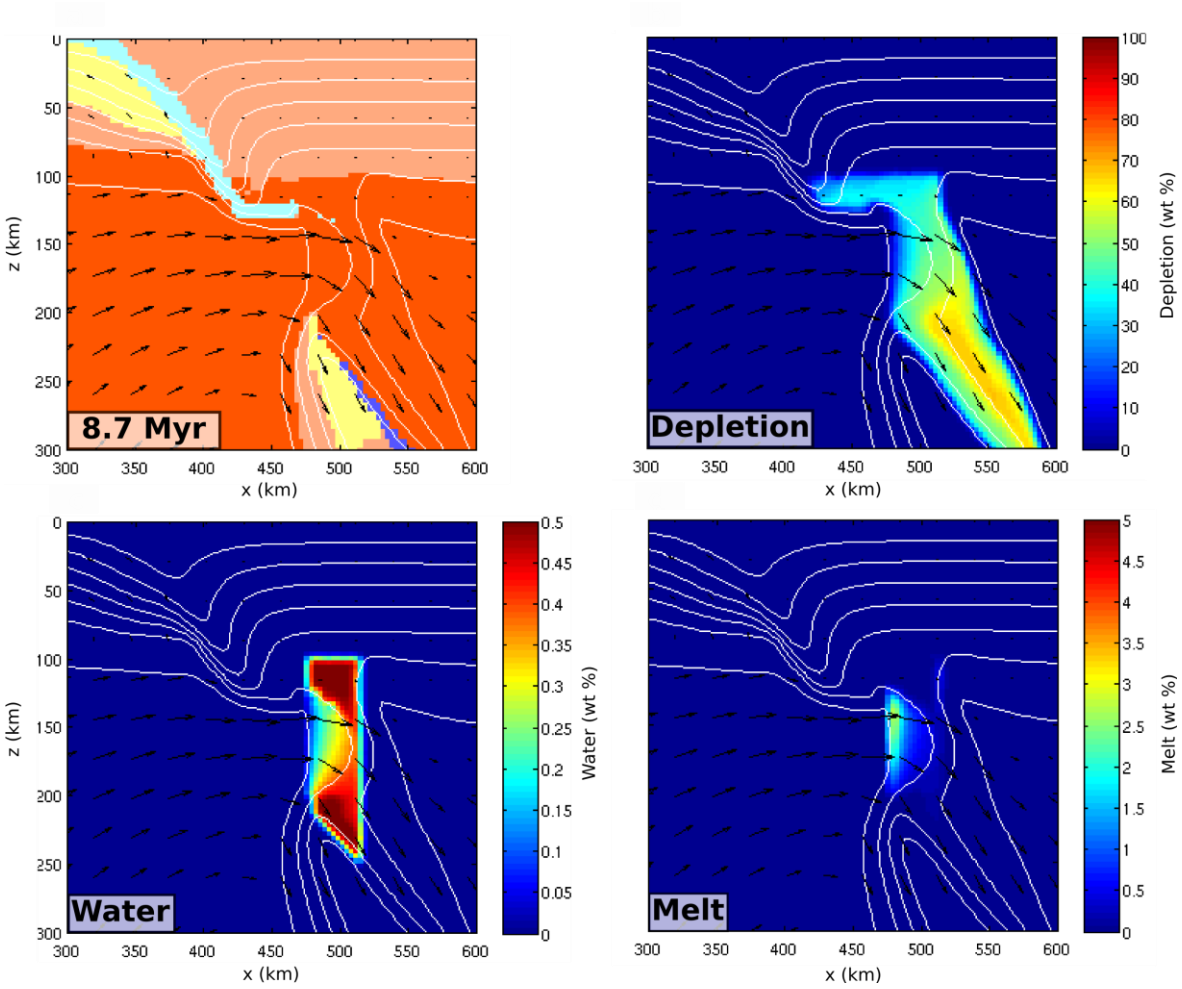


**Figure B.1: Model calculation using parameterised solidus and hydrated mantle wedge.** An example of a model calculation where the parameterised solidus is used to determine the amount of melting and the depletion is tracked to determine the amount of subsequent melting. The mantle wedge is hydrated above crustal material with 0.5 wt% $H_2O$. In this example continental collision and slab breakoff have taken place, resulting in an inflow if asthenospheric mantle through the slab window. Melting of hot, undepleted asthenosphere occurs within this area, which acts to absorb some of the free water. The upper left plot shows the compositional geometry: weak zone (light blue), oceanic crust (dark blue), continental crust (yellow), lithospheric mantle (light orange), asthenospheric mantle (dark orange). The black arrows represent the flow pattern, and the white lines the temperature profile, contoured an interval of 200°C starting from 0°C at the surface.

## B.3 Migration of free water

The method of free water migration is outlined below. This is used in Chapter 4 in conjunction with the thermodynamic lookup tables, to determine how any free water 'released' from a particle is redistributed to other particles. A number of assumptions are made by implementing this method: water is only capable of migrating vertically upwards;

water migration happens significantly faster than the mantle flow; water is able to percolate material instantaneously (i.e. material has an infinite permeability). The first two of these are considered further in Chapter 2.5.2.

Beginning at the bottom of the model, the total amount of water released from all particles within this element is determined using the lookup tables (see Magni et al. (2014) for further details) (Fig. B.2). Any free water is re-distributed across the particles within the same element which have not released any water (i.e. are undersaturated) to see if they can absorb this water. This step is repeated until either all free water has been reabsorbed by the

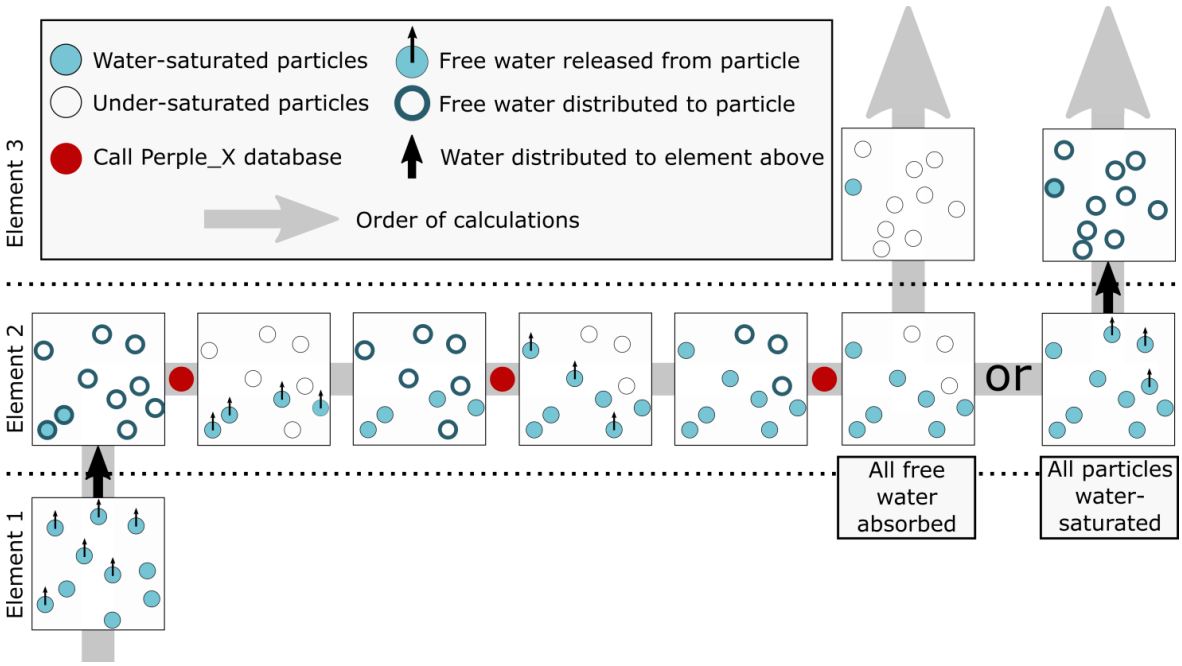


**Figure B.2: Method of free water migration.** An example of a calculation for the flow of water upwards through three elements is shown. Squares represent individual elements, whilst small circles represent individual particles. Starting with element 1, all particles that are water-saturated release any remaining free water, which is transferred to the overlying element. The total amount of free water is calculated and redistributed equally over the particles in element 2. These particles refer to the lookup tables to determine the stable mineralogy, and any particles that are water-saturated, and so have free water as a stable phase, redistribute this water over the remaining under-saturated particles in this element. The lookup tables are again referred to and any remaining free water redistributed, until all the free water has been absorbed by particles within the element, or all particles have become water-saturated. For the latter, the remaining total free water is redistributed equally over the particles in the element above, and in either case the calculation is repeated for element 3, as for element 2, referring to the lookup tables and redistributing any free water over under-saturated particles.

particles in the element, or all particles in that element cannot absorb further water (i.e. have become saturated). Any remaining free water is transferred to the overlying element. The absorption steps outlined above are repeated for this element and in turn for all overlying elements. Any free water remaining at the top of the model is assumed to evaporate. This process is completed for all elements for every timestep and hence this method assumes that the migration of water occurs significantly faster than the mantle flow and tectonic processes.

## B.4 Implementation of thermodynamic (de)hydration reactions with a parameterised solidus

In Section B.5 the parameterised solidi of Katz et al. (2003) and that determined from the thermodynamic database for undepleted mantle material are compared. In order to reliably compare the results that these two solidi produce, the same water migration scheme needs to be used. Below the implementation of the water migration as described in Section B.3 with the parameterised solidus is described. This method (i.e. determining the amount of mantle melting using a parameterised solidus, whilst still using a thermodynamic database to track the hydration and dehydration reactions of minerals) is often implemented in numerical studies (e.g. Li et al. (2013)).

The parameterised solidus is considered when the conditions are supra-solidus and the thermodynamic lookup tables when the conditions are sub-solidus. The amount of bulk hydration within the particle is used to calculate the amount of melting according to the parameterised solidus. If a particle meets the conditions to melt (or has previously undergone melting, and so is considered to some extent depleted) the stable mineralogy is ignored for this particle. Any water that remained in the residue and was not absorbed by the melt, as according to the parameterised solidus, is re-distributed across the remaining under-saturated particles within the element. This water is assumed to be a free phase and not bound in hydrous minerals within the particle, as the lookup table will no longer be referred to for this particle, and hence it is unknown whether the material would be able to absorb this water or whether it would be released. At the temperatures and pressures required for melting, any water is unlikely to be stable within minerals, as hydrous minerals are unstable at high temperatures (excluding the melt phase). The amount of melt according to the solidus is stored for each particle. If the particle has not melted, the stable mineralogy is calculated in subsequent timesteps.

## B.5 A comparison of different mantle solidi

Below the difference that using the parameterised solidus of Katz et al. (2003) or that determined from the thermodynamic database has on the results of mantle melting is assessed (see Bouilhol et al. (2015) for further details). Fig. B.3 compares these solidi, and shows that the thermodynamic solidus, when water is in excess, approximately equals the parameterisation with 0.1 wt% $H_2O$.

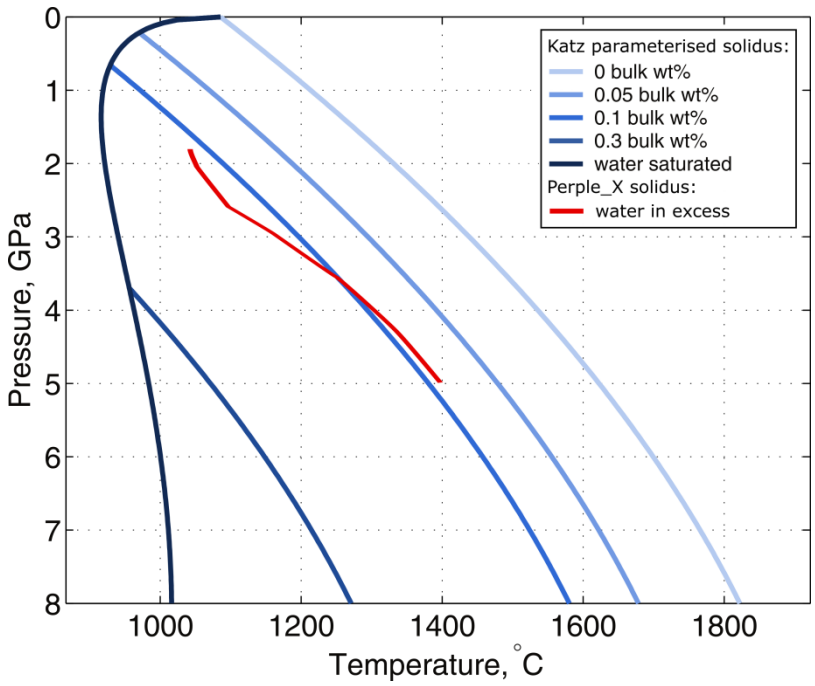


**Figure B.3: A comparison of mantle solidi.** Shown are the solidi from the parameterisation for varying water contents and that determined from Perple_X for water saturated material. The latter is significantly higher (note that this is only shown for water saturated material), reaching a difference of over 400 °C at a pressure of 5 GPa. After Bouilhol et al. (2015) and Katz et al. (2003).

For the reference model, the asthenospheric solidus used has little effect on the melt generation. During oceanic subduction the mantle wedge reaches a sufficient temperature to melt as a result of the fluid influx from the downgoing oceanic slab according to both solidi (Fig. B.4). During continental collision and breakoff, no water is available to depress either solidus sufficiently to generate any asthenospheric melting across the model. For differing collisional dynamics, which may promote the generation of melt, if water is in excess in the asthenosphere, it may be that the mantle is likely to melt regardless of the solidus used; however, the depth that this melting takes place at could vary significantly. For example, asthenospheric mantle with a temperature of 1350 °C (the mantle potential temperature used in the models) could melt at pressures greater than 8 GPa according to the parameterised

solidus if water saturated, but would have to be at a pressure less than 4.5 GPa to melt according to the thermodynamic solidus (Fig. B.3). However, it is less likely that the asthenosphere will become hydrated at greater depths, as material in general will be drier due to shallow dehydration reactions. With these considerations in mind, the solidus of the thermodynamic database is implemented for the asthenospheric mantle in Chapter 4. No significant differences are expected in the results, although it should be noted that these results may represent a lower limit for the amount of asthenospheric melting. This comparison has only been carried out for the fertile asthenospheric mantle, as the parameterised solidus is considered to be too low to be used for depleted mantle material.

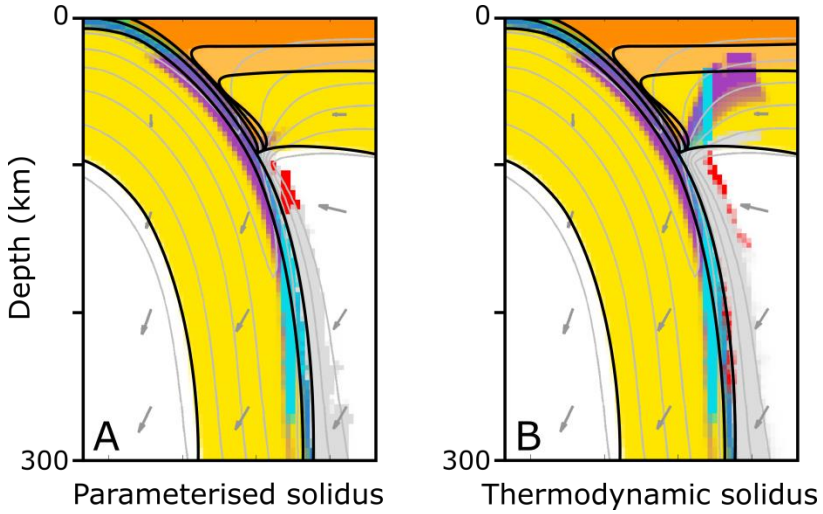


**Figure B.4: A comparison of subduction-related melting when the parameterised solidus and the thermodynamic solidus are implemented.** The parameterisation results in melting at lower temperatures within the mantle wedge, shifting the locus of melting nearer to the slab; however, melting occurs at a similar depth for both solidi. More hydration of the overriding plate occurs when using the thermodynamic database. This is probably a result of the absorption of more water by the melt when using the parameterised solidus. Note that the parameterisation only includes melting of the asthenospheric mantle, and not of the oceanic crust. . It should also be noted that, although both methods include an approximation for material depletion, these are different, which may also have an effect on the melting results.

## B.6 Depletion approximation with pre-determined lookup tables

Two similar methods to approximate the depletion of material are considered below. These are used where the thermodynamic lookup tables are consulted to determine the presence of melt, as an approximation of the decrease in likelihood that material that has previously melted will melt again. Both methods define an extraction threshold; an amount of melt, at which it is considered that the melt has reached a sufficient quantity to be extractable away

from the source rock. It is only at this point that the composition of the bulk rock would change from the initial composition; before melt extraction, the melt and residue may have differing compositions, but can continue to chemically interact with each other.

The simplest way to deal with depleted material is for these particles not to refer to the lookup tables again to determine the stable mineralogy (including the free water and any melt) (Fig. B.5 - Method 1). In other words, depleted material doesn't melt, hydrate or interact petrologically anymore with the rest of the model domain. Another, slightly more refined, version of this, is to only refer to the lookup tables for these depleted particles, if they again show melt to be present as a stable phase; otherwise they continue to refer to the lookup tables to determine the stable mineralogy (Fig. B.5 - Method 2). The latter method allows the determination of the amount of free water released from that particle, which is either re-distributed over the element or transferred to the element above. Although depleted mantle material may undergo different (de)hydration reactions than the original material, this second method assumes that depleted material is capable of holding as much water as fertile material, which may be a reasonable approximation. This may provide a more accurate method of modelling the water migration, as the first method assumes that water can 'jump' across areas that are considered depleted, without any water being absorbed across this area.

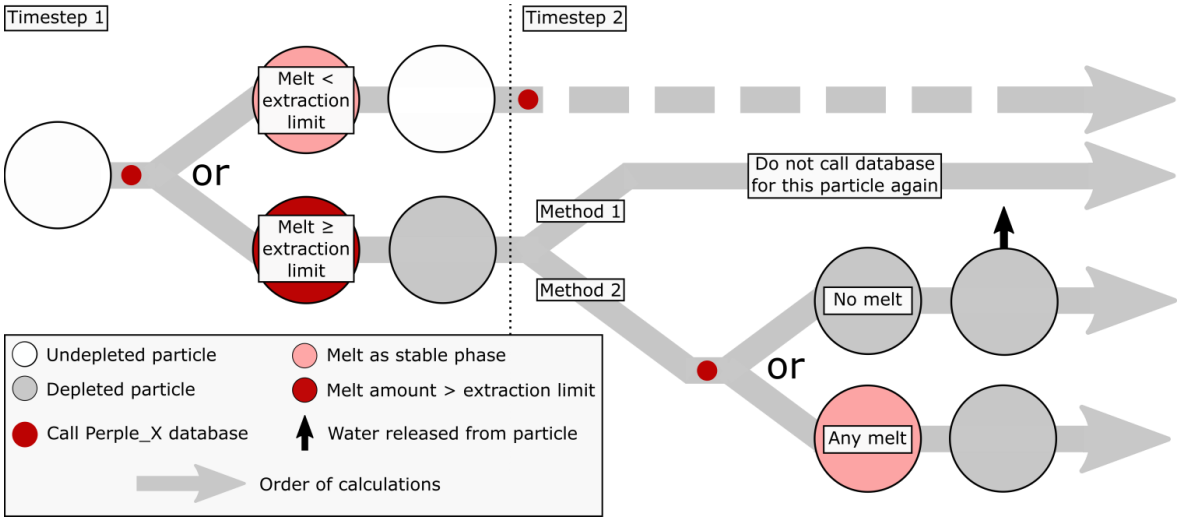


**Figure B.5: Two methods of approximating melt depletion.** If melt does not exceed the extraction threshold, the material is not considered depleted and continues to refer to the lookup tables to determine the stable mineralogy (including the melt and free water). However, if the amount of melt exceeds this threshold, the particle is considered depleted. In subsequent timesteps the material either does not calculate the stable mineralogy (Method 1), or refers to the lookup tables to determine the amount of free water release (Method 2), unless any melt is present.

A comparison of the results from both methods shows very little difference in the melting and water migration (Fig. B.6). This is probably because material that has undergone melt extraction remains at conditions at which it can theoretically melt again (after which there would be no difference in the water migration scheme between both methods anymore), or this material is too hot to reabsorb any water. The first method is applied in Chapter 4, as a simpler way to approximate the melt depletion.

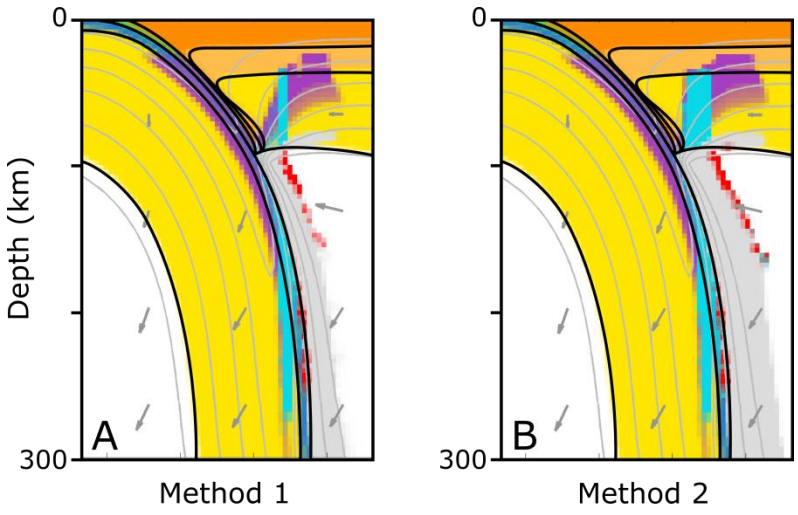


**Figure B.6: A comparison of subduction-related melting when the melt depletion approximations are implemented.** Slight differences are observed in the location of melting and the hydration area of the overriding lithosphere, but show the same general pattern of dehydration, mantles wedge.